THE HYDROCRACKING OF FISCHER - TROPSCH WAX

- Using n-Tetradecane as a Model Compound

by

ATHANASIOS KOTSIOPOULOS

BSc (Chem. Eng.) (Cape Town)

A thesis submitted to the University of Cape Town
in partial fulfilment of the requirements for the degree of
Master of Science in Engineering
MSc (Eng.)

March 2005

Acknowledgements

This thesis would not have been possible without the help and support of a few key people and organizations.

I would like to firstly thank Albemarle Catalysts (formerly Akzo Nobel Catalysts) and The Petroleum Oil and Gas Corporation of South Africa (PetroSA). Without their financial support and insight into the importance and development of Fischer-Tropsch wax hydrocracking globally, the Catalysis Research Unit at the University of Cape Town and myself, would not have had this opportunity to undertake a very new and intellectually challenging project.

I would also like to thank the NRF, THRIP and the University of Cape Town for their financial support throughout this study. Their continuous support was greatly appreciated.

Experimentation could not have been possible without the skillful workmanship of Jo Mäcke. Mark Wüst gratefully repaired electrical glitches.

Finally, I would like to thank my supervisors, Jack Fletcher and Walter Böhringer. Jack's continuous interest, advice and guidance were always appreciated. Weekly meetings with Jack always ensured that work was on track and heading in the right direction.

Walter's willingness to help and provide anybody with advice is indescribable. He has taught me so much with respect to research with his never-ending knowledge. Many late nights were spent preparing presentations and reports without any objections. Walter's input into this thesis is exceedingly valued and will never be forgotten.

Synopsis

Increasingly stringent legislation has been applied to transportation fuels to minimise or eliminate aromatics and sulphur compounds in diesel fuel. This has led to manufacturers determining alternative production methods to comply to legislation.

Part of the current diesel fuel is being produced by hydrocracking heavier fractions derived from crude oil. These hydrocracking processes utilise bi-functional catalysts which have a metal (hydrogenating/dehydrogenating) function and an acid (cracking) function. The most common of these hydrocracking catalysts are combinations of either noble metals and acid zeolites, such as Pt/HY, or combined sulphides of group VIA and VIIIA metals on amorphous acidic supports, such as $CoMo/SiO_2$-Al_2O_3.

For good quality diesel, the fuel should have a high cetane number and the aromatics and sulphur content should also be kept to a minimum (e.g. EU legislation: sulphur content must be below 10 ppm (wt) by 2008). Fischer-Tropsch wax is made up predominantly of long-chain linear paraffins with exceptionally low aromatics and heteroatom content (sulphur- and nitrogen-containing compounds) and therefore a good source for very 'clean', good quality diesel.

The objective of this study was therefore to investigate the suitability of a conventional bi-functional hydrocracking catalyst namely, $CoMo/SiO_2$-Al_2O_3 in unsulphided form for the hydrocracking of Fischer-Tropsch wax using n-tetradecane as a model compound. The purpose of using the catalyst in unsulphided form was not to introduce any sulphur to the already sulphur-free feedstock.

For the investigations a high pressure test apparatus was designed and constructed. The apparatus consisted of an isothermal trickle bed reactor followed by a vapouriser which ensured that the product stream was in the vapour phase prior to going to on-line gas chromatographic analysis.

Experiments focussed mainly on the effects of temperature, pressure, space velocity and hydrogen/n-tetradecane ratio on the hydrocracking reactions.

The outcome of experimentation did not reveal bi-functional, 'true' hydrocracking as expected i.e. at low conversions: no methane, very little ethane, slightly higher propane selectivity and high molar selectivities of equally distributed, highly branched mid-carbon number products between C_4 and C_{10}, with heavier carbon number fractions, C_{11}-C_{13}, mimicking the lighter fractions. Instead what was observed was a very high molar selectivity for methane with very little, almost equally distributed, negligibly branched, C_2 - C_{10} fractions and increasing tail ends beyond C_{10}. This product was indicative of hydrogenolysis reactions rather than bi-functional, 'true' hydrocracking reactions.

The excessive molar selectivity of methane and increasing tail ends was attributed to a successive methyl abstraction type hydrogenolysis mechanism occuring over isolated metallic cobalt species, while the almost equally distributed C_2 - C_{10} range was considered to be due to a 'platinum-type' hydrogenolysis mechanism over the oxidic CoMo-phase which cleaves all bonds with equal probability. To explain the observed trends, a simple mathematical model was formulated for the successive methyl abstraction hydrogenolysis mechanism. What was obtained from the model was a trend that was similar in shape to what was obtained experimentally, particularly at low hydrogen/n-tetradecane ratios, thereby supporting the hypothesis that the observed results were a combination of the 'platinum-type' hydrogenolysis mechanism and the methyl abstraction type hydrogenolysis mechanism.

Results also indicate that process conditions had a significant effect on the conversion. However, their major or only influence on selectivities was by conversion and process conditions as such did not have much of a direct influence on selectivity. Increasing conversion resulted in increasing light gas (C_1-C_3) selectivity and decreasing C_{11}-C_{13} selectivity with a shift in the mid-carbon number range to lower carbon numbers (indicative of secondary reactions) but effects became significant only at very high conversion ($>$ 98% cracking conversion of tetradecane). Increasing temperature, decreasing pressure, decreasing space velocity and increasing hydrogen/n-tetradecane ratio all resulted in an increase in conversion.

Unexpectantly, conversion declined with increasing total pressure. From experiments varying either the total pressure or the hydrogen/n-tetradecane ratio, consistent correlation of conversion with the n-tetradecane partial pressure was obtained but not with hydrogen partial pressure. Since conversion declined with increasing n-tetradecane partial pressure, it is concluded that adsorbed n-tetradecane is inhibiting reactions.

It can be speculated that the apparent paradox of increasing methane selectivity at low hydrogen/n-tetradecane ratios may be explained with 'platinum-type' hydrogenolysis

demanding more space on the catalyst surface than methyl abstraction due to different adsorption geometries (flat versus perpendicular) and therefore being suppressed at high catalyst surface occupation by n-tetradecane.

High isomerisation was observed at low hydrogen/n-tetradecane ratios. Low hydrogen/n-tetradecane ratios result in increased olefin partial pressure, hence, accelerated acid catalysed reactions on the SiO_2-Al_2O_3 support.

It can be concluded that non-sulphided conventional hydrocracking catalysts such as CoMo/SiO_2-Al_2O_3 proved suitable for Fischer-Tropsch wax hydrocracking. The high yields of linear paraffins, due to minimal isomerisation through the hydrogenolysis mechanism, would be of interest with regard to providing high cetane number diesel. Also, no sulphur is introduced to the product.

The future challenge is to minimise methane selectivity, i.e. avoid/reduce the presence of metallic cobalt and keep conversion somewhat below 100%.

List of Symbols

[ ]	Indicates erroneous data
A_i	GC peak areas corresponding to individual carbon species i
α	Represents the probability of a long hydrocarbon fragment to remain adsorbed on the catalyst surface to undergo repeated methanolysis
C_{20+}	Hydrocarbon fractions above carbon number 20
CH_4 or C_1	Methane
C_i	Iso- and normal paraffins of species i
CoMo	Cobalt Molybdenum
C_x-C_y	Iso- and normal paraffins in the range between carbon numbers x and y
$\Delta\ G_{f,x}{}^o$	Gibbs free energy of formation of species x
$\Delta\ G_R{}^o$	Gibbs free energy of reaction
$\Delta\ G_{rxn,298K}$	Gibbs free energy of reaction at STP
$\Delta\ H_{rxn,298K}$	Heat of reaction at STP
EU	European Union
FCC	Fluid catalytic cracking

FID	Flame ionisation detector
F-T	Fischer-Tropsch
GC	Gas chromatograph / gas chromatography
GTL	Gas to liquids process
H_2/n-C_{14}	Hydrogen to n-tetradecane molar ratio
H/C	Hydrogen to carbon ratio
HDM	Hydrodemetallisation process
HDN	Hydrodenitrogenation process
HDS	Hydrodesulphurisation process
HPC	Heavy paraffin conversion (hydrocracker)
HPLC	High performance liquid chromatography
HPS	Heavy paraffin synthesis (Fischer-Tropsch reactor)
K	Equilibrium constant
LHSV	Liquid hourly space velocity
LPG	Liquified petroleum gas
min	Minute
n-C_{14}	n-Tetradecane
n-C_i	Normal paraffins of species i
N_{C_i}	Number of carbon atoms in the respective compound i

$\dot{n}$	Molar flow rate
n_i	Number of moles of each species i
NiMo	Nickel Molybdenum
NiW	Nickel Tungsten
NO_x	Nitrous oxides
P	Pressure
$P_{C_{14}}$	Partial pressure of n-tetradecane
P_{C_7}	Partial pressure of n-heptane
P_{H_2}	Partial pressure of hydrogen
ppm	Parts per million
P_x^{vap}	Vapour pressure of compound x
R	Ideal gas constant
REP	Reproduced results
sccm	Standard cubic centimeters per minute
S_{C_i}	Molar selectivity of the respective compound i
SiO_2 - Al_2O_3	Silica-alumina
SMDS	Shell middle distillate synthesis
SO_x	Sulphur oxides

STP	Standard temperature and pressure
T	Temperature
TOS	Time-on-stream
US, USA	United States of America
wt	Weight
X	Conversion

Contents

List of Figures

List of Tables

Background 1

1.1 Introduction

Hydrocracking is a refinery process which is able to produce a range of products. Initially the focus of this process was to achieve a high yield in the gasoline range, particularly in the US, but with the increased demand in diesel throughout the world, the focus has now shifted to produce a high yield of middle distillates (UOP, 1998).

Crude oil has a high content of heteroatoms which are the main cause of pollutants emitted from end user applications such as furnaces or cars. Also crude oil has a high concentration of aromatics, which may be advantageous in the production of gasoline (increases octane number), but has a negative impact on the cetane value for diesel (Dry, 2001). It is known that diesel engine performance is related to the cetane number, that is to say that higher cetane numbers improve engine performance that ultimately results in less fuel consumption and reduced emissions. With these qualities, crude oil derived feedstocks had to undergo pretreatment to lower any heteroatom and aromatic concentrations in the streams to achieve an acceptable product in the gas oil range (i.e. low heteroatom content and high cetane rating).

Products from the Fischer-Tropsch (F-T) synthesis appear to hold the answer for a cleaner and highly efficient diesel fuel. Products obtained at low synthesis temperatures using either iron or cobalt catalysts from this process result in a high yield of linear paraffins (wax) with 'relatively no sulphur or nitrogen' (Dry, 2001). After hydrocracking, the diesel fraction may have a cetane number of up to 75 (Shah et al., 1988; Dry, 2001).

The idea of hydrocracking F-T wax seems like a rather straight forward concept and a highly advantageous means of obtaining a high yield of high quality middle distillates. This, however, is not the case. Although the literature is rather extensive in the area of hydrocracking of crude oil derived feedstocks, very little is reported on the hydrocracking of F-T wax.

The only plant hydrocracking Fischer-Tropsch wax on commercial scale (Shell at Bintulu, Malaysia) is said to be using a rather conventional catalyst. It is questionable if a sulphided catalyst (that requires constant co-feeding of sulphur compounds for stabilisation) is the best choice for hydrocracking a sulphur free feedstock.

Another challenge is tailoring the properties of the produced diesel with respect to contrary criteria such as high cetane number (requires linear paraffins) and good cold flow properties (requires branched paraffins) for application in cold climates.

Therefore the challenge lies in the development of tailored catalysts and the corresponding process conditions.

Most of the literature which applies to the hydrocracking of linear paraffins will be reported in the present study and is assumed to relate to the hydrocracking of wax. This was found to be acceptable by comparing available literature on the hydrocracking of F-T wax with hydrocracking trends found on 'shorter' linear paraffins.

1.2 Industrial Relevance

As emission from petrol and petrol engines has been regulated, so too are the emissions from diesel and diesel engines. Regulations redefined the gasoline specification to enforce the US 'Reformulated Gasoline' Act, which was to eliminate the use of lead (Fernandez and Keller, 2000) and reduce the benzene and aromatics content to a minimum.

With the increasing demand of diesel, it has become necessary that the emissions from engines using this fuel source are also regulated. Specifications that have been targeted are (UOP, 1998):

- Aromatic and polyaromatic hydrocarbons - which result in particulate formation, influence combustion temperature and in that way affect NO_x formation
- Sulphur - which contributes to the amount of particulates and SO_x
- Density - which affects the ignition and increases combustion temperature and NO_x formation when it is higher
- Cetane value - which enables better combustion, higher engine efficiency and lower emissions when it is higher

The result is that industries need to modify their processes to adhere to any regulations imposed. Factors which could be improved to provide cleaner diesel include catalyst and process technology, feedstock selection and fuel additives.

At present the most concerning factor of diesel emissions is sulphur. In the United States, sulphur levels were reduced to 500 ppm (wt) in 1993. More stringent specifications since have been imposed by regions such as California and Western Europe (UOP, 1998) e.g. EU legislation requires that the sulphur content must be below 10 ppm (wt) by 2008 (Andrews et al., 2000).

Diesel fuel is primarily used by transportation companies in the United States of America (USA) while in Japan, Europe and other parts of the world, it is a significant fuel for personal transportation by passenger cars. Many publications forecast that the demand for diesel will grow faster than the demand for any type of energy in general (UOP, 1998). The increasing demand for diesel can be related to the fact that diesel engines have a greater fuel efficiency compared to petrol engines, with the added advantage that this produces less CO_2 per kilometre travelled (Dry, 2001), making it a more environmentally friendly source of energy.

Many refineries, particularly in the USA, were built with large fluid catalytic cracking units with the aim to produce predominantly gasoline. This meant that as the demand for gasoline increased, so did the production of light cycle oil, which was commonly blended into fuel oil. With the shift in the demand towards diesel, the light cycle oil now has to be blended into the diesel. Light cycle oil has a high aromatic and sulphur content. The use of light cycle oil as blendstock in diesel results in the reduction of the cetane number and an increase in sulphur levels i.e. it greatly reduces the quality of the diesel. On the other hand blendstocks produced by hydrocracking have low sulphur content and high cetane value and hence make excellent diesel (UOP, 1998).

With the increasing demand in diesel, refiners need to convert existing refinery streams into high-quality diesel. Depending on the refiners equipment and overall processing strategy, they may use combinations of desulphurisation, aromatics saturation, selective ring opening and hydrocracking to produce the quality diesel required (UOP, 1998). Diesel from F-T wax hydrocracking would be a particularly valuable, additional blendstock for refineries to improve diesel quality and meet imposed regulations.

1.3 Cracking

Low boiling fractions are obtained when converting heavy crude oil fractions. Different processes are applied (Dufresne et al., 1987):

- Thermal processes
  - Coking
  - Vis-breaking (volatile by-products)

  Thermal processes are able to break carbon-carbon bonds, do not increase the overall hydrogen content, but result in an increase of the H/C ratio of the volatile product fraction compared to the feed, since co- or main products are coke or a more heavy (although less viscous) fuel oil, respectively
- Catalytic processes
  - Catalytic cracking

  Catalytic cracking does not increase the overall hydrogen content but volatile products have a slightly enhanced H/C ratio due to low yields of co-product coke
  - Mild hydrocracking,
  - Conventional hydrocracking

  Increases overall hydrogen content

In the catalytic processes, hydrogen pressure is of significant importance when good quality middle distillates are required, since middle distillates must have a sufficient hydrogen to carbon ratio (H/C ratio) to obtain a satisfactory cetane number. Catalytic cracking produces low quality middle distillates (light cycle oil) while yielding a good quality naphtha cut (due to the absence of hydrogen). On the contrary, mild and conventional hydrocracking is performed in the presence of hydrogen. Mild hydrocracking, which is operated at low hydrogen pressure (30 - 70 bar, 380 - 440°C), produces a large quantity of low-sulphur fuel oil, with a hydrogen content slightly higher than that of the feed, and small quantities of medium-quality distillates (Dufresne et al., 1987). Conventional hydrocracking is operated at higher hydrogen pressure (100 - 140 bar, 350 - 450°C) which produces a higher H/C ratio resulting in good quality middle distillates.

1.3.1 Hydrocracking

Hydrocracking is a combination of catalytic cracking and hydrogenation to produce naphthas, distillates and lubricating oils (SET Laboratories Inc., 2002). This is achieved by a sequence of hydrogenation/dehydrogenation and carbon-carbon bond cleavage reactions of high molecular weight components from heavy petroleum fractions. The use of high temperatures and pressures, a catalyst and hydrogen is indicative of this process. Hydrocracking is usually employed for feedstocks that are difficult to process by catalytic cracking. The difficulty in processing these feedstocks lies in the high content of polycyclic aromatic hydrocarbons and high concentrations of catalyst poisons, i.e. sulphur and nitrogen compounds, when crude oil derived feedstocks are converted (Scherzer and Gruia, 1996).

Typically, hydrocracking consists of two stages (SET Laboratories Inc., 2002; Scherzer and Gruia, 1996; Maxwell, 1987; Dufresne et al., 1987). The first stage is a hydrotreatment step in which heteroatom removal (hydrodesulphurisation, hydrodemetallisation and hydrodenitrogenation), hydrogenation (mostly of polyaromatics) and minor hydrocracking reactions occur. The catalysts utilised in this step consist of sulphided systems, such as $CoMo/Al_2O_3$ and $NiMo/Al_2O_3$. Relatively high temperatures and pressures are employed in order to obtain a sufficient degree of heteroatom removal and hydrogenation of aromatics (Maxwell, 1987). The second stage is where the actual hydrocracking reactions occur. The severity, which is related to the temperature and pressure of the process, is greater in this stage. The catalysts used in this step are bi-functional catalysts which have both a strong acidic and a strong hydrogenation/dehydrogenation function e.g. sulphided NiW/SiO_2-Al_2O_3 or (non-sulphided) Pt/H-Y. In the case of the latter type of catalyst, interstage removal of H_2S from the product stream is ultimately required (see figure 1.1). When the feedstock to the hydrocracker has a high paraffin content, the high hydrogen pressure prevents the formation of polycyclic aromatics and thereby serves as a means to reduce tar formation and coke build-up on the catalyst.

Typically fixed bed reactors, operated in trickle bed mode, are used in hydrocracking in which multiple catalyst beds are utilised due to the highly exothermic nature of the process (aromatics saturation). For this reason, recycle hydrogen gas, which acts as a cooling agent ('cold shots'), is introduced between the catalyst beds (Scherzer and Gruia, 1996).

As mentioned above, the most common configuration is a two-stage hydrocracker (figure 1.1), which consists of two stages with inter-stage product removal (Maxwell, 1987).

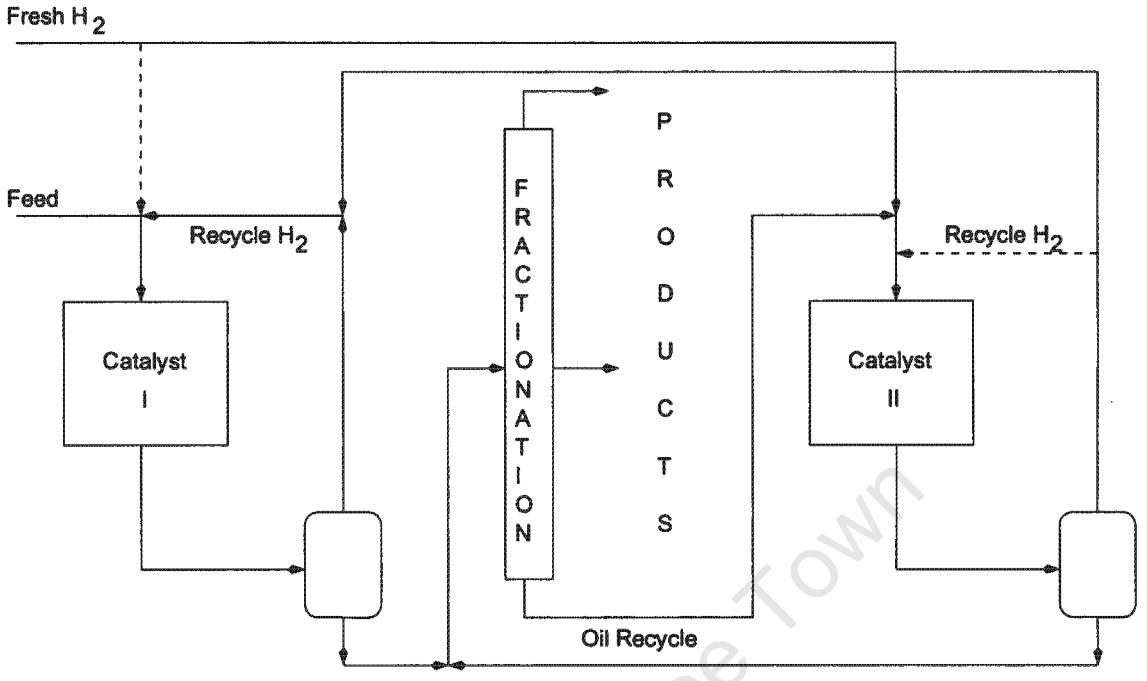

Figure 1.1: Two-Stage Hydrocracker (adapted from the schematic proposed by Scherzer and Gruia, 1996)

Gaseous products removed from the first stage include H_2S and NH_3. Removal of these catalyst poisons and supply of fresh, pure hydrogen allows the refiner a greater choice in catalysts that may be used in the second stage, e.g. Pt/H-Y.

The series-flow hydrocracker (figure 1.2) also has two reactor stages but does not have inter-stage product removal. In the second stage a different catalyst can be applied at different conditions (temperature, space velocity). The constraint of this configuration is that the second stage is only possible with the use of catalysts, which are sufficiently resistant to NH_3 and H_2S, e.g. NiW/SiO_2-Al_2O_3.

The single-stage hydrocracker (figure 1.3) is the most simple configuration but requires a catalyst which is sufficiently resistant to NH_3 and H_2S and is able to perform multiple tasks such as heteroatom removal, hydrogenation and hydrocracking.

1.3.1.1 Mild Hydrocracking

This is a relatively new process in which the conventional vacuum gas oil hydrodesulphurisation (HDS) process is switched to a mild hydrocracking mode to produce more middle distillates (Maier et al. 1984; Sonnemans et al. 1984; Dufresne et al. 1987).

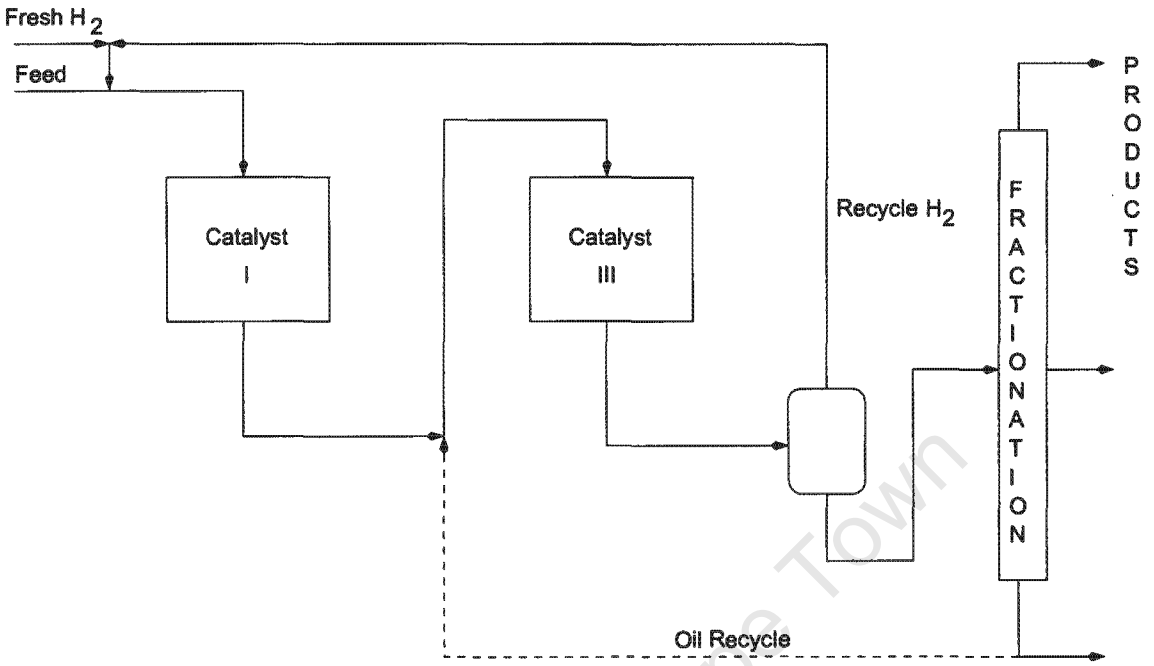

Figure 1.2: Series-Flow Hydrocracker (adapted from the schematic proposed by Maxwell, 1987)

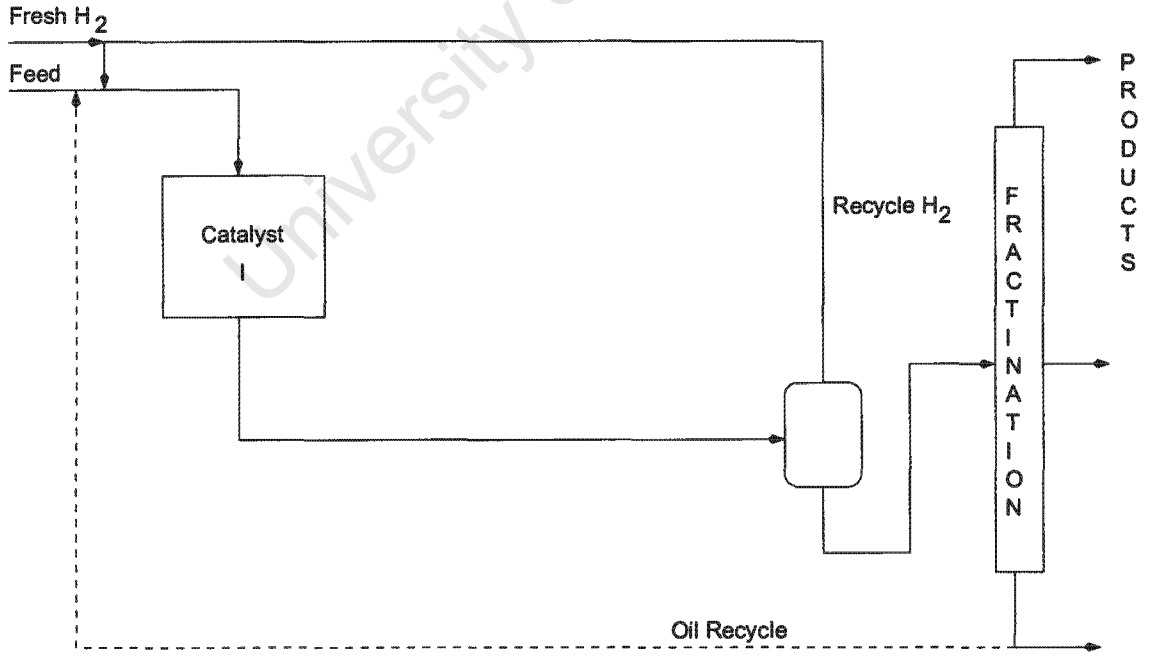

Figure 1.3: Single-Stage Hydrocracker (adapted from the schematic proposed by Maxwell, 1987)

The main feedstock is vacuum gas oil although other heavy gas oils can be used. The process is very similar to hydrotreatment and therefore results in a very similar product. The quality of the gas oil cut of mild hydrocracking is very close to the diesel oil specification in terms of cetane number and therefore may be blended in the diesel pool (Dufresne et al., 1987).

As this process is a switch from hydrotreatment, the operating conditions remain quite similar, notably the hydrogen pressure, which is often in the range 30 to 45 bar (Dufresne et al., 1987). A lower level of aromatic hydrogenation and conversion is therefore achieved than with conventional hydrocracking.

Mild hydrocracking in a hydrotreater may be achieved (in single-stage mode, analogous to figure 1.3) by either of the following (Dufresne et al., 1987):

1. An increase in the operating temperature compared to hydrotreating, using the conventional hydrotreating catalyst. The consequence is that all reaction rates increase - especially the cracking reaction rate which thus results in an increase of middle distillate production. The disadvantage of this method is that aromatics hydrogenation is thermodynamically limited, resulting in a comparably high concentration of polyaromatics (coke precursors), which cannot be cracked at these operating conditions. This inevitably brings about quick deactivation of the hydrotreating catalyst.

2. A partial change of the non-acidic hydrotreating catalyst for one that is slightly acidic, using a more acidic carrier, either a halogen doped alumina or silica-alumina. The acidic component will produce more cracking conversion. This allows for the catalyst to be used alone or if necessary to be coupled with a conventional hydrotreating catalyst placed upstream in the reactor.

1.3.1.2 Conventional Hydrocracking

This process is performed at hydrogen pressures greater than 100 bar and at 350 - 450°C. Bi-functional catalysts are used with a hydrogenation function (noble metals or combined sulphides of group VIA and VIIIA elements), and an acidic function (comprised of either amorphous silica-alumina or an acid zeolite (H-Y)). The high hydrogen pressure enables deep hydrogenation of polynuclear aromatics and deeper hydrodenitrogenation i.e. less catalyst coking and poisoning (Dufresne et al. 1987).

The process may run as either a single-stage (figure 1.3) or two-stage process (figures 1.1 and 1.2). In two-stage mode there is (Dufresne et al., 1987) a:

- hydrotreatment step and, optionally, a fractionation step where H_2S and NH_3 are removed together with gases and other light cuts, and a
- hydrocracking step in which the unconverted heavy fraction from the first step is converted using a hydrocracking catalyst

The advantage of hydrocracking is that it is flexible. It can process different types of feedstocks (e.g. vacuum gas oils, FCC cycle oils or thermal gas oils) to produce a range of products (e.g. naphtha and middle distillates). The disadvantage is the necessity to use high hydrogen pressure which is economically unfavourable (`http://www.cheresources.com/refining5.shtml`, 2004).

Typical feedstocks, products and process conditions for conventional and mild hydrocracking are compared in table 1.1.

Table 1.1: Conventional and Mild Hydrocracking – Feedstocks, Products and Process Conditions (Dufresne et al., 1987)

Conventional Hydrocracking		Mild Hydrocracking	
Feedstocks		*Feedstocks*	
Vacuum Gas Oils		Vacuum Gas Oils	
Cat. Cracking Gas Oils		Cat. Cracking Gas Oils	
Coking Gas Oils		Coking Gas Oils	
Deasphalted Oils		Deasphalted Oils	
Products		*Products*	
Middle Distillates		Low Sulphur Fuel Oil (60-80%)	
(Diesel Fuel + Jet Fuel)		Middle Distillates (40-20%)	
Naphtha			
Propane + Butane			
Operating Conditions		*Operating Conditions*	
Temperature	350 to 450°C	Temperature	380 to 440°C
H_2 Pressure	80 to 150 bar	H_2 Pressure	30 to 70 bar
LHSV	0.3 to 1.5 h^{-1}	LHSV	0.2 to 1.5 h^{-1}
Process Design		*Process Design*	
One or Two Stages		One Stage	

1.4 Mechanisms

1.4.1 Hydrocracking Mechanism

The bi-functional mechanism for catalytic hydrocracking has been postulated based on pure component work (Coonradt and Garwood, 1964; Schweitzer et al., 1999). This mechanism (figure 1.4) shows that the hydrocracking of n-paraffins undergoes a series of steps over the hydrogenation/dehydrogenation function i.e. the metal or metal sulphide, and over the acid function (i.e. amorphous silica-alumina or an acid zeolite) of a bi-functional catalyst. The initiation of the cracking of paraffins occurs at the metal/metal-sulphide component of the catalyst. At this point the paraffins are dehydrogenated to form olefins. The olefins are rapidly adsorbed on the acid sites of the catalyst forming carbenium ions. More stable carbenium ions are formed by isomerisation. Provided the dehydrogenation/hydrogenation activity of the catalyst is sufficiently high, reactions are in equilibrium up to this step (figure 1.4). Smaller carbenium ions and olefins are formed via β-scission (Shah et al., 1988). This is the rate determining step. Paraffins are eventually formed again as a result of olefin saturation at the metallic component of the catalyst. Secondary cracking results if the hydrogenation/dehydrogenation function of the catalyst is comparably weak so that the carbenium ions continue to isomerise and crack or the olefins are readsorbed on the acid function (Shah et al., 1988).

Since acid catalysed skeletal isomerisation of carbenium ions is far more rapid than cracking, a 'pool' of branched carbenium ion isomers and their corresponding hydrocarbons forms rapidly (which is equilibrated or close to being equilibrated – Martens and Jacobs, 2001), followed by slow cracking (figure 1.5). From this carbenium ion 'pool' the most reactive species are cracked with preference. These species contain a stable, tertiary carbenium ion in the 1,3-position to a quartary carbon atom (see figure 1.6, Weitkamp et al., 1983). β-Scission results in a stable, tertiary carbenium ion again. According to Alvarez et al. (1996) such tertiary-tertiary cracking is 50 times faster than tertiary-secondary or secondary-tertiary cracking of carbenium ions of a lower degree of branching.

The tertiary-tertiary mechanism implies also that the formation of fragments smaller than C_4 is unfavourable (since it unavoidably implies secondary or primary carbenium ions). All internal bonds beyond the γ-bond can be cracked via a tertiary-tertiary mechanism (after isomerisation) and hence have equal reactivity. The consequence of hydrocracking, for instance, n-tetradecane (n-C_{14} paraffin) is an even carbon number distribution of the

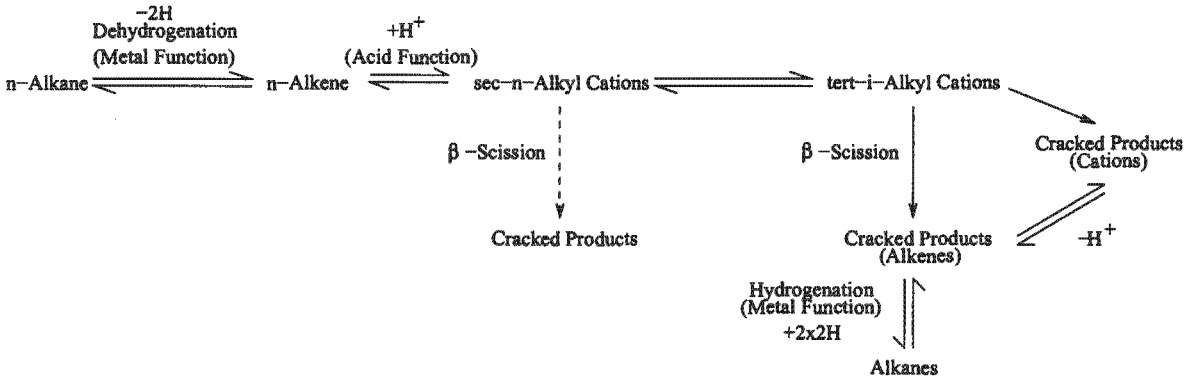

Figure 1.4: Bi-Functional, 'True' Hydrocracking Mechanism (based on the mechanism proposed by Shah et al., 1988)

cracked products in the C_4 to C_{10}, as shown in figure 1.7. C_3 fragments, whose formation requires a secondary carbenium ion and consequently has a far lower rate (see above), are cleaved off to a small extent, resulting in noticeable but low C_3 and C_{11} selectivity. The resulting 'flat' ideal primary cracking distribution, obtained at low conversion, is the primary product from ideal bi-functional, 'true' hydrocracking of long paraffins. Secondary cracking occurs increasingly at higher conversions, shifting the carbon number distribution to smaller carbon numbers with a maximum in C_4. The resulting 'skewed' secondary cracking distribution is shown in figure 1.7 as well.

In order to produce maximum paraffin selectivity within a desired range (e.g. C_{10}-C_{20} middle distillates) from Fischer-Tropsch (F-T) wax these heavy paraffins have to undergo selective hydrocracking. According to Sie et al. (1991), the selective cracking of wax has to meet two criteria:

1. The chain length of the fragments should be predominantly in the desired range, and
2. Components above the desired range should be cracked in preference to those which are already in or below the desired range.

Sie et al. (1991) observed that only very small quantities of lights (methane, ethane and propane) were formed when cracking a F-T product fraction consisting of mostly hexadecane while at low conversion a relatively equal distribution (on a molar basis) of carbon numbers in the intermediate range was obtained, such as shown in figure 1.7. This equal distribution was attributed to primary cracking. A similar observation was made by Froment (1987) for the cracking of n-decane over Pt/USY (a bi-functional catalyst).

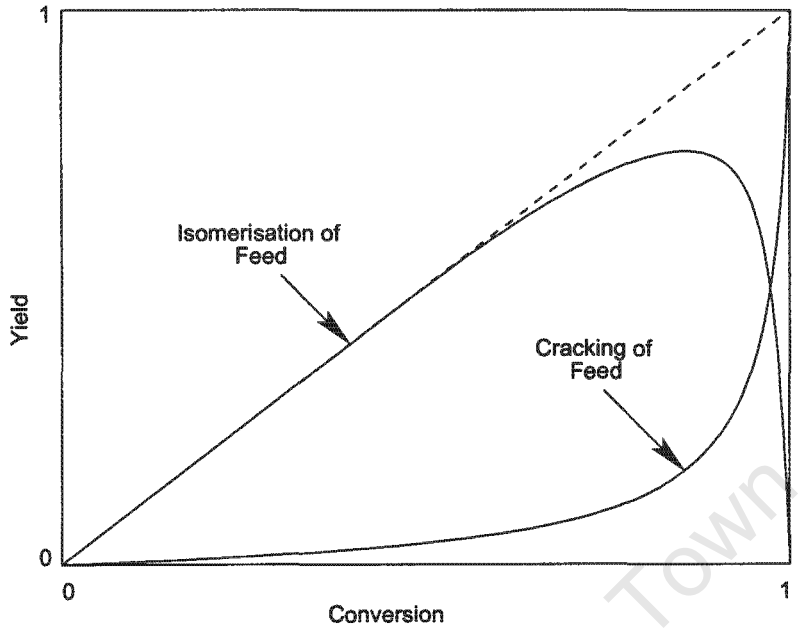

Figure 1.5: Yield of Isomerised and Cracked Products over a Bi-Functional Hydrocracking Catalyst as a Function of Conversion (Martens and Jacobs, 2001)

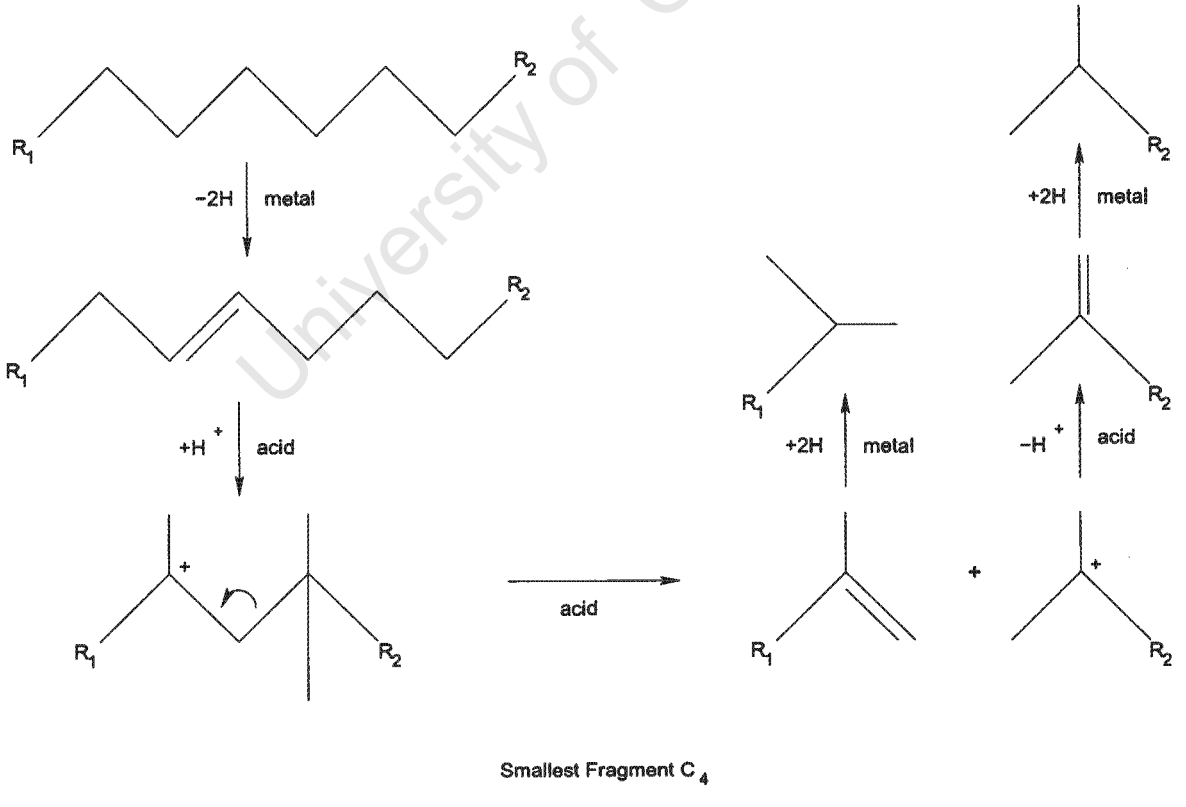

Figure 1.6: Bi-Functional, 'True' Hydrocracking Mechanism Based on the Mechanism Proposed by Weitkamp et al. (1983)

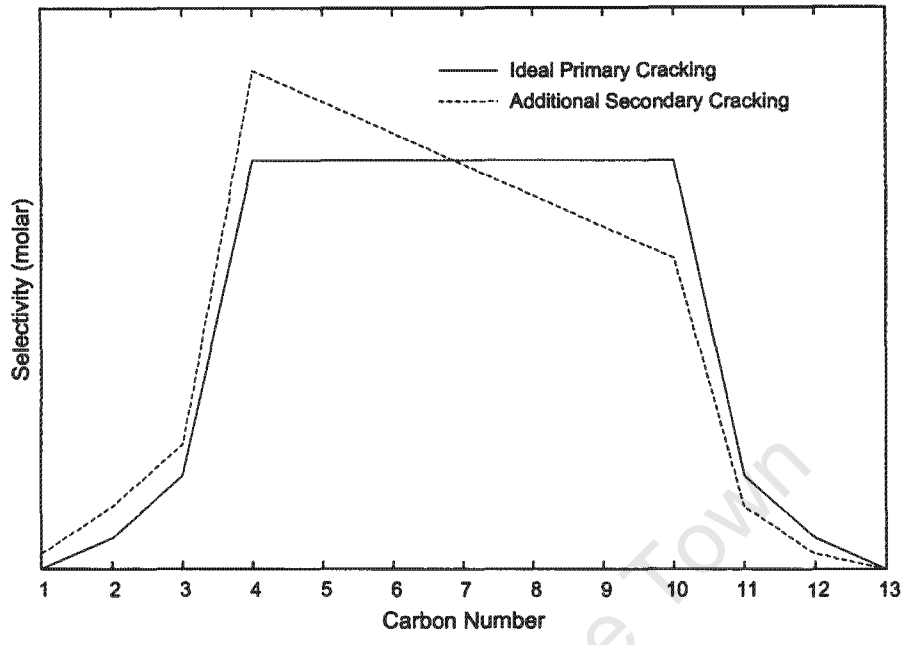

Figure 1.7: Theoretical Bi-Functional Hydrocracking Product Carbon Number Distribution from n-C_{14} Paraffin Conversion

Froment (1987) found, as well, that the product distribution comprised small quantities of methane, ethane and propane, which were negligible compared to the equally distributed, intermediate cracked products. Bi-functional hydrocracking of a long chain F-T product also resulted in minor formation of propane and negligible formation of methane and ethane (Sie et al., 1991), see figure 1.8.

From the product carbon number distribution observed, Sie et al. (1991) concluded that β-scission of the α, β or γ carbon-carbon bonds from the terminal carbon atoms is disfavoured. It was deduced that scission most likely occurs on the remaining more centrally situated carbon-carbon bonds of the paraffin chain that have a high and approximately equal probability of cracking.

The minor reactivity of the first three bonds from the terminal carbon brought about the relationship that the intrinsic cracking reactivity of paraffins is proportional to the number of carbon-carbon bonds minus 6 or the carbon number minus 7, the straight line in figure 1.9, 'intrinsic reactivity' (Sie et al., 1991).

The second of the conditions expressed by Sie et al. (1991) (see above) was shown to hold true by the observation obtained from the hydrocracking of n-paraffins in the C_{10}-C_{17} range over a bi-functional catalyst. Sie et al. (1991) observed that with increasing carbon number, the reactivity of the paraffins increased to a greater extent than predicted by

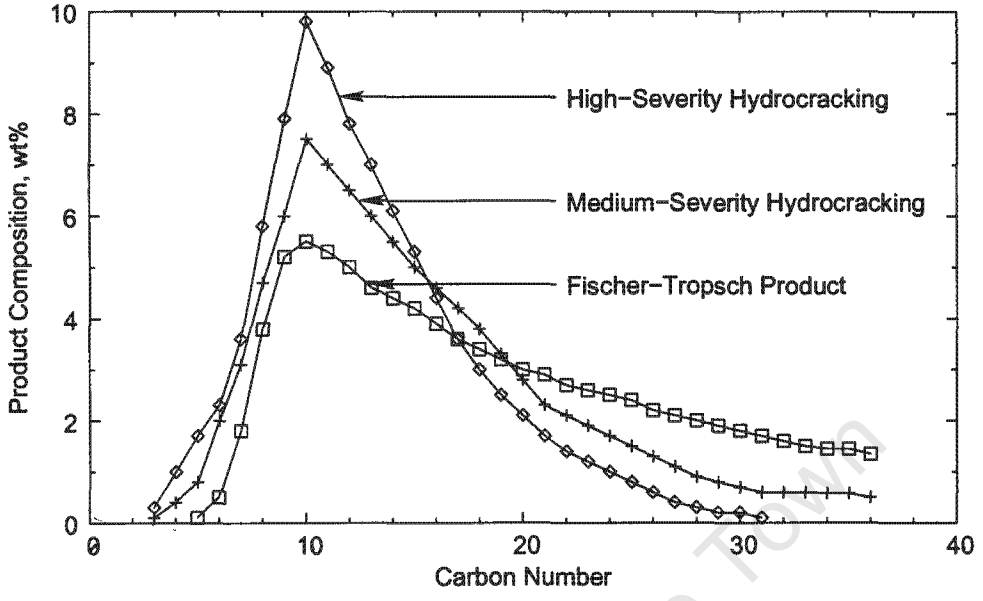

Figure 1.8: Carbon-Number Distribution from Hydrocracking a Fischer-Tropsch Product over an Undisclosed Bi-Functional Catalyst at Varying Degree of Severity (Sie et al., 1991)

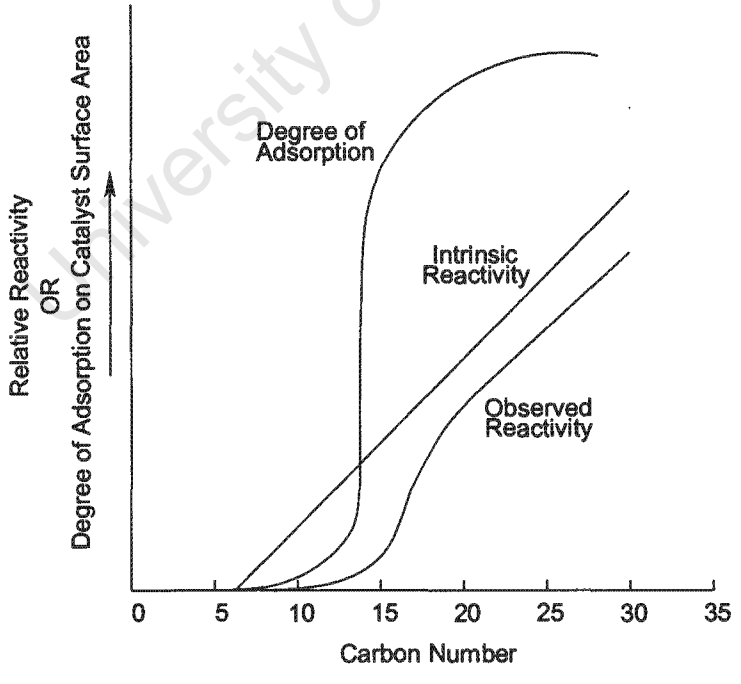

Figure 1.9: Schematic Representation of the Reactivity of n-Paraffins in Bi-Functional Hydrocracking (Sie et al., 1991)

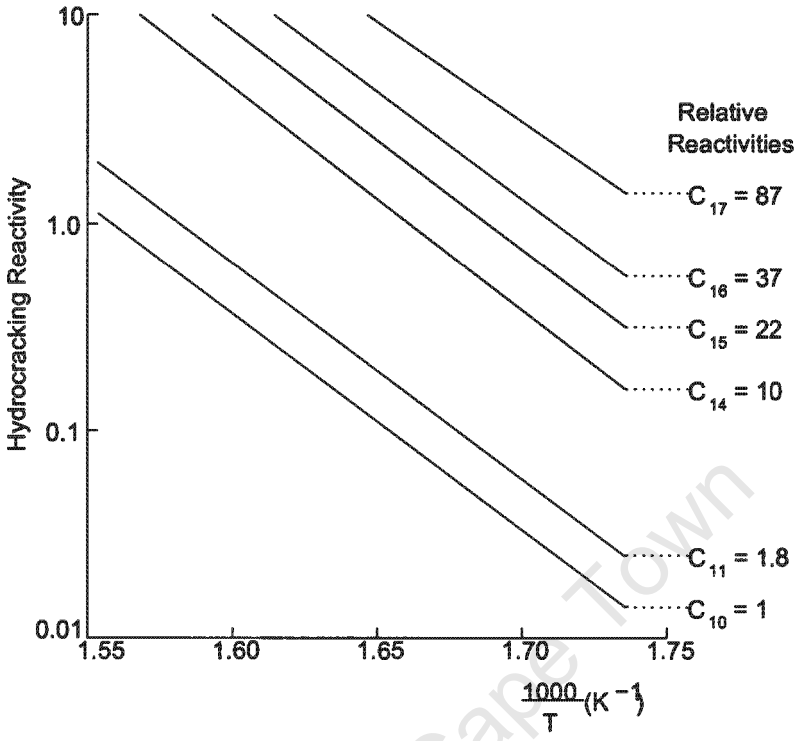

Figure 1.10: Hydrocracking of Paraffins of Different Chain Length over an Undisclosed Bi-Functional Catalyst (Sie et al., 1991)

the intrinsic reactivities of bonds (figure 1.9 curve labelled 'observed reactivity' and figure 1.10).

Carbon number dependency of adsorption was to further highlight the chain length dependence of the observed cracking rate (Sie et al., 1991). It was suggested that the lighter hydrocarbons will tend to escape from the reactor faster while heavier components will stay condensed or adsorbed on the catalyst with preference (figure 1.9). Therefore, the heavier hydrocarbons will remain longer in the reactor and therefore have a greater probability of being cracked. The adsorption curve of figure 1.9 shows that initially the curve follows an exponential increase corresponding to a linearly increasing heat of adsorption with increasing number of carbon atoms (Sie et al., 1991). As the degree of adsorption reaches 100% the effect levels off above a certain chain length.

What was concluded from the above was that approximately 80 wt% of a C_{20+} paraffin cut can be converted to a C_{10}-C_{20} range product with the remaining 20 wt% ranging below the C_{10} fraction with minor selectivity of products C_1-C_3, resulting from breakage of α, β or γ bonds.

This meets the criteria of selective hydrocracking proposed by Sie et al. (1991), see above.

A kinetic model proposed by Archibald et al. (1960) on the hydrocracking of wax was referred to by Shah et al. (1988). The model is based on rules developed from the hydrocracking of n-paraffins. The rules are stated as follows (Shah et al., 1988):

- only alkanes larger than C_6 may be cracked
- C_3 is the smallest product molecule
- probability of β-scission of carbon-carbon bonds giving C_3 products is half the probability of β-scission of the other bonds
- all other carbon-carbon bonds have equal probability of β-scission

The similarity of the model of Archibald et al. (1960) and the findings of Sie et al. (1991) lies in the first, second and fourth statement, which correspond to the observations and conclusions made by Sie et al. (1991).

An apparent difference in Sie's and Archibald's rules lies in the reactivity of higher paraffins. Both the authors claim equal reactivity of the internal bonds from the γ-bond onwards, i.e. for paraffins greater than C_6 (for Sie's see the straight line 'intrinsic reactivity' in figure 1.9). Whereas Archibald's model appears to refer to a single phase reaction system, Sie's appears to refer to a dual phase reaction system with enhanced adsorption and residence time of the higher paraffins resulting in higher apparent reactivity (see the S-shaped curves in figure 1.9)

1.4.2 Hydrogenolysis

Hydrogenolysis of hydrocarbons is a mechanism which involves the homolytic scission of carbon-carbon bonds over transition metals or transition metal sulphides and oxides. The difference between hydrocracking and hydrogenolysis lies in the type of catalyst used and therefore the intermediates formed. With hydrocracking, bi-functional catalysts are utilised in which the reactant is at first adsorbed on the hydrogenation/dehydrogenation function of the catalyst and the resulting olefinic intermediates are eventually adsorbed on the acid function of the catalyst to form carbenium ion intermediates. Hydrogenolysis, in contrast, occurs over transition metal or transition metal sulphide and oxide catalysts where the reactant is adsorbed on the surface to immediately form alkyl radicals as intermediates (Sinfelt, 1969).

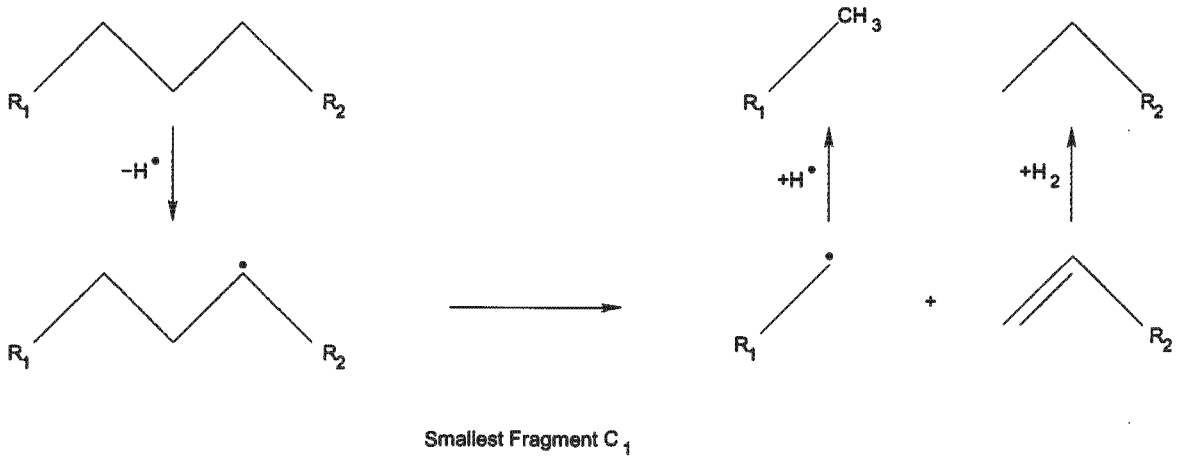

Figure 1.11: Simplified Hydrogenolysis Mechanism for Platinum and Iridium Metal Catalysts

Hydrocarbon chemisorption on the hydrogenolysis catalyst surface involves the split of carbon-hydrogen bonds. This phenomenon indicates that carbon-hydrogen bonds are more reactive than carbon-carbon bonds. The adsorbed alkyl radical undergoes homolytic carbon-carbon bond scission forming another (adsorbed) alkyl radical and an olefin (Kemball and Taylor, 1948; Cimino et al., 1954; Sinfelt, 1969). The final step in the hydrogenolysis mechanism is saturation and desorption of the adsorbed species (Sinfelt, 1973).

The carbon number distribution obtained from hydrogenolysis depends on the type of catalyst used. Metallic nickel based catalysts, for instance, are very selective to terminal bond cracking of saturated paraffins (Gates et al., 1979; Sinfelt, 1973) i.e. methane formation, whereas other hydrogenolysis catalysts, e.g. platinum, form more equally distributed products.

1.4.2.1 Hydrogenolysis over Group VIIIA Noble Metal Catalysts

Sinfelt (1973) set out to determine the hydrogenolysis selectivity of group VIIIA noble-metal catalysts using n-heptane as reactant. Unsupported metal powders were used to eliminate any bi-functional catalysis caused by a carrier. The results showed that hydrogenolysis was the predominant reaction over all noble-metals. Although platinum and palladium on the one hand, and iridium and rhodium on the other have similar low and high hydrogenolysis activities, respectively, selectivities of these pairs of metals exhibited very different product carbon number distributions.

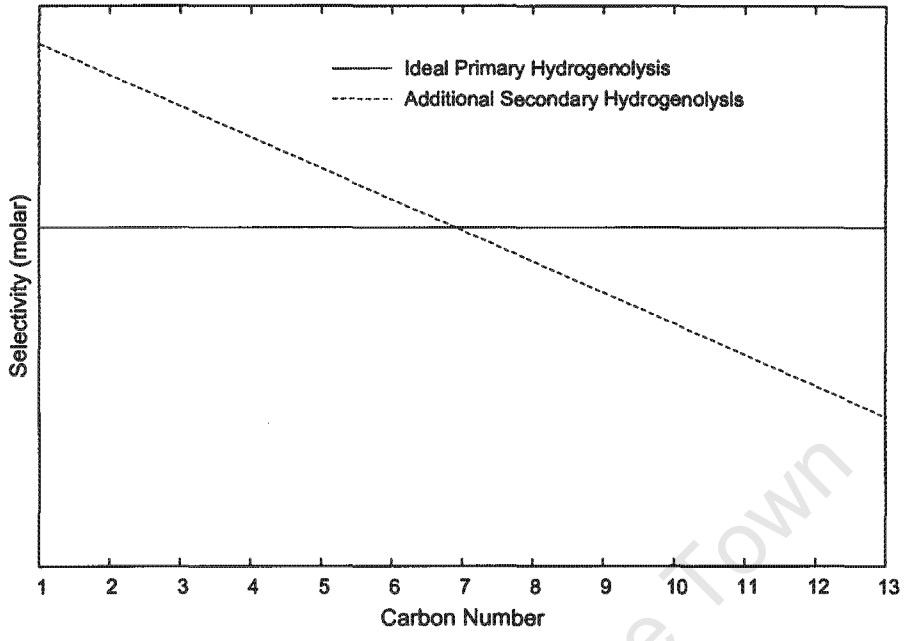

Figure 1.12: Theoretical Product Carbon Number Distribution from Hydrogenolysis of n-C_{14} Paraffin over Platinum and Iridium Metal Catalysts

- Hydrogenolysis over platinum and iridium produced comparable molar selectivities of primary products over the entire carbon number range.
- Palladium and rhodium showed a high selectivity to terminal bond scission at low conversions yielding mainly methane and the corresponding higher n-paraffin with a carbon number one less than the feed molecule, with minimal intermediate products.
- Platinum showed a high degree of skeletal isomerisation and dehydrocyclisation in the product.

So, when a platinum or iridium catalyst is used, the cleavage of carbon-carbon bonds tends to be non-selective giving a broad carbon number distribution of primary products ranging from methane to higher order normal paraffins (figures 1.11 and 1.12). While palladium and rhodium are selective to methane and paraffins with carbon numbers just below the feed (figures 1.13 and 1.14).

To explain the different product distributions observed over group VIIIA noble-metal catalysts, Sinfelt (1973) employed the 1,3-chemisorbed intermediates proposed by Anderson and Avery (1967). In this mechanism, a double bond forms between a carbon atom and the metal surface, while the next but one carbon atom is single bonded (1,3-chemisorption).

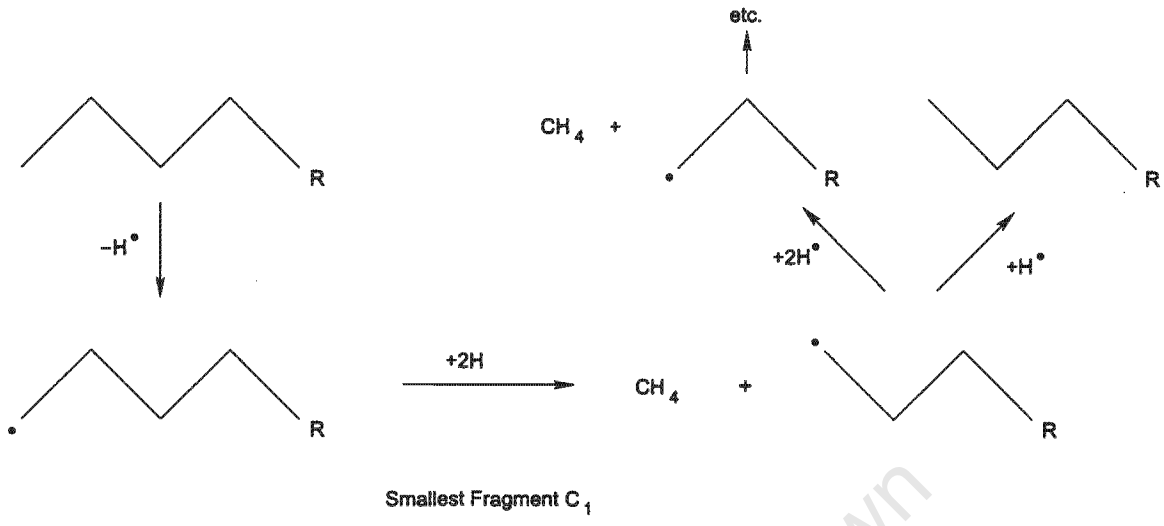

Figure 1.13: Simplified Consecutive Methyl-Abstraction Type Hydrogenolysis Mechanism for Palladium and Rhodium Metal Catalysts as well as Nickel, Cobalt and Iron Catalysts

Sinfelt (1973) made the assumption that if the terminal carbon atom of a chain was adsorbed on the catalyst with a double bond, the adjacent carbon-carbon single bond would cleave preferentially. This would result in methane and the corresponding higher paraffin and this type of mechanism would explain the carbon number distributions observed with palladium and rhodium catalysts (figure 1.14). Gates et al. (1979) suggested that carbon-metal bonds are stronger than carbon-carbon bonds thereby supporting the view that carbon-carbon bonds adjacent to carbon-metal bonds will be cleaved preferentially.

For platinum and iridium, Sinfelt (1973) proposed that these metals could exist in different valence states allowing the carbon-metal double bond to rapidly shift along the chain from the terminal carbon atom to the internal carbon atoms. This type of mechanism would explain the almost equal probability of bond cleavage along the entire carbon chain resulting in a non-selective or equal product carbon number distribution for platinum and iridium (figure 1.12).

1.4.2.2 Hydrogenolysis over Group VIIIA Non-Noble Metal Catalysts

Hydrogenolysis over the non-noble metals of group VIIIA, i.e. nickel, cobalt and iron, results in high selectivity of methane which is consistent with successive methyl-abstraction-type reactions as over palladium and rhodium (see section 1.4.2.2) (Sinfelt, 1973; Gates et al., 1979). With these types of metals, cleavage of the hydrocarbon

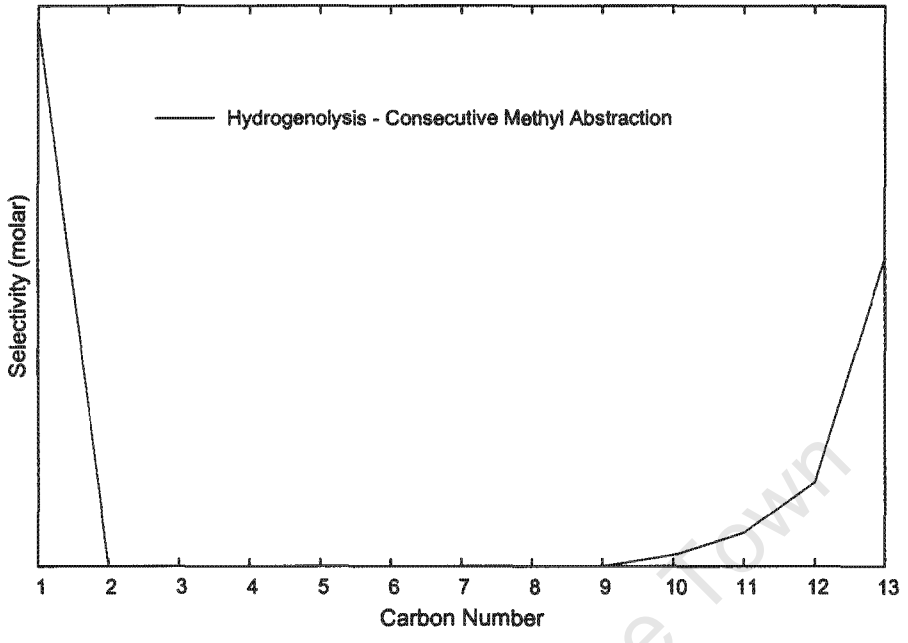

Figure 1.14: Theoretical Product Carbon Number Distribution for Consecutive Methyl-Abstraction Type Hydrogenolysis of n-C_{14} Paraffin over Palladium and Rhodium Metal Catalysts as well as Nickel, Cobalt and Iron Catalysts

chain predominantly occurs at the terminal carbon atom producing equimolar quantities of methane and the corresponding higher alkyl species (Sinfelt, 1973). The higher alkyl species can either be hydrogenated and desorb from the metal catalyst or can undergo further demethylation to produce more methane as well as tail ends from the carbon number distribution obtained from the methyl abstraction mechanism (figures 1.13 and 1.14).

The order of methanolysis activity and selectivity increases from iron to cobalt to nickel. Where with iron catalysts, C_2 fragments are readily formed as compared to the negligible amounts observed in the presence of nickel and cobalt catalysts (Sinfelt, 1973).

1.4.2.3 Hydrogenolysis over Sulphided Group VIA/VIIIA Metal Catalysts

Sulphided catalysts of the CoMo, NiMo and NiW type play an enormous role in petroleum refining with almost every product stream having been treated over such type of catalysts. A comprehensive review of the application of such catalysts has been given by Topsøe et al. (1996). Specific investigations into mild hydrocracking over these catalysts has been discussed in the foregoing sections.

Mechanistic studies were focussed on heterocompound conversion i.e. hydrodesulphurisation, hydrodenitrogenation and, to some extent, hydrodeoxygenation, with more papers suggesting hydrogenolysis mechanisms via adsorbed radicals (Topsøe et al., 1996; Schulz et al., 1987; Schulz and Rahman, 1993) corresponding to what is termed as the 'non-selective' hydrogenolysis mechanism in this work.

1.4.2.4 Hydrogenolysis over Non-Sulphided (Oxidic) Group VIA/VIIIA Metal Catalysts

Little work has been published on hydrotreating / hydrocracking reactions over the typical refining catalysts in their non-sulphided (oxidic) form. However, no fundamental differences have been observed between the sulphided and the non-sulphided form of such catalysts, e.g. in hydrodenitrogenation reactions over sulphided and oxidic NiW/Al_2O_3 and the distribution of the resulting hydrocarbons (Schulz and Eichhorn, 1981; Eichhorn, 1979).

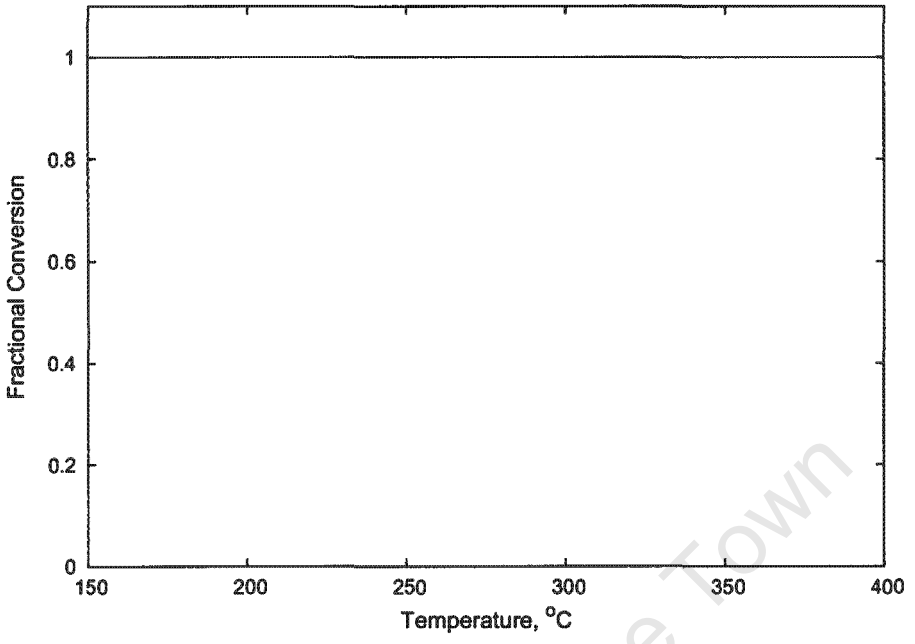

Figure 1.15: Effect of Temperature on Hydrocracking Equilibrium Conversion ($n{-}C_{14} + H_2 \rightleftharpoons 2\ n{-}C_7$)
(For data see Appendix B)

1.5 Thermodynamics

Only the overall reaction scheme was considered for thermodynamic evaluation of the hydrocracking of n-paraffins. The following reaction was taken as an example:

$$n{-}C_{14} + H_2 \rightleftharpoons 2\ n{-}C_7 \tag{1.1}$$

$$\Delta G^o_R = 2\,\Delta G^o_{f,n-C_7} - \Delta G^o_{f,n-C_{14}} \tag{1.2}$$

$$K = \frac{P^2_{C_7}}{P_{C_{14}} \cdot P_{H_2}} \tag{1.3}$$

From the above reaction scheme it was found that the overall hydrocracking reaction is moderately exothermic ($\Delta H_{rxn,298K}$= -44.0 kJ/mol). At standard conditions (298K) the

Gibbs free energy of reaction and the equilibrium constant is $\Delta G_{rxn,298K}$ = -49.7 kJ/mol and K = 5.1 $\times 10^8$ respectively (thermodynamic data from Daubert and Danner, 1989 and calculation based on Sandler, 1989). Note that the reaction (1.1) is equimolar, i.e. independent of pressure.

If the Gibbs free energy is less than zero and the equilibrium constant is greater than one, at equilibrium the partial pressure of products exceeds that of the reactants. This means that products are favoured at equilibrium (Atkins, 1994). Le Chatelier's principle, on the other hand, states that a system at equilibrium will respond to a disturbance to counter or minimise the disturbance. Therefore, in this case, an increase in the system temperature will favour products due to the exothermic nature of the reaction.

$$X = \sqrt{\frac{1}{1+\frac{4}{K}}} \tag{1.4}$$

When evaluating the effect of temperature on equilibrium conversion from the thermodynamic data, it is noted that total conversion is effectively achieved (e.g. >99 mol% at 350°C for n-C_{14} + H_2 $\rightleftharpoons$ 2 n-C_7 at 1/1 molar feed ratio) and remains essentially unaffected by a change in temperature over the range to be considered for hydrocracking paraffins (see data in Appendix B). Under typical hydrocracking conditions, i.e. H_2/n-C_{14} molar ratio >> 1, equilibrium conversion will be higher. Hydrocracking is effectively not thermodynamically limited (figure 1.15).

1.6 Hydrocracking of Fischer-Tropsch Wax

1.6.1 Gas-to-Liquids via Fischer-Tropsch Synthesis - A Brief Overview

The classic Fischer-Tropsch process converts synthesis gas in a typical H_2/CO molar ratio of approximately two to marketable liquid transportation fuels with light gas and wax (long chain hydrocarbons) as by-products (Eilers et al., 1990; Corke, 1998; Shah et al., 1988). The main steps in this process are illustrated in figure 1.16. In gas-to-liquids (GTL) mode, the feed is natural gas. Syngas manufacture is via steam reforming or partial oxidation and the F-T process is operated at maximum wax selectivity. This wax is selectively hydrocracked to maximum middle distillates.

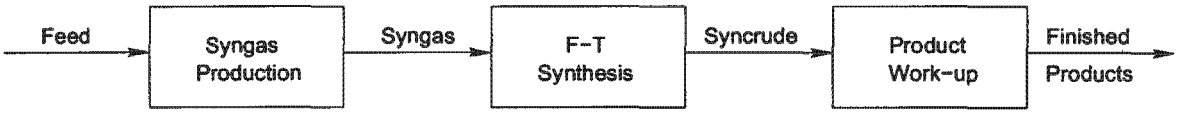

Figure 1.16: Process of Converting Natural Gas to Marketable Liquid Hydrocarbons (Corke, 1998)

Sulphur, a catalyst poison in the Fischer-Tropsch reaction and also an environmental pollutant, is first removed from the natural gas prior to syngas production. Established high temperature and high pressure syngas production processes include (Corke, 1998):

1. Steam reforming
   Reactants: Steam and natural gas
   Operating temperature: 800 - 900°C
   Operating pressure: ca. 20 bar
   Catalyst: Nickel
   Reactions:
   $CH_4 + H_2O \rightleftharpoons CO + 3H_2$
   $CO + H_2O \rightleftharpoons CO_2 + H_2$
   Products: Mixture of hydrogen, carbon oxide and carbon dioxide
   Characteristics: High hydrogen to carbon oxide molar ratio
   Application in GTL: Low H/C natural gases e.g. with high CO_2 content

2. Partial oxidation
   Reactants: Natural gas and air or pure oxygen
   Operating temperature: 1200 - 1500°C
   Operating pressure: 140 bar or higher
   Catalyst: none
   Reaction:
   $2\,CH_4 + O_2 \rightleftharpoons 2\,CO + 4\,H_2$
   Products: Mixture of hydrogen and carbon monoxide
   Characteristics: Near ideal (2:1) hydrogen to carbon oxide molar ratio for F-T synthesis
   Application in GTL: Methane rich natural gas with low CO_2 content

3. Autothermal Reforming
   Reactants: natural gas, steam and oxygen
   Autothermal reforming is a hybrid system where partial oxidation precedes steam reforming in a single reactor vessel
   Characteristics: Syngas composition is controlled by combination of feed streams in order to obtain ideal hydrogen to carbon oxide ratios (Eilers et al., 1990)

In Fischer-Tropsch synthesis the syngas is converted to longer chain hydrocarbons, typically paraffinic and olefinic in nature, over iron and cobalt catalysts. The Fischer-Tropsch process typically occurs at temperatures ranging between 200 - 340°C and pressures between 10 - 40 bar (Corke, 1998; Dry, 1996). Iron catalysts are utilised in both high temperature Fischer-Tropsch synthesis producing short chain olefins and low temperature Fischer-Tropsch synthesis producing longer chain olefins and paraffins, while cobalt catalysts are used in low temperature synthesis, producing essentially long chain paraffinic hydrocarbons. The reaction that takes place is (Dry, 2004):

$$CO + 2\,H_2 \rightarrow (CH_2) + H_2O$$

or

$$n\,CO + 2n\,H_2 \rightarrow n\,(CH_2) + n\,H_2O$$

Products, as previously mentioned, are predominantly n-paraffins (including a heavy paraffinic wax) and α-olefins. By-products are iso-paraffins and internal olefins as well as small quantities of oxygenates (Dry, 1996; Shah et al., 1988; Eilers et al., 1990). Depending on the Fischer-Tropsch reactor configuration and operating conditions used, the yield and product characteristics may vary (Dry, 1996; Shah et al., 1988). Typical Fischer-Tropsch product distributions for fixed bed and entrained bed (Synthol) reactors are given in table 1.2. In table 1.3 the composition of wax from four commercial production or pilot plants are characterised.

Products from the Fischer-Tropsch synthesis can undergo various work-up steps such as mild hydrocracking of the wax. Mild hydrocracking reduces the boiling range of the heavy Fischer-Tropsch product yielding high quality jet fuel and diesel fuel with diesel fuel having improved cold flow properties compared to straight run Fischer-Tropsch diesel, and cetane numbers up to 75 (Dry, 2001; Shah et al., 1988).

Table 1.2: Fischer-Tropsch Product Distributions (Shah et al., 1988)

Product	wt%	
	Fixed-Bed Reactor	Entrained Bed (Synthol) Reactor
C_{4-}	13.3	43
C_5-C_{11} (Gasoline)	18	40
C_{12}-C_{18} (Diesel)	14	7
C_{19+} (Wax)	52	4
Water Soluble Chemicals	2.7	6

Table 1.3: Composition of Raw Fischer-Tropsch Waxes of Different Origin (Shah et al., 1988)

Compound Type	Arge Wax	Air Products	Union Carbide	Mobil
	wt%			
Paraffins	88.0	89.7	90.5	64.6
Mono-olefins	5.6	7.0	6.2	23.2
Diolefins	0.1	0.2	0.1	1.4
Monoaromatics	0.3	0.2	0.5	0.8
Oxygenates	6.0	2.9	2.7	10.0
	% Branched Molecules			
	2.3	44.0	13.0	31.0
	Average Carbon Number			
	43	26	29	48

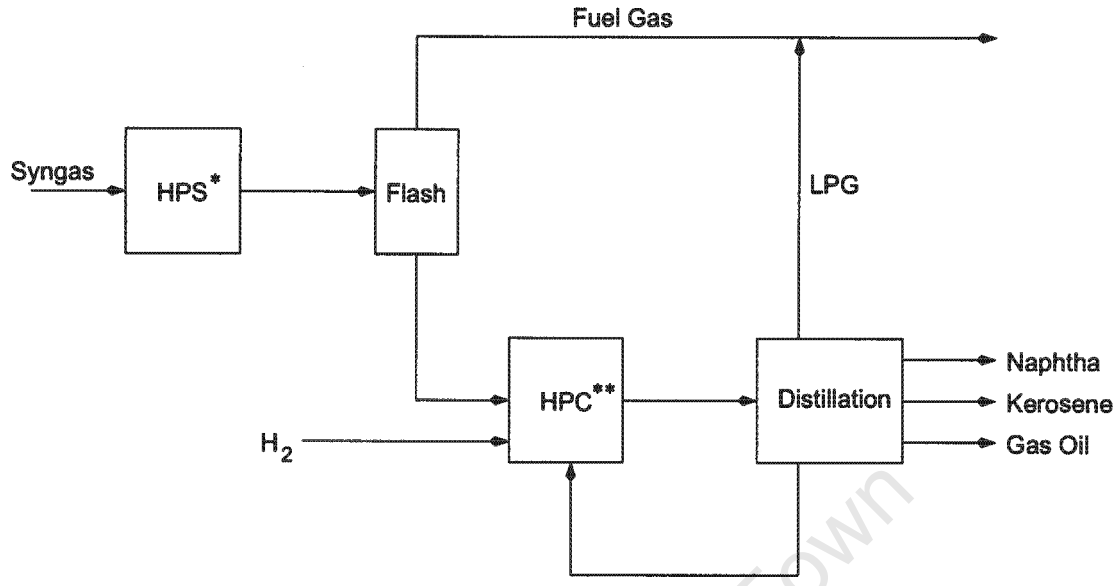

Figure 1.17: Shell Middle Distillate Synthesis (SMDS) Process (Sie et al., 1991)
*Heavy Paraffin Synthesis (Fischer-Tropsch Reactor)
**Heavy Paraffin Conversion (Hydrocracker)

1.6.2 SMDS Process

The Shell Middle Distillate Synthesis (SMDS) process converts synthesis gas preferentially into middle distillates in a two-stage process (figure 1.17, Sie et al., 1991).

The first stage of the SMDS process is a low temperature Fischer-Tropsch synthesis, termed 'Heavy Paraffin Synthesis (HPS)'. This process is directed towards producing high yields of heavy paraffins or wax in order to limit formation of light gases and products in the gasoline range. This is achieved by operating the process with a chain growth probability above 0.90 (Sie et al., 1991; Eilers et al., 1990).

The second stage of the SMDS process is the mild hydrocracking of the Fischer-Tropsch product, in a stage termed 'Heavy Paraffin Conversion (HPC)'. In a trickle-flow hydrocracker, operated under mild conditions, the Fischer-Tropsch products are selectivitely converted to products in the middle distillate range using a non-disclosed type of catalyst at a temperature and a pressure in the range of 300 - 350°C and 30 - 50 bar, respectively (Sie et al., 1991; Eilers et al., 1990).

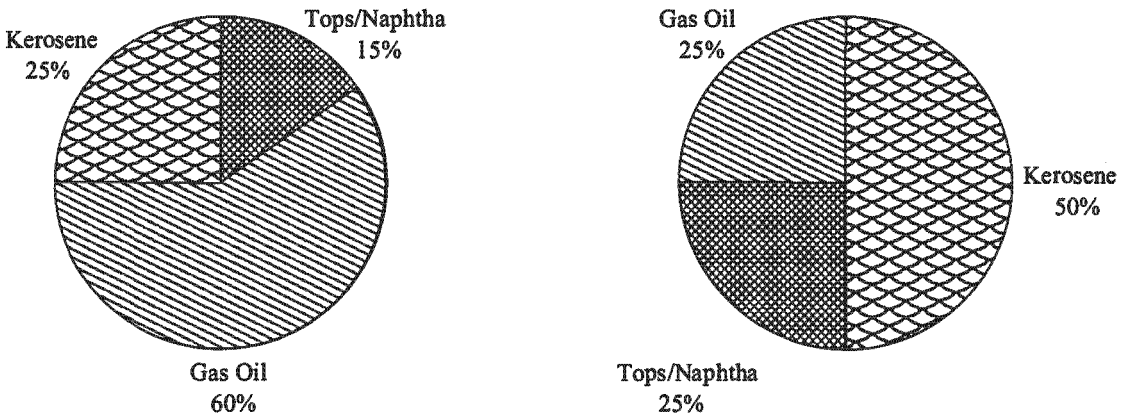

(a) Gas Oil (Diesel) Mode (b) Kerosene (Jet Fuel) Mode

Figure 1.18: Variable Product Yields From SMDS Process (Sie et al., 1991)

Tasks performed by the hydrocracker include (Sie et al., 1991; Eilers et al., 1990):

- hydrogenation of the olefins in the Fischer-Tropsch product
- removal of the small amounts of oxygenates in the Fischer-Tropsch product, mainly primary alcohols
- hydroisomerisation
- hydrocracking to isoparaffins of the desired carbon number or boiling range

Fractionation follows the hydrocracking stage where the fraction boiling above the gas oil range is recycled to the hydrocracker. Manipulation of the single-pass conversion ensures selectivity towards the desired product range, kerosene (jet fuel) or gas oil (diesel), making the SMDS process flexible (figure 1.18).

1.6.3 Process Variables

Hydrocracking is a very flexible process which may utilise a range of feedstocks and produce a wide range of products, such as, liquified petroleum gas (LPG), naphtha and middle distillates, to name a few (Scherzer and Gruia, 1996). The resulting products generally have a very low level of sulphur and nitrogen (compared to the respective crude oil derived feedstocks) and olefins.

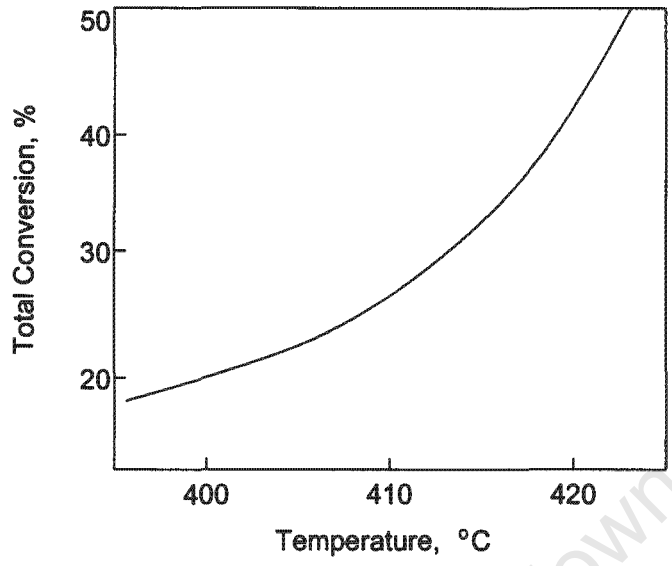

Figure 1.19: Effect of Temperature on Conversion in Mild Hydrocracking Operation (Weismantel, 1992; Scherzer and Gruia, 1996)

The type of feedstock, process configuration, catalyst(s) and process variables such as temperature, hydrogen partial pressure and space velocity influence the yield and quality of the resulting products, where reaction severity is often reflected by temperature and hydrogen partial pressure. Generally, to produce a high boiling range product, e.g. diesel, the severity of the process is reduced (Scherzer and Gruia, 1996; Sie et al., 1991).

1.6.3.1 Temperature

An increase in reaction temperature results in an increase in feedstock conversion (figure 1.19) and light gas yields (which is indicative of enhanced secondary cracking). Alternatively, if the temperature is decreased, the conversion is decreased, also resulting in a higher yield of heavier products.

Temperature is often increased with time-on-stream to counter catalyst activity loss (due to coking at prolonged time-on-stream), and to maintain the overall conversion and product yield.

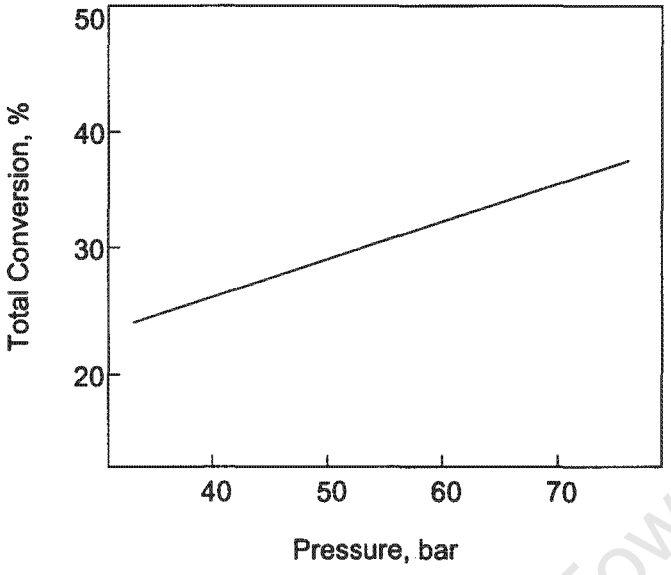

Figure 1.20: Effect of Pressure on Conversion in Mild Hydrocracking Operation (Weismantel, 1992; Scherzer and Gruia, 1996)

1.6.3.2 Hydrogen Partial Pressure

The degree of hydrogenation of unsaturated compounds and the hydrocarbon cracking conversion is closely related to the hydrogen partial pressure (Scherzer and Gruia, 1996), see figure 1.20.

Depending on the type of feedstock, an increase in hydrogen partial pressure can have two effects:

- An increase in the rate of hydrogenation of unsaturated products, and
- A decrease in the rate of isomerisation and cracking reactions.

With highly aromatic feedstocks, the increasing hydrogenation effect is dominating, if the feedstock is highly paraffinic the decreasing isomerisation/cracking effect tends to dominate (Scherzer and Gruia, 1996; Dufresne et al., 1987).

Increased hydrogen partial pressure also has the advantage of reducing coke precursors and cleaning the catalyst surface (Scherzer and Gruia, 1996; Shah et al., 1988).

Shah et al. (1988) found that a decrease in hydrogen partial pressure accelerated the rate of olefin formation.

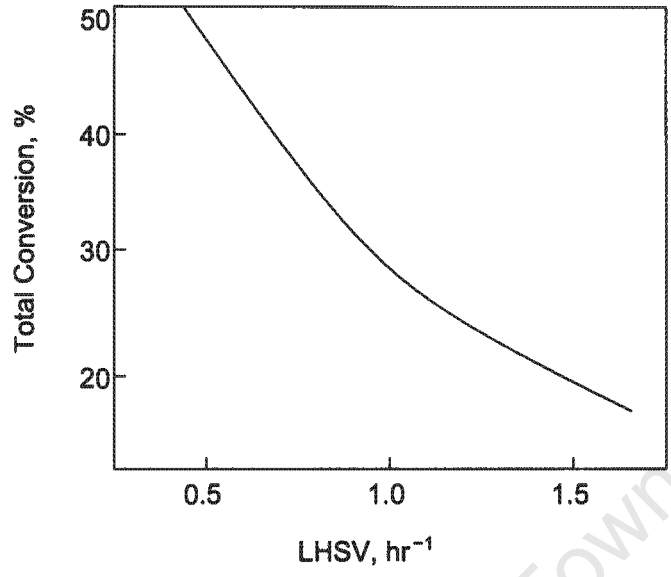

Figure 1.21: Effect of Space Velocity on Conversion in Mild Hydrocracking Operation (Weismantel, 1992; Scherzer and Gruia, 1996)

1.6.3.3 Liquid Hourly Space Velocity (LHSV)

Liquid hourly space velocity (LHSV), by definition, measures the total liquid throughput per unit volume of catalyst, therefore any adjustment in LHSV will affect the temperature requirements (to maintain constant conversion) and product distribution (Shah et al., 1988). For any given catalyst the overall conversion will decrease with an increase in space velocity while keeping all other process variables constant (figure 1.21).

1.6.4 Conclusions from Fischer-Topsch Wax Hydrocracking

Shah et al. (1988) were able to propose possible operating conditions for the hydrocracking of Arge F-T wax that would maximise distillate yield. Their findings were as follows:

- Greater distillate yields are achieved when operating at pressures lower than ca. 70 bar (range ca. 35-70 bar).
- More distillates are achieved with higher hydrogen gas rates.
- An operating scheme with a recycle of the heavy fraction boiling above the distillate range tends to give higher distillate yields than a single-stage once-through operation.

1.7 Catalysts

Bi-functional hydrocracking catalysts consist of constituents that provide acid and metal sites which allow for hydrocracking, hydroisomerisation and hydrocyclisation reactions to occur (Sie et al., 1991; Scherzer and Gruia, 1996; Maxwell, 1987; Dufresne et al., 1987; Sinfelt, 1973).

The acid sites provide the cracking, isomerisation and cyclisation function of the catalyst. The acid component may consist of either (Scherzer and Gruia, 1996):

- Amorphous mixed oxides e.g. silica-alumina,
- Zeolites - most common of which is zeolite Y, or
- Mixtures of zeolite and amorphous oxides.

Generally, amorphous mixed oxides are being replaced by zeolites which tend to be more selective (Thompson and Mathews, 1989).

The metal sites of the bi-functional hydrocracking catalyst provide the hydrogenation and dehydrogenation function. This component may consist of (Scherzer and Gruia, 1996; Maxwell, 1987):

- noble metals - e.g. platinum and palladium, or
- non-noble transition metal combinations - metals of group VIA and group VIIIA in sulphided form e.g. nickel or cobalt combined with tungsten or molybdenum.

Amorphous supports, usually silica-alumina, are mostly used in combination with non-noble metals of group VIA and VIIIA in sulphided form (Maxwell, 1987; Dufresne et al., 1987; Scherzer and Gruia, 1996).

The metal or metal sulphide function of the catalyst initiates the first step in the hydrocracking mechanism by dehydrogenation to make the feedstock more reactive for cracking (Sie et al., 1991; Scherzer and Gruia, 1996), i.e. produce olefins that are reactive over the acid function.

Depending on the activity and selectivity required by the hydrocracking process, the hydrogenation and cracking functions are 'balanced' by fine tuning the metal to acid

ratio. This 'balancing' determines the degree of secondary cracking and that way the selectivity to middle distillates and gasoline, respectively. It is generally observed that noble metal and zeolite combinations have the strongest affinity towards hydrogenation and cracking activity, respectively, while non-noble metal combinations and alumina are weaker than the aforementioned (Maxwell, 1987; Scherzer and Gruia, 1996).

Although the amorphous acid function of hydrocracking catalysts is often replaced by crystalline zeolites, amorphous supports are still widely used. Amorphous supports are mostly utilised in processes where middle distillates or lube oil blending stock is the desired product. This is a mild hydrocracking process where the catalyst is similar in composition to hydrotreating catalysts (Dufresne et al., 1987) see also sections 1.3.1.1 and 1.3.1.2.

1.7.1 Zeolites

Zeolites have ion exchange, sorption, catalytic and molecular sieve properties and are crystalline aluminosilicates (Scherzer and Gruia, 1996).

Acid zeolites are considered to have a more severe acid / cracking function than their amorphous counter-parts and are said to have the following advantages over amorphous catalysts (Scherzer and Gruia, 1996; Marcilly and Franck, 1980):

1. Greater cracking activity due to the higher acidity
2. Better thermal/hydrothermal stability
3. Better resistance to nitrogen and sulphur compounds
4. Lower coking tendency
5. Easier regenerability

Usually, zeolite based hydrocracking catalysts have a higher naphtha selectivity.

Heavy crude oil derived feedstocks (carbon numbers above 25) comprise of constituents that do not enter zeolite pores due to steric hindrance (Scherzer and Gruia, 1996). This phenomenon was also observed by Muñoz Arroyo et al. (2000) when studying the hydroconversion of a mixture of n-paraffins (that were cracked) and of a hydrotreated gas oil (that was not cracked) over Pt loaded medium pore shape selective zeolite, ZSM-22.

Zeolites commonly used in hydrocracking are zeolite Y (or any modified form thereof e.g. ultrastabilised), mordenite, ZSM-5 and beta to name a few (Scherzer and Gruia, 1996).

1.7.2 Metals

The hydrogenation and dehydrogenation function is provided by the metal or metal sulphide in bi-functional hydrocracking catalysts.

Noble metals tend to have higher hydrogenation activity than sulphided non-noble transition metals. The hydrogenation/dehydrogenation activity of these catalyst constituents decreases in the following order (Scherzer and Gruia, 1996; Maxwell, 1987; Franck and Le Page, 1981):

$$noble\,metal > sulphided\,transition\,metals >> sulphided\,noble\,metals$$

From the above order, it can be seen that the presence of sulphur drastically reduces the activity of noble metal catalysts. Therefore, these catalysts are often used downstream of a hydrotreating process where the majority of the sulphur (in the form of H_2S) has been removed from the feedstock. Feedstocks which have very high concentrations of sulphur containing compounds employ non-noble transition metal catalysts in sulphided form due to their high resistance to sulphur poisoning (Maxwell, 1987; Scherzer and Gruia, 1996; Dufresne et al., 1987; Maxwell, 1987).

The 'balance' between the hydrogenation and acid functions of the hydrocracking catalyst is important when considering the product selectivity that needs to be achieved. If a very high metal to acid ratio is present, hydrogenolysis reactions may predominate (Sinfelt, 1973).

2 Objective

Due to the increasing constraints enforced by legislation in terms of cleaner fuels, there is a growing demand for processes which are able to produce fuels that meet these specifications. Therefore, hydrocracked Fischer-Tropsch wax appears to hold the answer. Fischer-Tropsch wax is composed of predominantly long chain linear paraffins. It is practically free of heteroatoms, sulphur and nitrogen. The aim was, therefore, to develop a method whereby the wax could be hydrocracked over a non-sulphided hydrocracking catalyst i.e. without the introduction of sulphur to an already sulphur-free feedstock.

The objective of this study was to determine the suitability of a conventional bi-functional catalyst $CoMo/SiO_2$-Al_2O_3, in unsulphided form, to the hydrocracking of Fischer-Tropsch wax.

As a model compound, n-tetradecane was used since the same information about the hydrocracking trends and hence the catalyst performance can be extracted from the experimental results irrespective of the chain length of the linear paraffin used as long as it is not too short.

It is important to note that this study is the first undertaking by the Catalysis Research Unit at the University of Cape Town in the field of hydrocracking and therefore focuses predominantly on screening the effects of the process conditions on the hydrocracking trends and on the mechanisms that should be considered when interpretating the results.

Experimental 3

3.1 Experimental Apparatus

A diagrammatic flowsheet of the apparatus designed, constructed and used for experimentation is presented in figure 3.1. The apparatus consists of a trickle bed reactor followed by a vapouriser, which is used to ensure that all downstream products from the reactor are in the vapour phase before going to on-line gas chromatographic analysis. Inert gas is introduced between the reactor and the vapouriser for both pressure control and dilution of the reactor effluent. Vapourised products pass through a throttle system prior to sampling via a 6-port valve.

A description of all major components as well as a summary of the operation of sensitive areas in the system follows.

3.1.1 Feed Supply

Liquid n-C_{14} is fed by a metering pump (Hewlett Packard 1100 Series HPLC pump) with the feed pot sitting on a balance. Hydrogen is fed via thermal mass flow controllers (Brooks Instruments) with flow ranges of 0-20 and 0-100 sccm depending on the applied conditions. Gaseous feed streams pass through a guard catch pot (100 ml), the purpose of which is to prevent the mass flow controllers from contamination with liquid feed in the event of downstream blockage of the apparatus.

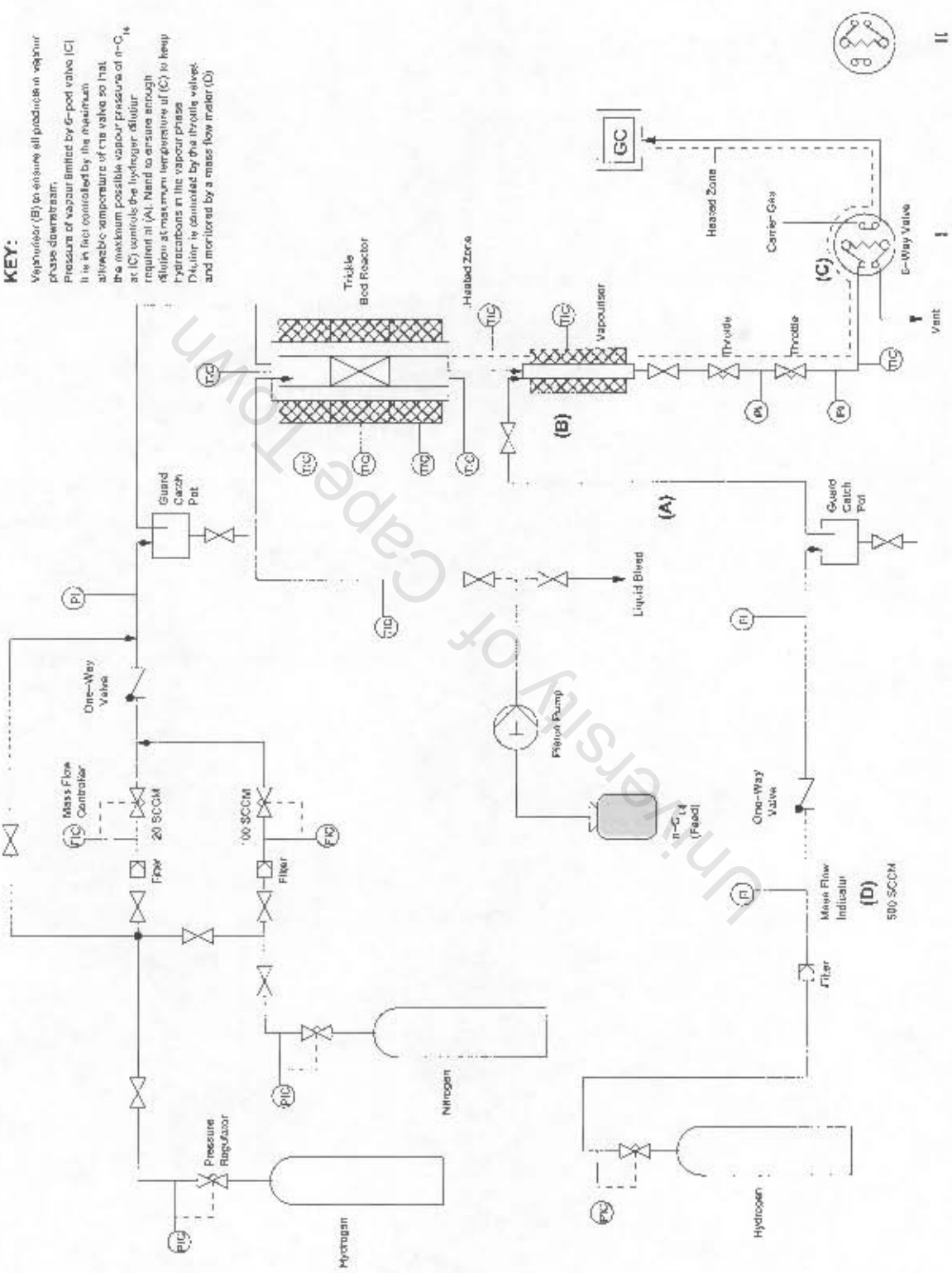

Figure 3.1: Experimental Setup

3.1.2 Trickle Bed Reactor

The trickle bed reactor (figure 3.2) consists of a stainless steel cylinder with an internal diameter of approximately 20 mm and 350 mm in length. In the centre of the reactor tube is a thermowell of approximately 3 mm outer diameter, which runs through the whole length of the reactor.

The reactor is concentrically enclosed by a wider stainless steel jacket (internal diameter approximately 23 mm). The jacket makes provision for the feed inlet line (n-tetradecane) and the hydrogen feed gas line. The jacket is surrounded by three heating coils over the top, mid and bottom sections, having lengths of 80, 160 and 80 mm respectively. These heating coils ensure that maximum heat transfer is achieved and that the reactor operates under isothermal conditions. The reactor has been found to be isothermal down the entire length of the catalyst bed (Appendix C).

The packed reactor volume comprises of three zones (figure 3.2):

- An inert silicon carbide pre-heating and (partial) evaporation zone that also evens out the flow pattern (top)
- A diluted catalyst zone (middle)
- An inert silicon carbide support zone for the catalyst bed (bottom)

The diluted catalyst zone is made up of 3 g catalyst extrudates (3 cm^3), in oxidic form, diluted in 6 cm^3 of inert silicon carbide, 0.8 mm, making a 2:1 (silicon carbide:catalyst) dilution ratio, on a volume basis and yielding an effective bed length of approximately 4 cm in the reactor. The pre-heating and support zones (above and below the catalyst bed) are composed of 35 cm^3 inert silicon carbide each. Dilution of the catalyst bed with inert silicon carbide serves to limit any temperature and radial concentration gradients within the bed.

3.1.3 Vapouriser

The function of the vapouriser is to ensure that all products from the trickle bed reactor are in the vapour phase before going to on-line gas chromatographic analysis. It is similar

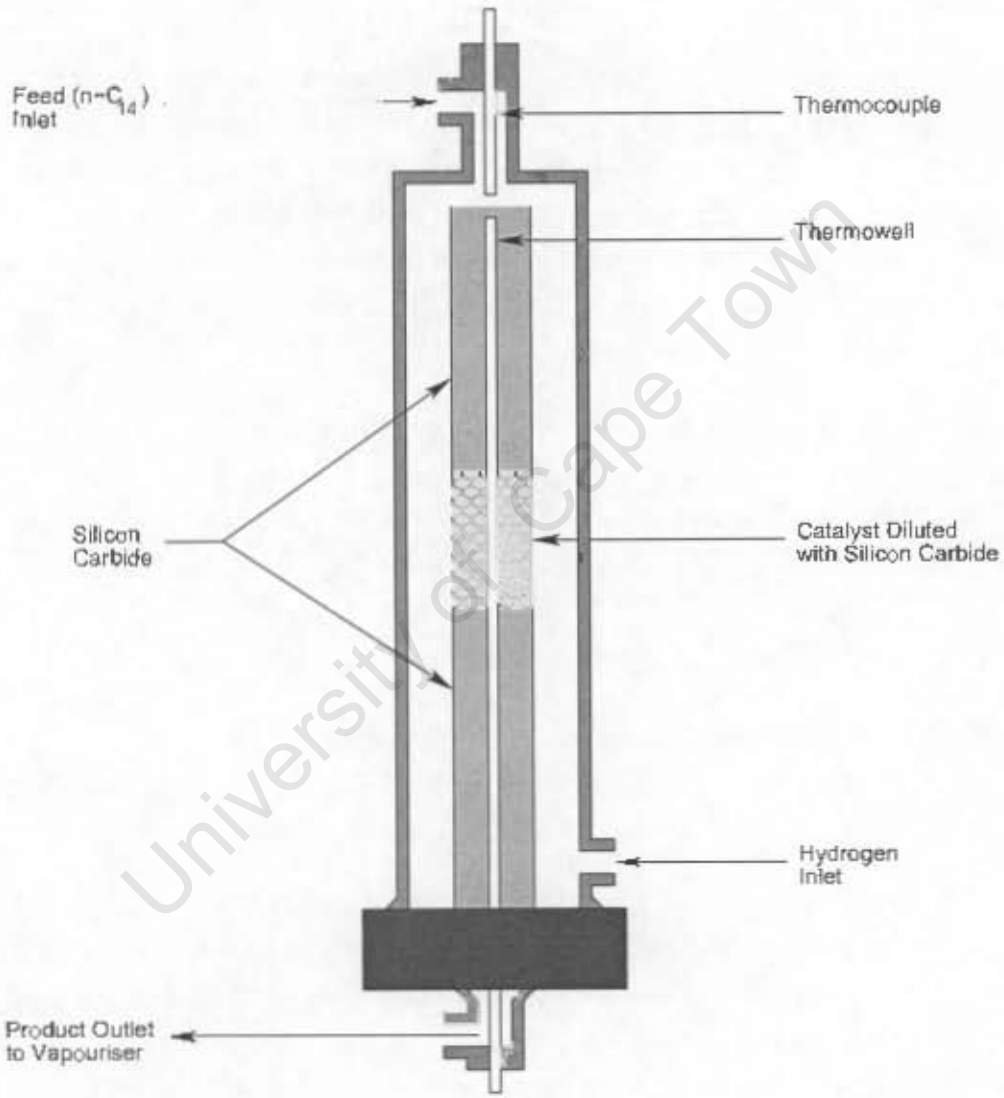

Figure 3.2: Schematic Sectional Drawing of the Trickle Bed Reactor

3.2 Experimental Operating Conditions

For the purpose of understanding the mechanism behind the hydrocracking of wax, a model compound, n-tetradecane (n-C_{14}) was used as a feed compound for experimentation. The reason and validity of using n-C_{14} as the model compound was discussed in chapter 2.

3.2.1 Catalyst

The concept of wax hydrocracking is fairly new with no commercially recognised or 'standard' catalyst being employed. Therefore, for these initial studies, a commercial "distillate hydrocracking catalyst" [1] was employed, comprising of cobalt and molybdenum oxides on an amorphous silica-alumina support, provided by Albemarle Catalysts (previously Akzo-Nobel Catalysts). The catalyst was in the form of 1/16" extrudates of ca. 5 mm length. 3 g of catalyst was loaded in the form obtained and diluted with silicon carbide (see section 3.1.2).

In contrast to applications in hydrocracking petroleum fractions, the catalyst was applied in unsulphided form.

Conditions such as reaction temperature, pressure, liquid hourly space velocity (LHSV) and hydrogen to feed (H_2/n-C_{14}) ratio were used to investigate the suitability of this catalyst in terms of wax hydrocracking, such that future investigations into catalyst performance can be compared.

3.2.2 Reaction Temperature

Experiments to determine the effect of reaction temperature on the hydrocracking conversion and selectivity ranged from 300°C to 350°C in 10°C increments. Initial experiments were conducted at 350°C with a low liquid hourly space velocity of 0.2 ml/(ml·h), high total system pressure, 80 bar, and high H_2/n-C_{14} molar ratio, 116:1.

Due to the high overall C_{14} conversion observed at 350°C (see section 4.3), subsequent runs were conducted at the lower end of the temperature range (300°C) and then incrementally increased by 10°C until the temperature was again returned to the other extreme, 350°C.

[1] A catalyst that is optimised for maximum distillate (i.e. diesel and jet fuel) selectivity from hydrocracking heavier crude oil derived feedstock in a sulphur containing environment.

is fed via a pressure controller and mass flow meter. The flow rate of the pressure regulating/dilution gas stream is controlled by the throttle valves in the product line, see section 3.1.3.1. Delivery hydrogen pressure to the mass flow controller upstream the reactor that is controlling the feed hydrogen flow is set approximately 5 bar above the reaction pressure.

3.1.5 6-Port Valve

Sampling required for gas chromatographic analysis occurs via a 6-port valve (with a 1.25 cm^3 sample loop, (C) in figure 3.1). This valve has a maximum allowable temperature of 175°C and was operated at 150°C, which is the basis for all dilution calculations and the bottom/outlet temperature of the vapouriser. The sample loop is charged in position I and the sample is introduced in the carrier gas stream to the gas chromatograph in position II.

3.1.6 Throttle System

For on-line gas chromatographic analysis, samples need to be taken at or slightly above atmospheric pressure. For this reason a two stage throttle system was employed to reduce the system pressure to atmospheric.

The system pressure is reduced progressively in stages. The pressure is first reduced, for example from 80 bar to 8 bar, through the first throttle valve, then further lowered via the second throttle valve to 1 bar prior to the sampling loop. This method of pressure reduction is flexible. The positioning of the throttle valves depends on the reaction conversion, feed space velocity, H_2/n-C_{14} ratio and, most importantly, the dilution gas requirement. It was found by trial and error, that if the reaction temperature was low (i.e. below 350°C) or a high space velocity was employed, the 10:1 pressure reduction in the first throttle valve did not allow for sufficient dilution. Therefore adjustments to the two stage pressure reduction system had to be altered accordingly, where sometimes the system pressure could only be reduced to a minimum of 4 bar upstream of the sample loop.

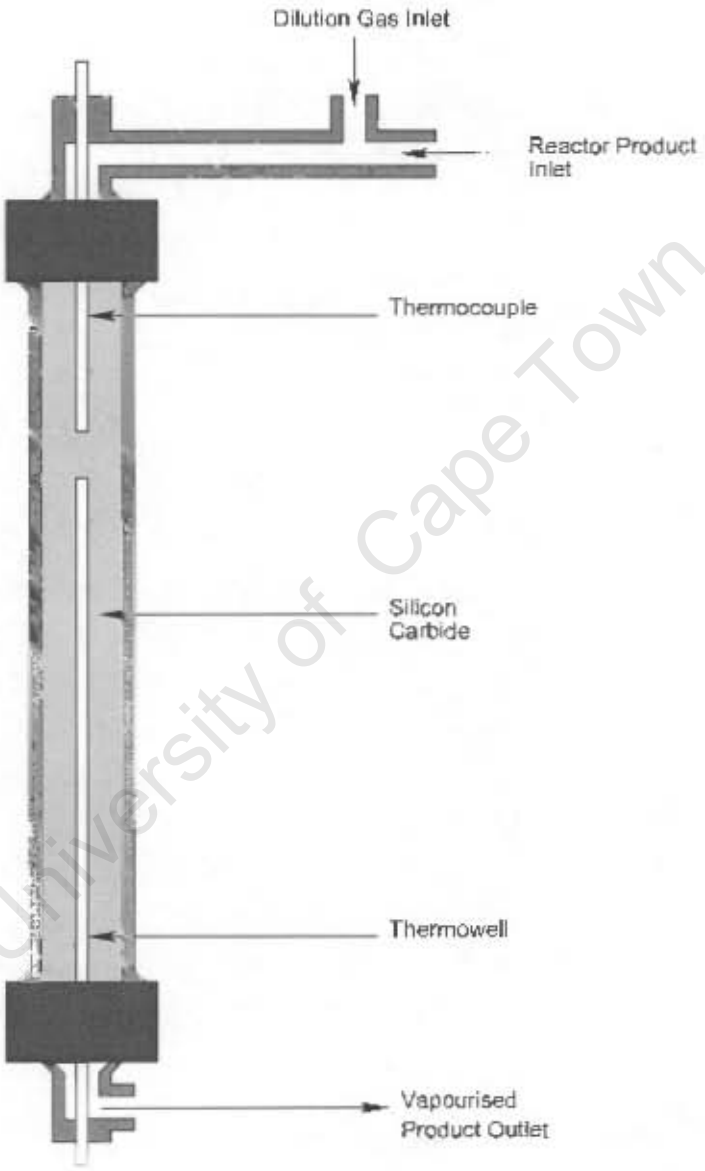

Figure 3.3: Schematic Sectional Drawing of the Vapouriser

in construction to the reactor, having an internal diameter of 16 mm and a length of 350 mm packed with inert silicon carbide, 0.8 mm (figure 3.3).

The vapouriser is heated by means of a heating tape which is tightly wrapped around the length of the cylinder. Heating is concentrated at the base of the vapouriser to produce a temperature gradient, and that way ensure smooth but complete vapourisation of any liquid products from the reactor. The silicon carbide helps in retarding the flow of the liquid products through the cylinder thus increasing radial heat transfer, increasing the gas/liquid interface and maximising the vapourisation rate.

A further function of the vapouriser is to act as a dilution vessel. Dilution is achieved by means of hydrogen fed between the reactor and the vapouriser (stream labeled (A) in figure 3.1). In that way the vapour pressure of the products is lowered so as to meet the temperature limitation of the 6-port gas sampling valve (175°C; see '*KEY*' in figure 3.1).

3.1.3.1 Dilution

The dilution of products in the vapouriser is monitored by means of a mass flow indicator, (D) in figure 3.1. The mass flow indicator is actually a 0-500 sccm mass flow controller with a set point of 100%. The flow through the indicator varies according to the dilution required to reduce the vapour pressure according to the maximum allowable temperature of the 6-port valve (see section 3.1.5). The total dilution gas flow is actually controlled by the throttle valves downstream the vapouriser and the flow of hydrogen that is required, in addition to the feed hydrogen, is monitored by the sensor unit of the mass flow controller. Actual minimum dilution gas flow rates are calculated by equation (3.1) in section 3.5.1 and given in Appendix B. Note that too high a dilution ratio and dilution gas flow rate is unfavourable with regard to gas chromatographic analysis.

3.1.4 Pressure Control by Dilution Gas

The hydrogen gas fed between the reactor and the vapouriser (stream labelled (A) in figure 3.1) has a dual function. Firstly, it serves as a dilution gas (see section 3.1.3.1), and secondly it acts to control pressure in the reactor.

Pressure regulation is achieved by setting the pressure of the diluent gas stream fed downstream the reactor to the desired reaction pressure. Note that the diluent gas

All experiments were conducted at the same space velocity, pressure and H_2/n-C_{14} molar ratio of 0.2 ml/(ml·h), 80 bar and 116:1 respectively.

3.2.3 Reaction Pressure

Experiments to determine the effect of reaction pressure on the hydrocracking activity and selectivity were conducted at conditions more typical of industrial hydrocracking.

The H_2/n-C_{14} molar ratio was reduced to 10:1 and the LHSV was increased to 1.3 ml/(ml·h). The reaction pressure was kept at 80 bar. Experiments at 320°C, 330°C and 350°C were conducted at these new conditions. From these experiments, 330°C was chosen as the reference temperature for subsequent pressure variation experiments (inclusive of space velocity and H_2/n-C_{14} ratio experiments, see sections 3.2.4 and 3.2.5), which included investigations at 80 bar, 40 bar and 20 bar at the aforementioned industrial conditions. See Appendix B for dilution gas flow rates.

3.2.4 Space Velocity

Investigations into the effect of liquid hourly space velocity (LHSV) on the cracking reactions were conducted at 1.3 ml/(ml·h), 1.0 ml/(ml·h) and 0.5 ml/(ml·h) at 330°C and 40 bar with a constant H_2/n-C_{14} molar ratio of 10:1 (see Appendix B for dilution gas flow rates).

Attempts to reduce the space velocity to below 0.5 ml/(ml·h) at these conditions proved to be difficult because the desired feed flow rate could not be achieved, therefore these experiments were abandoned. It emerged during data evaluation that the experiment at 0.5 ml/(ml·h), 330°C, 40 bar and H_2/n-C_{14} 10:1 was flawed as well (data points presented in brackets in the results).

3.2.5 H_2/n-C_{14} Molar Ratio

H_2/n-C_{14} ratio experiments were conducted to determine the effect of varying the hydrogen feed flow rate by keeping all other conditions constant, and to establish whether there is any correlation between the H_2/n-C_{14} ratio and the total system pressure (which in effect is essentially made up by the hydrogen partial pressure).

Experiments included investigations at molar H_2/n-C_{14} ratios of 30:1, 10:1 and 3:1 at a liquid hourly space velocity of 0.5 ml/(ml·h), 330°C temperature and 40 bar pressure (see Appendix B).

3.3 Experimental Operating Procedures

3.3.1 Catalyst Loading Procedure

The trickle bed reactor operates in a down-flow orientation. The catalyst loading to the reactor occurs from bottom to top. This entails securing the reactor in an upright position in a bench vice and then sequentially loading the various packed layers with the bottom, support zone for the catalyst bed loaded first.

The first layer of inert 0.8 mm SiC granulate, 35 cm^3, is poured into the reactor by means of a funnel. The quantities of diluent, SiC, and catalyst (2:1 on a volume basis with 3 g of catalyst) are accurately measured, thoroughly mixed with a spatula and then funneled into the reactor as well. Thereafter, the final 35 cm^3 layer of inert SiC, which acts as the pre-heating zone, is packed into the reactor using the same procedure as explained above. After each layer is added to the reactor, the external wall of the reactor wall is gently tapped to ensure the layer is thoroughly compacted.

It is important to note that no silane treated glass wool is used in the reactor packing procedure as a support at the bottom end, as it was found to plug the reactor when a liquid phase is present.

3.3.2 Catalyst Pretreatment and Reduction

The catalyst-loaded reactor is secured into the stainless steel heating jacket and connected to the n-C_{14} and H_2 feed lines and with the outlet line to the vapouriser. Prior to catalyst pretreatment and reduction, a leak test is performed over the entire system. For the leak test, the system is pressurized with nitrogen (N_2) to 80 bar (at approximately 5 bar per minute) and then closed up to monitor the pressure. After the leak test the system is depressurized back to atmospheric pressure by venting the gas into the atmosphere.

3.3.2.1 Catalyst Pretreatment

Catalyst pretreatment occurs under N_2 gas flow (100 ml/min) at atmospheric pressure.

The following procedure is used to pretreat the catalyst:

1. The reactor is first ramped from room temperature to 90°C in a time period of 1.5 hours and held at 90°C for 1 hour.

2. From 90°C, the temperature is ramped to 100°C at a rate of 1°C per minute (i.e. a 10 minute time period) where it is then again kept for 1 hour.

3. Following the same ramp rate as in step 2, the temperature is raised to 110°C and held at this temperature for the same time period. This mild pretreatment is carried out in order to allow any moisture to desorb from the catalyst.

4. The final step in the pretreatment process is to raise the reactor temperature to 350°C in a period of 4 hours (1°C/min).

Once the final temperature is achieved, the system pressure is increased to 80 bar with N_2 gas bypassing the inlet mass flow controllers (see flow sheet, figure 3.1).

3.3.2.2 Catalyst Reduction

After the catalyst pretreatment process and system pressurization to 80 bar at 350°C with N_2, the N_2 is closed off (closing off the bypass line) and H_2 is introduced to the system (at 100 sccm and 80 bar) via the mass flow controllers. The guard catch pot (100 ml) acts as a kind of backmixing device (mean residence time, calculated as a CSTR = 1.3 hours) so that the catalyst is reduced under flowing H_2/N_2 mixture with slowly increasing H_2 concentration for approximately 5 hours.

This reduction step also serves as a 'stabilisation period' in which the system pressure and gas flow rates are constantly monitored and adjusted.

3.3.3 Reactor Operation

3.3.3.1 Start-Up Procedure

After the catalyst pretreatment and reduction steps, the following procedure is used in preparation for the experiment. Within all steps of the start-up procedure the two stage pressure reduction procedure as described in section 3.1.6 is always maintained.

1. Once the system pressure and gas flows have stabilised, the temperature controllers for the heating coils on the reactor heating jacket are set to precisely meet the desired temperature levels and isothermal profile inside the reactor (see Appendix C).
2. Temperatures are allowed to stabilise for 1 hour.
3. Once the temperatures have stabilised, the feed vent valve is opened ('liquid bleed' in figure 3.1) while the feed valve to the reactor is kept closed.
4. The n-C_{14} feed is purged to rid feed lines of any air or other gas.
5. Once the n-C_{14} feed stream is bubble free, the vent valve is closed while simultaneously opening the feed valve, redirecting the n-C_{14} stream to the reactor.
6. The feed line to the reactor is then primed for a few seconds.
7. The pump is then adjusted to the desired feed rate.

3.3.3.2 On-line Operating Procedures

Procedures followed when changing from one condition to another are outlined below for temperature, pressure, space velocity and H_2/n-C_{14} ratio. After each change in conditions, at least 24 hours re-stabilisation period is allowed to elapse prior to any sampling.

All the on-line procedures described below require that the throttle system be adjusted simultaneously for the new conditions as to allow sufficient dilution in the vapouriser and ensure fully vapourised streams through the throttle system and the sample loop (as described in section 3.1.6). See Appendix B for dilution gas flow rates.

Temperature

- Temperatures are ramped at a rate of 2°C per minute when the temperature is changed from a lower to a higher set-point.
- When the temperature is reduced, the lower set-point is set and the reactor is allowed to cool to the desired temperature naturally.

Pressure

- To increase the system pressure, the diluent/pressure control hydrogen (stream (A) in figure 3.1) is set to the desired set-point at a rate of 5 bar per minute. The feed hydrogen pressure on the delivery side of the mass flow controllers is simultaneously increased at the same rate thereby it is always kept at least 5 bar above the pressure of the diluent hydrogen stream as to allow the feed hydrogen to continue flowing freely through the reactor without any impairment of the flow rate or cause of back-flow.
- To reduce the pressure, the system is slowly depressurized to the desired level by venting the gas (through the throttle line in figure 3.1). The pressure on both (feed and diluent) hydrogen gas cylinders is simultaneously reduced to the required set-points maintaining the 5 bar pressure difference on the mass flow controllers.

Space Velocity

- When changing the space velocity, both the hydrogen and the n-C_{14} feed flow rates have to be adjusted accordingly such that the H_2/n-C_{14} ratio remains constant.
- Dilution gas flow rates also have to be adjusted via the throttle valves (see Appendix B for dilution gas flow rates).

H_2/n-C_{14} Ratio

- To change the H_2/n-C_{14} ratio, the n-C_{14} feed rate (i.e. space velocity) is kept constant while the hydrogen feed flow rate and dilution gas flow rate are adjusted.

3.3.3.3 Shut-down Procedure

1. At commencement of system shutdown, the feed pump is first switched off.
2. The hydrogen feed gas is closed off from the system and is replaced by nitrogen through the mass flow controllers, set at 100% flow, at the same pressure.
3. The nitrogen gas and diluent hydrogen are allowed to flow through the system for at least 24 hours to ensure that all remaining remnants of feed/products in the reactor and vapouriser are purged out of the system.
4. After the 24 hour period, the diluent hydrogen is closed off allowing only the nitrogen to continue flowing through.
5. All temperature controllers are switched off at this stage allowing the system to cool down under flowing nitrogen.
6. Once temperatures are down or close to room temperatures, the nitrogen gas is closed off. Remaining nitrogen in the apparatus is allowed to vent out naturally.

3.4 Product Analysis

3.4.1 Gas Chromatography

3.4.1.1 Sampling Procedure

Sampling for gas chromatographic analysis occurs by means of an on-line 6-port gas sampling valve with a sample loop. Diluted, vapourised products leaving the throttle system of the experimental apparatus are passed directly to the gas chromatograph, where they enter the 6-port valve, pass through the sample loop and then are vented out directly into a knock-out pot, which is partially filled with water. Upon sampling, the 6-port valve is switched to position I (figure 3.1) to allow the vapourised product gas pass through the sample loop. It is held in this position for approximately 20 seconds to completely flush and charge the sample loop. Thereafter, the valve is switched to position II (in figure 3.1) so that the carrier gas, H_2, transports the sample to the column.

Due to the diluted nature of the vapourised product gas, a fairly large, 1.25 cm^3, sample loop is required.

Table 3.1: Gas Chromatography Column Properties

Column material	Fused silica
Column phase	BP 1 (non polar, PONA) bonded phase
Column length	50 m
Column internal diameter	0.15 mm
Film thickness	0.2 μm
Maximum column temperature	360°C*
Minimum column temperature	-60°C

* In temperature programmed mode

Table 3.2: Two-Step Gas Chromatographic Temperature Programme and other Gas Chromatographic Conditions

Initial temperature	-30°C* / -50°C**
Hold time	2 min
1^{st} Temperature ramp	10°C/min
Final Temperature	50°C
Hold time	0 min
2^{nd} Temperature ramp	5°C/min
Final Temperature	220°C
Hold time	2 min

*Low conversion samples
**High conversion samples
A typical chromatogram from medium conversion product is shown in Appendix D, figure D.1

3.4.1.2 Gas Chromatographic Conditions

A Varian 3400 Gas Chromatograph (GC) fitted with a Flame Ionisation Detector (FID) in conjunction with a separate Hewlett Packard 3396 Series II integrator/printer, is used to determine the product composition. For start up, column temperatures below ambient temperature are required. For this purpose the GC is fitted with a cryogenic adapter, which utilises liquid carbon dioxide from a dip tube cylinder. The GC is fitted with a non-polar fused silica PONA capillary column having properties as indicated in table 3.1.

Gaseous/vaporous samples are introduced into the GC by means of the on-line 6-port gas sampling valve with 1.25 cm^3 sample loop, as described in section 3.4.1.1. A two-step temperature programme is used to separate the components in the sample, which is given in table 3.2.

From practical use of the gas chromatograph, it was found that at low conversion, if the starting temperature for the gas chromatographic analysis was too low, the GC column

would plug. This was attributed to condensing of unconverted feed in the very first section of the column. For this reason, analysis of low conversion samples was started at -30°C (see table 3.2). Also observed was that at a high conversion, i.e. high concentration of methane in the product, the methane peak was wide and there was insufficient separation of compounds methane and ethane in the chromatogram if the starting temperature was too high. Therefore, as seen in table 3.2, the starting temperature for high conversion samples was -50°C. A typical chromatogram from medium conversion product is shown in Appendix D, figure D.1

3.5 Data Work-Up

3.5.1 Dilution

As previously mentioned, the sampling valve has a maximum allowable temperature of 175°C and was operated at 150°C, which means that all unconverted feed and products passing through the sampling valve need to be in the vapour phase at this limiting temperature. As a precautionary measure, all calculations and settings relating to the dilution were performed for 120°C and 1 bar total pressure. The calculation used for dilution requirements is as follows:

$$H_2\ Dilution\ Gas\ Flow\ Rate = \frac{\dot{n}_{n-C_{14}} \times 22400}{\frac{P_{n-C_{14}}\ @\ 120°C}{P = 1\,bar}} \tag{3.1}$$

Note that the 'H_2 dilution gas flow rate' is made up by the sum of both feed hydrogen flow rate and dilution hydrogen flow rate.

3.5.2 Conversion and Selectivity

From the gas chromatogram data report, the peak areas, A_i, corresponding to the individual hydrocarbon species, i, were divided by the inherent number of carbon atoms, N_{C_i}, in the respective compound to obtain a value that is proportional to the number of moles of each species. This is possible since the signal of the flame ionisation detector

(FID) from hydrocarbons is proportional to the concentration of carbon eluted from the column. Using this method, the molar selectivity of each species was calculated as follows:

$$Molar\ Selectivity,\ S_{C_i} = \frac{n_i}{\sum_{i=1}^{13} n_i} \tag{3.2}$$

Where

$$n_i = \frac{A_i}{N_{C_i}} \tag{3.3}$$

so that

$$S_{C_i} = \frac{A_i}{N_{C_i} \cdot \sum_{i=1}^{13} \frac{A_i}{N_{C_i}}} \tag{3.4}$$

The total conversion of the feed ($X_{C_{14}}$), was calculated as follows:

$$X_{C_{14}} = \frac{\sum_{i=1}^{13} A_i}{\sum_{i=1}^{14} A_i} \tag{3.5}$$

whereby A_{14} includes the feed compound n-C_{14} and its isomers, i.e. all other C_{14} compounds.

To determine the total selectivity of specific product fractions, e.g. light gases methane, ethane and propane (C_1-C_3) the selectivities of the respective gases were summerised. To determine selectivity ratios, e.g. C_4/C_{10}, selectivities were divided.

4 Results

After the design, construction and commisioning of the experimental apparatus, a 3 month conditions screening programme was carried out by hydrocracking n-C_{14} over a commercial $CoMo/SiO_2$-Al_2O_3 catalyst in non-sulphided form (see section 3.2.1).

Hydrocracking reaction conditions were varied for temperature, pressure, liquid hourly space velocity (LHSV) and molar ratio (H_2/n-C_{14}) as specified in section 3.2 and summarised in table 4.1. Steady state conditions for each experiment were based on the reproducibility of feed conversion and product selectivity. Once the reaction had stabilised, conversion and selectivity over the product carbon number range were determined so as to observe the effect of varying these conditions.

All experiments were carried out over the same charge of catalyst. Reproducibility runs showed that there was no deactivation of the catalyst (section 4.2)

All references in this chapter (and subsequent chapters) to the *product*, refer to all products between C_1-C_{13} excluding all C_{14} isomers. Similarly, the *selectivity* of products refers to the selectivity of products in the range C_1-C_{13} excluding all C_{14} isomers. All C_{14} isomers are considered as unconverted feed. Accordingly, *conversion* refers to n-C_{14} and all C_{14} isomers as feed.

Data on carbon number distribution of total paraffins, n-paraffins and iso-paraffins, for all experiments are given in Appendix D, tables D.1 - D.19.

Note that in graphs where *selectivity* is plotted vs. carbon number, *selectivity* comprises the sum of both paraffins and iso-paraffins in the respective carbon number fraction.

Table 4.1: Experimental Programme

(Note that all these experiments were carried out over the *same* charge of catalyst)

Parameter Varied	Temperature °C	Pressure bar	LHSV h^{-1}	H_2/n-C_{14} molar ratio	TOS days	Phase** In	Phase** Out
	350	80	0.2	116	5	Vapour	Vapour
	300	80	0.2	116	8	Vapour	Vapour
	310	80	0.2	116	7	Vapour	Vapour
Temperature	320	80	0.2	116	6	Vapour	Vapour
	330	80	0.2	116	5	Vapour	Vapour
	340	80	0.2	116	5	Vapour	Vapour
	350*	80*	0.2*	116*	3	Vapour	Vapour
	320*	80*	0.2*	116*	11	Vapour	Vapour
	320	80	1.3	10	4	Mixed	Mixed
Screening	350	80	1.3	10	3	Mixed	Vapour
	350	40	1.3	10	2	Vapour	Vapour
	330	80	1.3	10	2	Mixed	Mixed
Pressure	330	40	1.3	10	4	Mixed	Vapour
	330	20	1.3	10	12	Vapour	Vapour
	330*	80*	1.3*	10*	4	Mixed	Mixed
	330*	40*	1.3*	10*	6	Mixed	Vapour
LHSV	330	40	1.0	10	7	Mixed	Vapour
	330	40	0.5	10	5	Mixed	Vapour
	330*	40*	1.3*	10*	4	Mixed	Vapour
H_2/n-C_{14}	330	40	0.5	3	5	Mixed	Vapour
Molar Ratio	330	40	0.5	30	3	Vapour	Vapour
	330*	40*	0.5*	3*	5	Mixed	Mixed

* Previous Results Reproduced

** See Appendix B for Reaction Phase Calculations

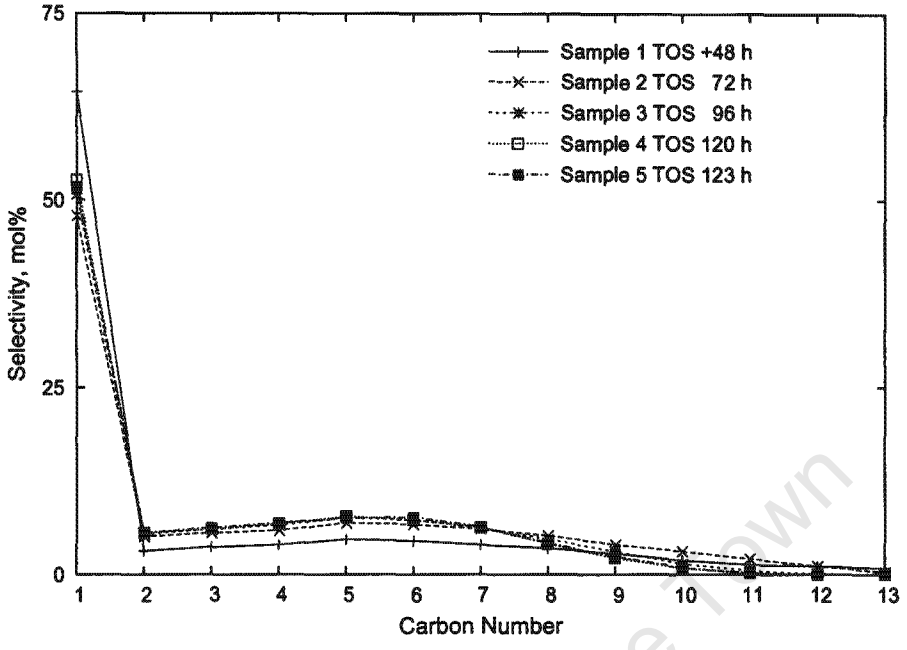

Figure 4.1: Achieving Steady State Conditions for Temperature Experiments
TOS refers to the moment conditions were changed from previous experiment to T=350°C, P=80 bar, LHSV=0.2 h^{-1}, H_2/n-C_{14}=116 mol/mol

4.1 Steady State

Steady state performance for each experiment was taken to be achieved after conversion and selectivities stabilised for at least two samples. Data from the last sample of each stabilisation series were taken to be representative of the respective set of reaction conditions. After steady state was achieved, process conditions for the next experiment, i.e. either temperature, pressure, liquid hourly space velocity or H_2/n-C_{14} molar ratio, were adjusted to determine their effect on the hydrocracking conversion and molar carbon number selectivities.

Figures 4.1 - 4.4 show how the molar carbon number distributions changed as steady state was achieved after changing conditions. In general, there was no significant change in the 'mid-carbon' number range distributions. The only significant changes in the carbon number distribution, prior to having achieved steady state conditions, were observed for C_1 and carbon numbers above C_{10} (or C_8 in the case of temperature experiments).

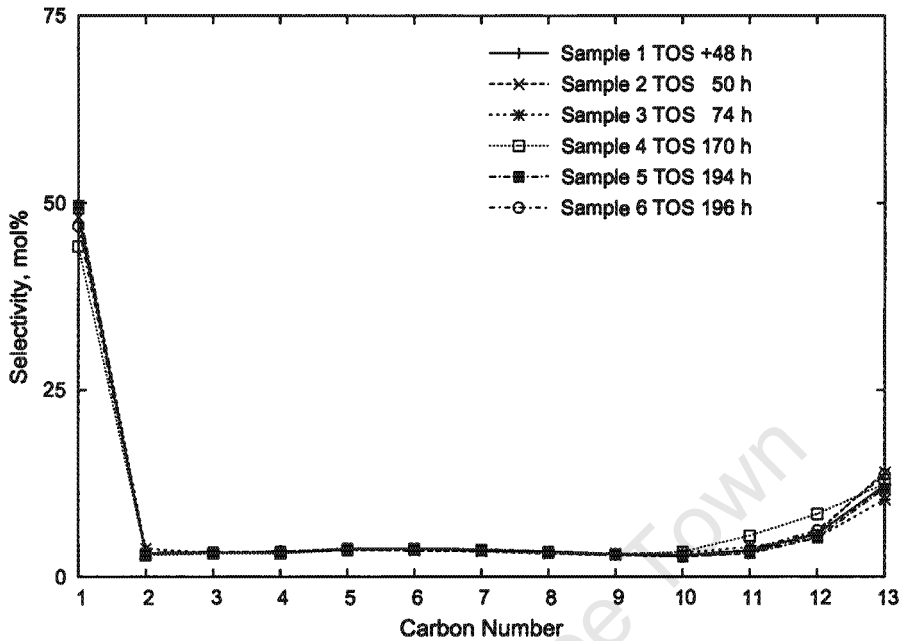

Figure 4.2: Achieving Steady State Conditions for Pressure Experiments
TOS refers to the moment conditions were changed from previous experiment to P=40 bar, T=330°C, LHSV=1.3 h^{-1}, H_2/n-C_{14}=10 mol/mol

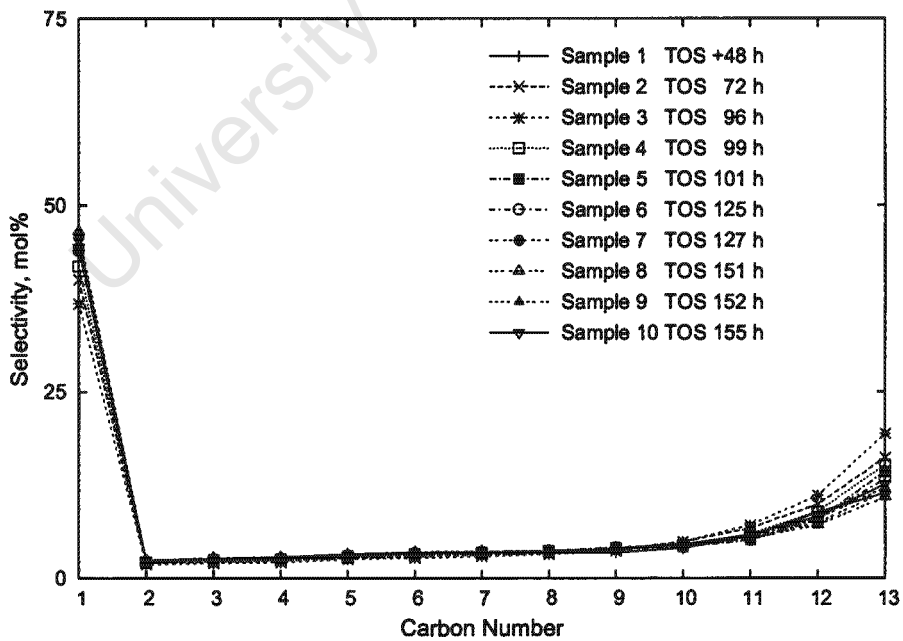

Figure 4.3: Achieving Steady State Conditions for Space Velocity Experiments
TOS refers to the moment conditions were changed from previous experiment to LHSV=0.5 h^{-1}, T=330°C, P=40 bar, H_2/n-C_{14}=10 mol/mol

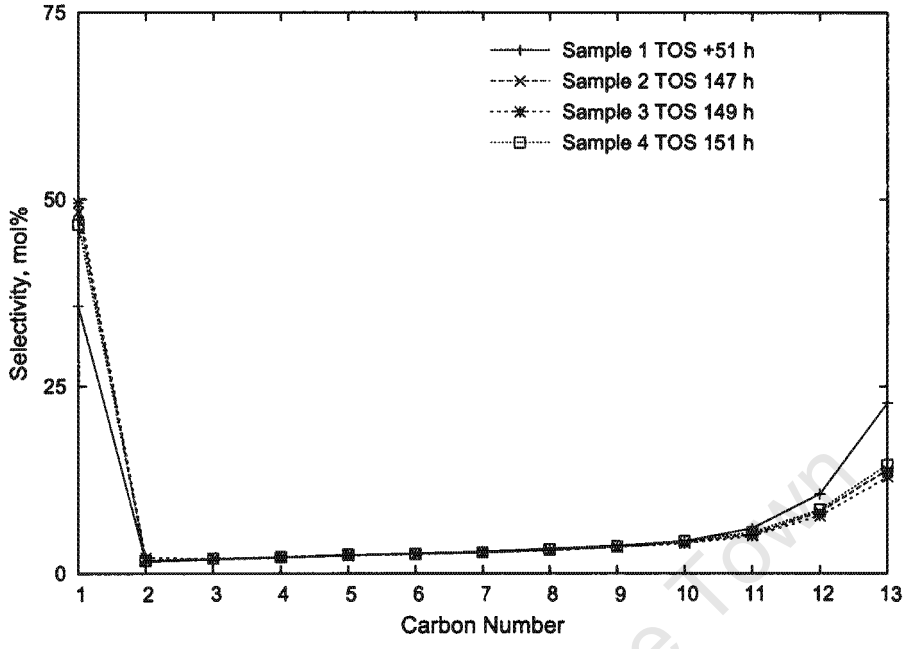

Figure 4.4: Achieving Steady State Conditions for Molar Ratio Experiments
TOS refers to the moment conditions were changed from previous experiment to H_2/n-C_{14}=3 mol/mol, P=40 bar, T=330°C, LHSV=0.5 h^{-1}

4.2 Reproducibility

To test the validity of the experiments conducted, the first experimental run of each series was repeated after the series was finished to determine the reproducibility of the results and to check whether there was any catalyst deactivation (table 4.1). Figures 4.5 - 4.8 indicate that the results are repeatable. The reproducibility of results also indicated that there was no catalyst deactivation.

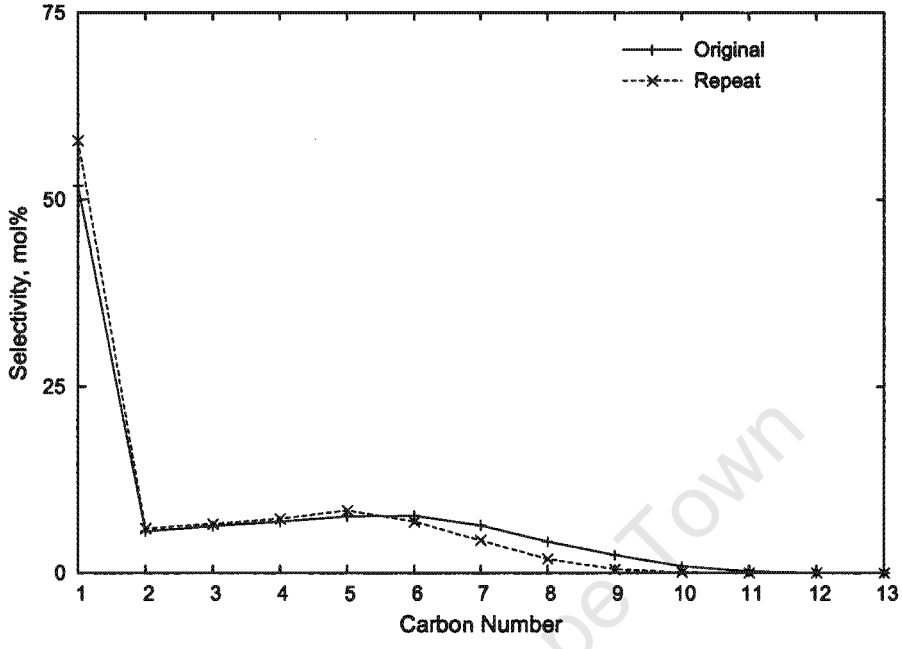

Figure 4.5: Reproducibility of Temperature Experiments
T=350°C, P=80 bar, LHSV=0.2 h^{-1}, H_2/n-C_{14}=116 mol/mol

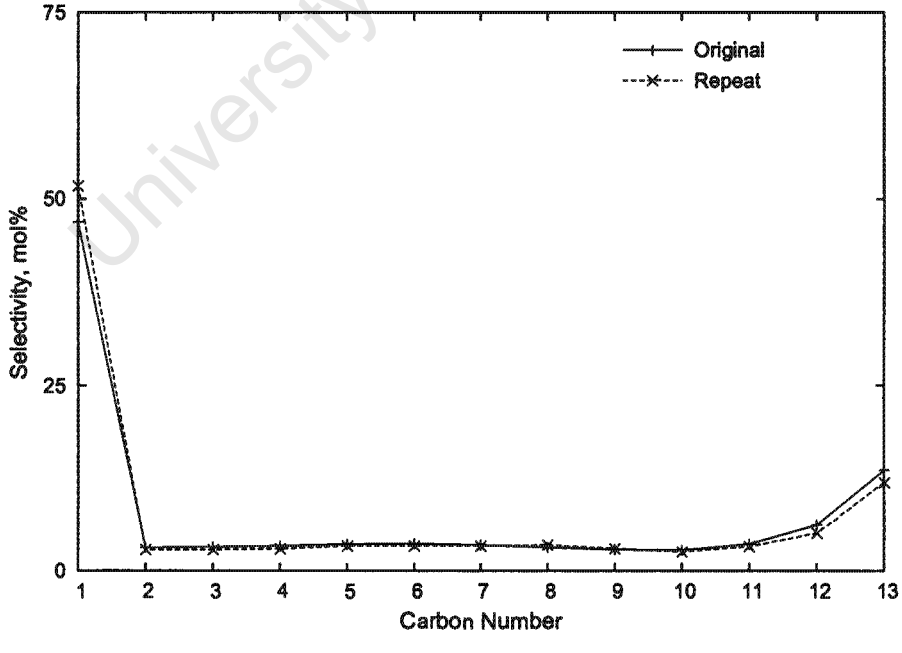

Figure 4.6: Reproducibility of Pressure Experiments
P=80 bar, T=330°C, LHSV=1.3 h^{-1}, H_2/n-C_{14}=10 mol/mol

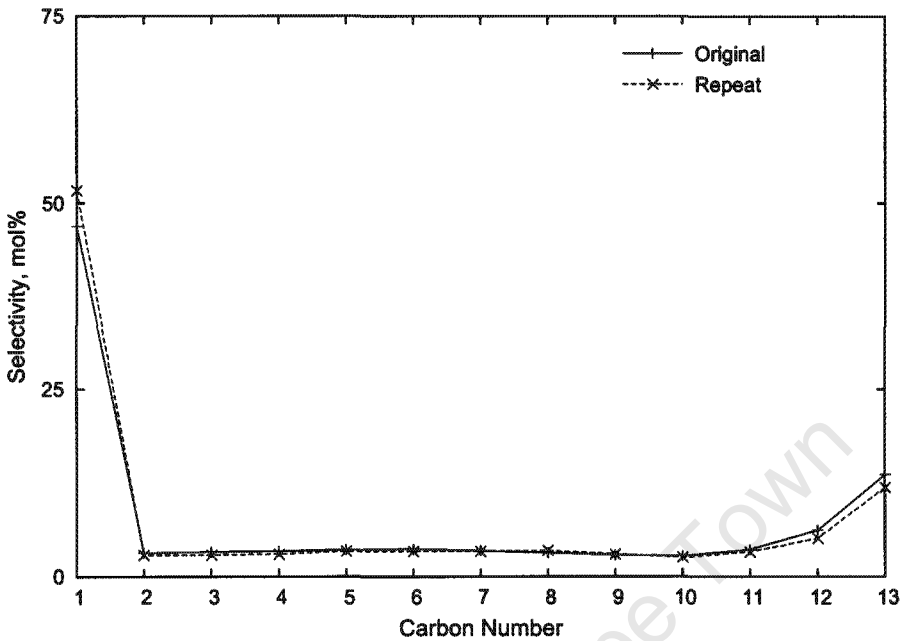

Figure 4.7: Reproducibility of Space Velocity Experiments
LHSV=1.3 h^{-1}, T=330°C, P=40 bar, H_2/n-C_{14}=10 mol/mol

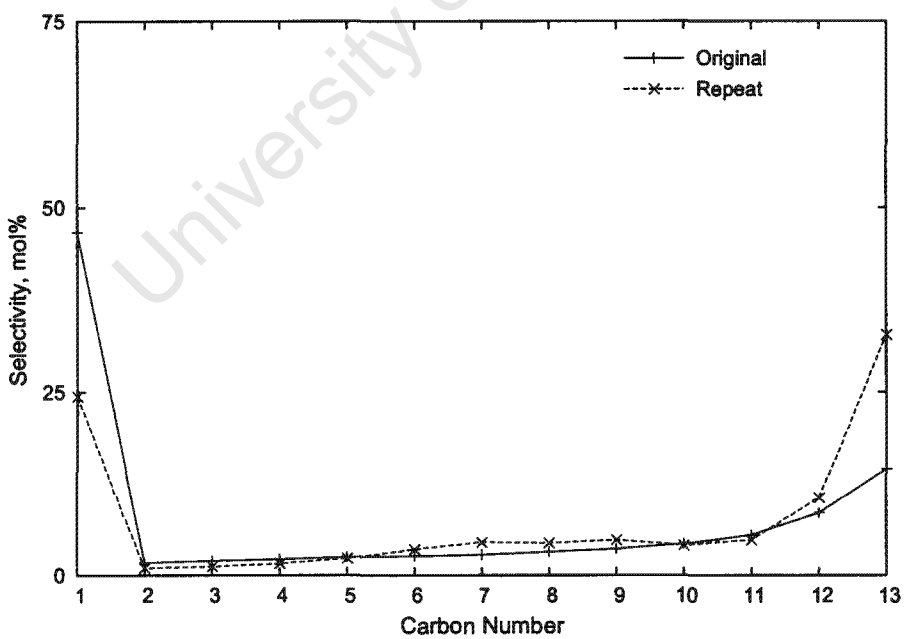

Figure 4.8: Reproducibility of Molar Ratio Experiments
H_2/n-C_{14}=3 mol/mol, P=40 bar, T=330°C, LHSV=0.5 h^{-1}
Note that operation at LHSV=0.5 h^{-1} was difficult and unstable, see section 3.2.4

Table 4.2: Effect of Temperature

P=80 bar, LHSV=0.2 h^{-1}, H_2/n-C_{14}=116 mol/mol

Temperature	Conversion	Selectivity, mol%			% Isomers in			Molar Ratio	
°C	%	C_1	C_1-C_3	C_{11}-C_{13}	$C_4^{\oslash}$	$C_{10}^{\oslash}$	Total	C_4/C_{10}	C_1/C_{13}
300	9.4	33.5	41.3	19.6	0.0	2.8	1.3	1.1	2.4
310	27.3	32.8	40.3	23.0	1.8	4.2	2.3	1.4	2.1
320	62.9	34.1	41.5	21.2	1.5	6.5	3.6	1.0	3.0
330	94.9	40.0	48.4	14.3	1.3	11.0	4.7	1.5	8.2
340	99.4	49.4	58.6	4.3	1.1	14.6	2.9	1.6	70.9
350	99.8	51.8	63.7	0.2	1.8	35.3	3.4	8.0	—*

* Contains no measureable amount of C_{13}
$^{\oslash}$ Percentage isomers in carbon number fractions

4.3 Temperature

Figure 4.9 shows that with increasing temperature conversion increases rapidly between 300 and 330°C, from 9.4% to 94.9%. At temperatures above 330°C conversion is complete.

For temperatures 300°C to 330°C the ratio of carbon numbers C_4 and C_{10}, which is the indicator for ideal (primary) hydrocracking, is close to unity (figures 4.10 and 4.11 and table 4.2). Within this temperature range, an increase in both light gases C_1-C_3 and tail ends C_{11}-C_{13} selectivity is noted. As the temperature increases to 350°C, a shift in the mid-carbon number range (C_4-C_{10}) towards the lighter end of the carbon number distribution (C_3-C_7) is observed with C_{11}-C_{13} selectivity tending to zero (figure 4.11), and C_1/C_{13} ratio tending to infinity (table 4.2).

Most notable of all the distribution curves is the high molar selectivity to methane, which increases further with increasing temperature. However, the selectivity for this gas is noticeably lower on a weight basis (based on carbon percent, figure 4.12), which is a more accurate indication of selectivity in terms of industrial economic significance.

From the molar distribution curves (figure 4.10) and the last column in table 4.2, it can be seen that for every mol C_{14} demethylated to C_{13} more than one mol of methane is produced. It is further evident in figure 4.13 that with increasing temperature, in particular when approaching 100% conversion, there is an increasing significance of light gases, C_1-C_3, selectivity.

The percentage skeletal isomers in the product is extremely low, see table 4.2, e.g. not exceeding 2% in the C_4 fraction whereas in higher carbon number fractions, such as C_{10},

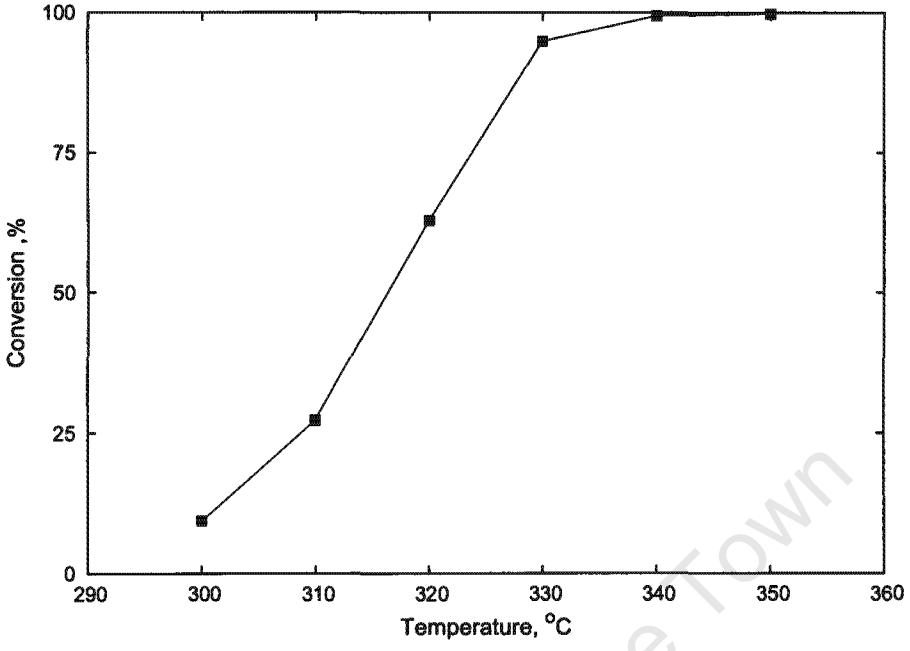

Figure 4.9: The Effect of Temperature on Conversion
P=80 bar, LHSV=0.2 h^{-1}, H_2/n-C_{14}=116 mol/mol

35% skeletal isomers are observed given the fact that the probability of skeletal isomer formation is greater for higher carbon number fractions.

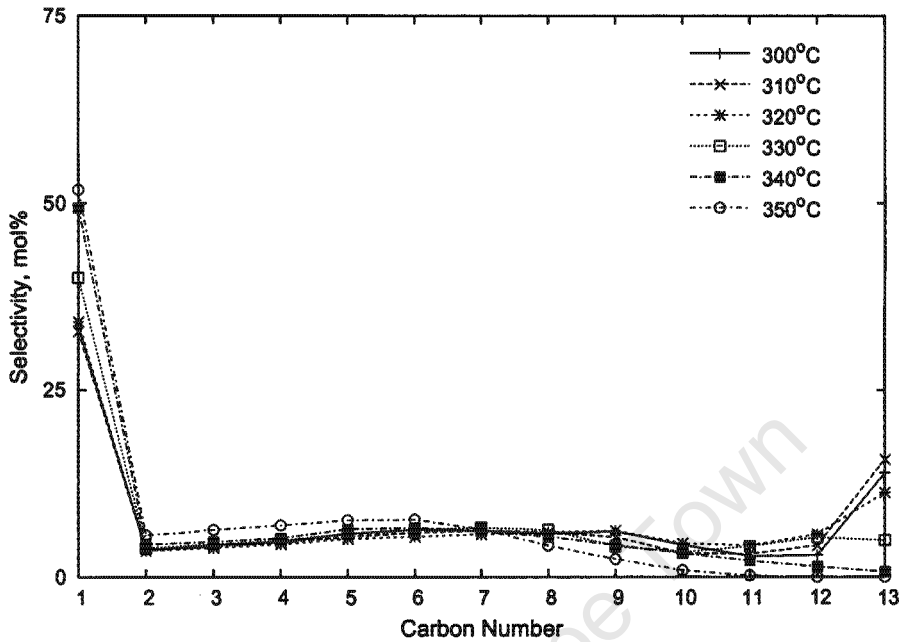

Figure 4.10: Molar Carbon Number Distribution of Products: Effect of Temperature
P=80 bar, LHSV=0.2 h^{-1}, H_2/n-C_{14}=116 mol/mol

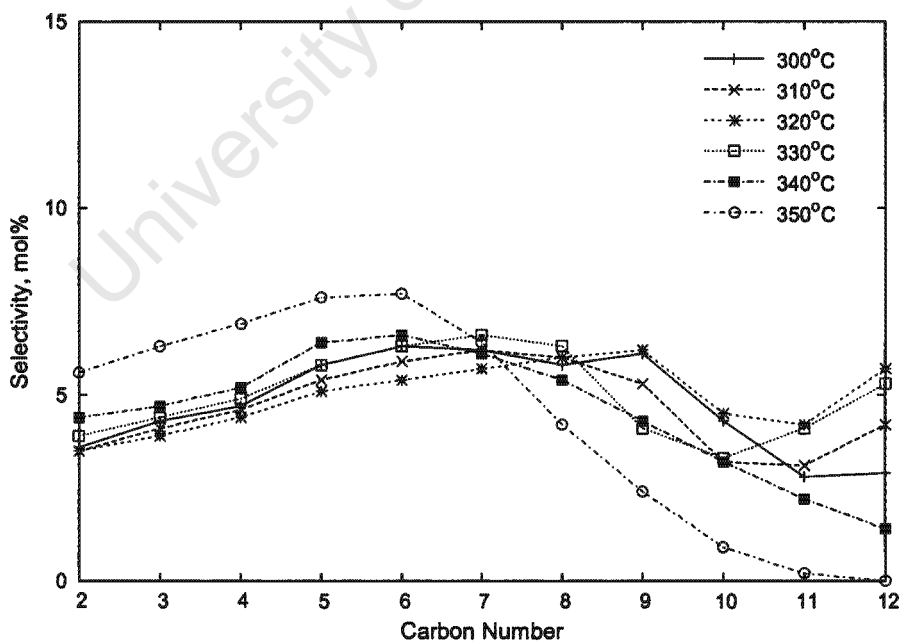

Figure 4.11: Molar Carbon Number Distribution of Products in C_2-C_{12} Range: Effect of Temperature
P=80 bar, LHSV=0.2 h^{-1}, H_2/n-C_{14}=116 mol/mol

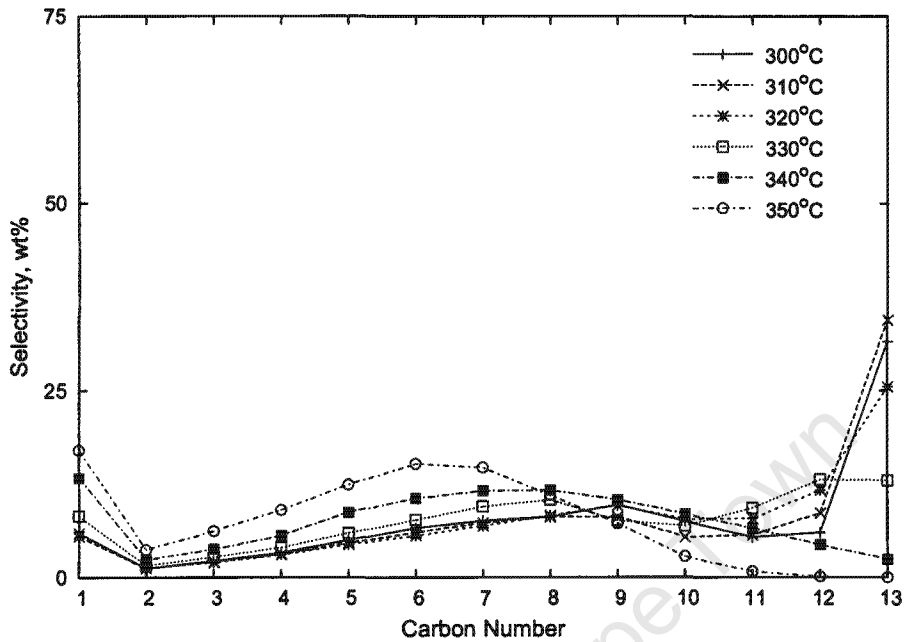

Figure 4.12: Weight Distribution of Paraffins: Effect of Temperature
P=80 bar, LHSV=0.2 h^{-1}, H_2/n-C_{14}=116 mol/mol

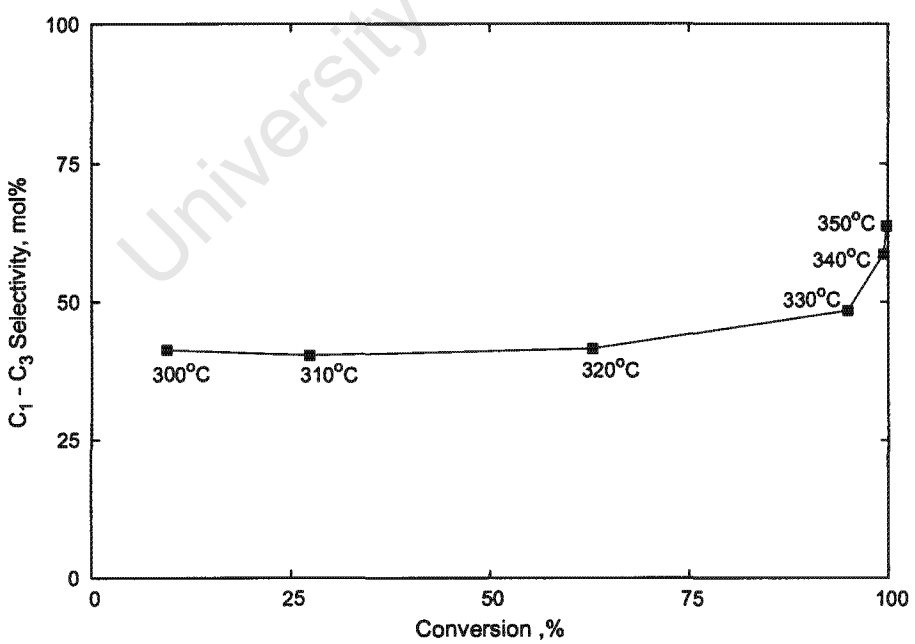

Figure 4.13: Selectivity of Lights: Effect of Temperature
P=80 bar, LHSV=0.2 h^{-1}, H_2/n-C_{14}=116 mol/mol

Table 4.3: Effect of Pressure

T=330°C, LHSV=1.3 h^{-1}, H_2/n-C_{14}=10 mol/mol

Pressure	Conversion	Selectivity, mol%			% Isomers in			Molar Ratio	
bar	%	C_1	C_1-C_3	C_{11}-C_{13}	$C_4^{\oslash}$	$C_{10}^{\oslash}$	Total	C_4/C_{10}	C_1/C_{13}
80	9.6	41.5	47.9	30.1	0.0	0.0	2.4	1.4	1.8
40	43.1	46.9	53.4	23.5	1.3	7.3	3.7	1.2	3.4
20	94.8	60.6	67.6	6.4	2.9	22.9	4.9	1.4	34.2

$^{\oslash}$ Percentage isomers in carbon number fractions

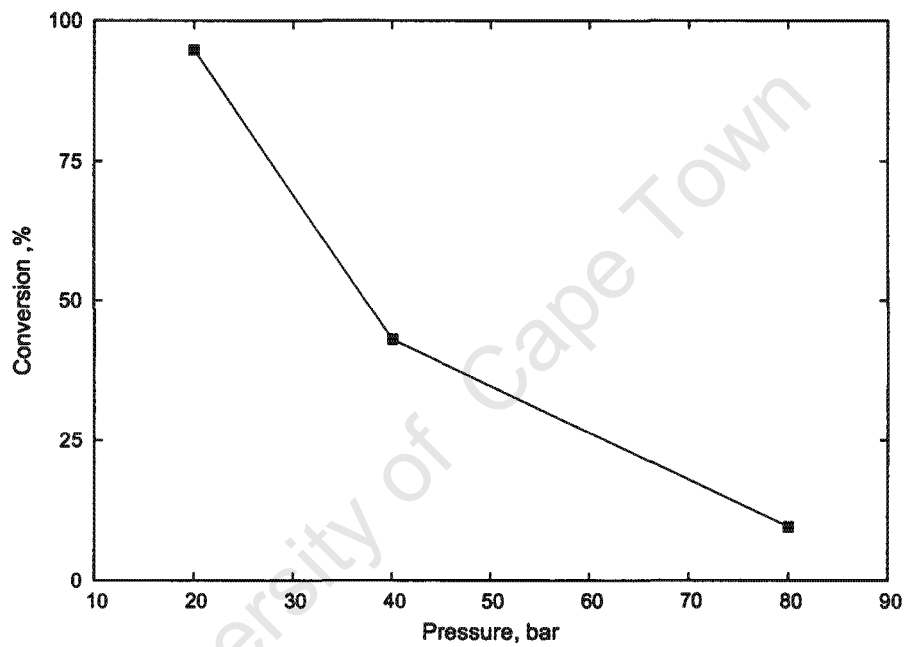

Figure 4.14: The Effect of Pressure on Conversion
T=330°C, LHSV=1.3 h^{-1}, H_2/n-C_{14}=10 mol/mol

4.4 Pressure

A significant impact is observed of pressure on conversion (figure 4.14). By decreasing the pressure from 80 bar to 20 bar at 330°C, the conversion increases from 9.6% to 94.8% (table 4.3).

Figure 4.15 indicates that by decreasing the pressure there is an increase in selectivity in methane and a decrease in heavy fractions, C_{11}-C_{13}. The ratio of C_4/C_{10} across all pressure experiments remains relatively unchanged at a little higher than 1 (table 4.3). The distribution between C_2 and C_{10} remains almost constant with the three curves obtained at the different pressures remaining rather flat and not deviating considerably

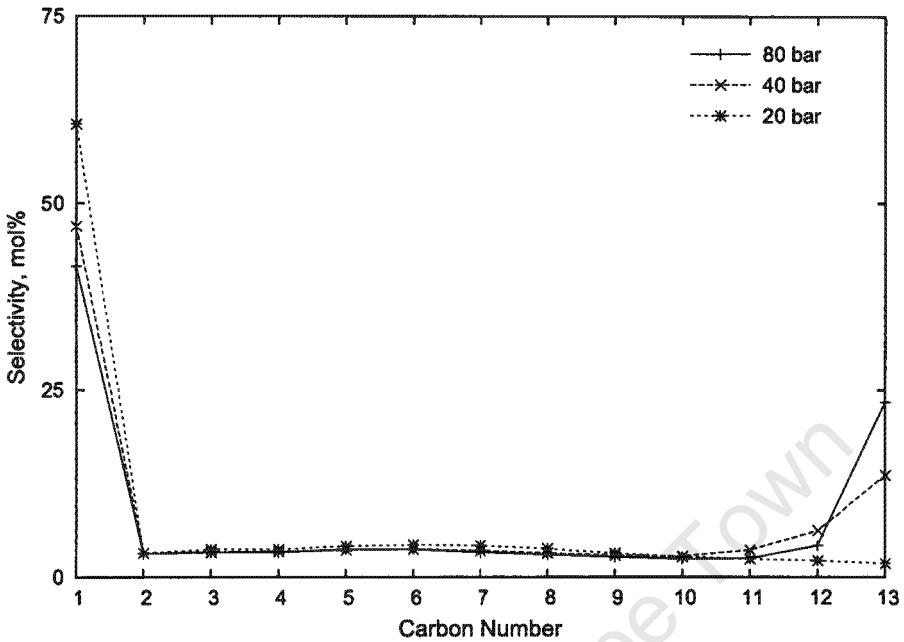

Figure 4.15: Molar Carbon Number Distribution of Products: Effect of Pressure
T=330°C, LHSV=1.3 h^{-1}, H_2/n-C_{14}=10 mol/mol

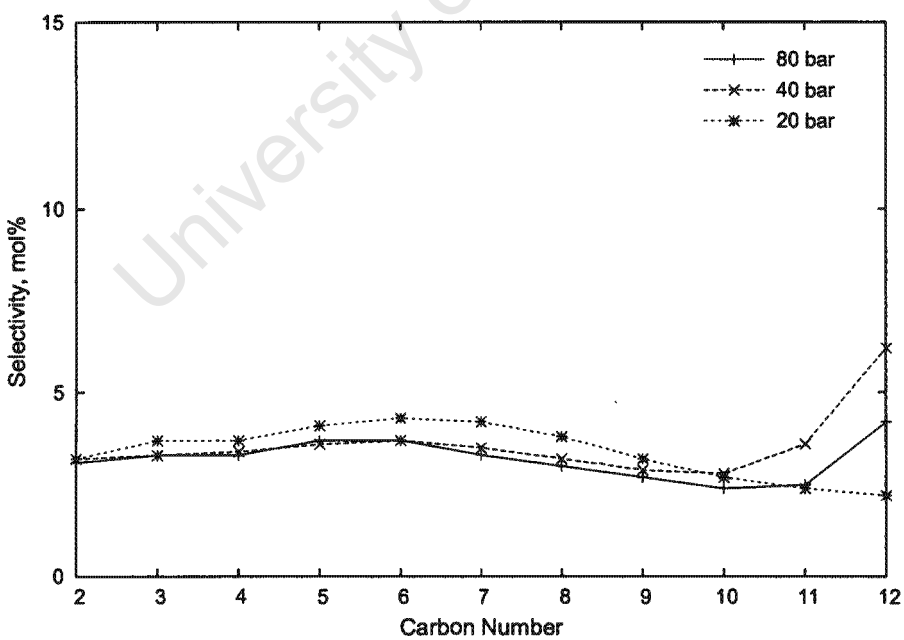

Figure 4.16: Molar Carbon Number Distribution of Products in C_2-C_{12} Range: Effect of Pressure
T=330°C, LHSV=1.3 h^{-1}, H_2/n-C_{14}=10 mol/mol

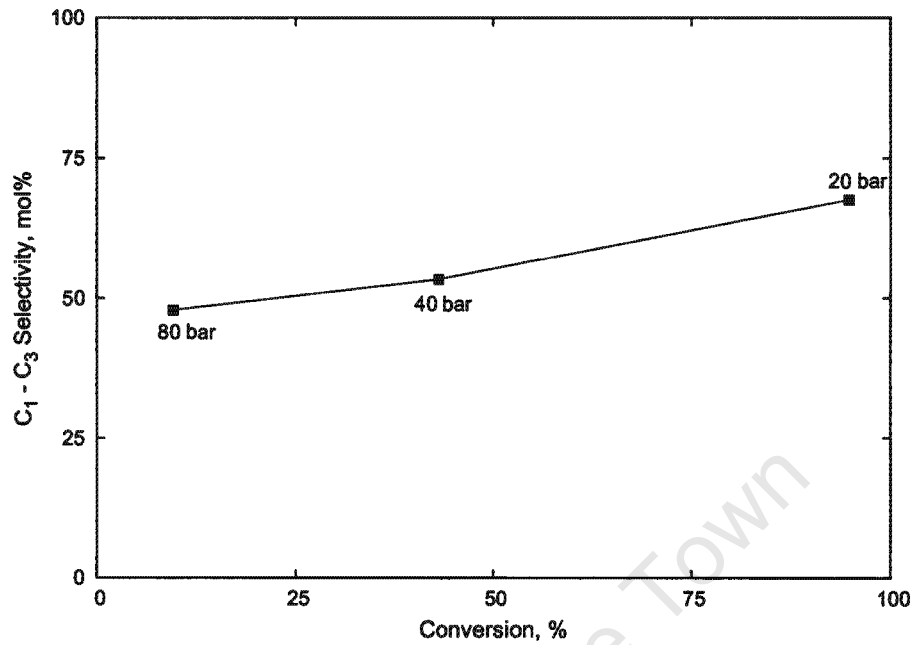

Figure 4.17: Selectivity of Lights: Effect of Pressure
T=330°C, LHSV=1.3 h^{-1}, H_2/n-C_{14}=10 mol/mol

from one another within this range (figure 4.16). The 80 bar curve tends to overlap the 40 bar curve over this range but differs over the C_{10} to C_{12} range, where experiments conducted at 40 bar yielded a higher C_{10}-C_{12} selectivity. The 20 bar curves in figures 4.15 and 4.16, which represent a product obtained at almost 100% conversion show a decreasing yield of tail ends C_{10} to C_{13}.

Over the range of pressure experiments conducted it can be seen in figure 4.17 that an increase in conversion (due to decreasing pressure) results in an increase in light gas selectivity, with the greatest change observed between 40 bar and 20 bar. The degree of isomerisation in individual carbon number fractions as a result of decreasing pressure tends to increase rapidly but still on a very low level. The degree of isomerisation in the total product also increases significantly (table 4.3).

Table 4.4: Effect of Space Velocity

T=330°C, P=40 bar, H_2/n-C_{14}=10 mol/mol

LHSV	Conversion	Selectivity, mol%			% Isomers in			Molar Ratio	
h^{-1}	%	C_1	C_1-C_3	C_{11}-C_{13}	$C_4^{\oslash}$	$C_{10}^{\oslash}$	Total	C_4/C_{10}	C_1/C_{13}
1.3	43.1	46.9	53.4	23.5	1.3	7.3	3.7	1.2	3.4
1.0	61.0	54.4	61.2	14.4	1.7	14.1	4.4	1.2	7.9
[0.5	67.0	44.4	49.2	26.6	2.3	20.5	10.6	0.6	3.5]

$^{\oslash}$ Percentage isomers in carbon number fractions

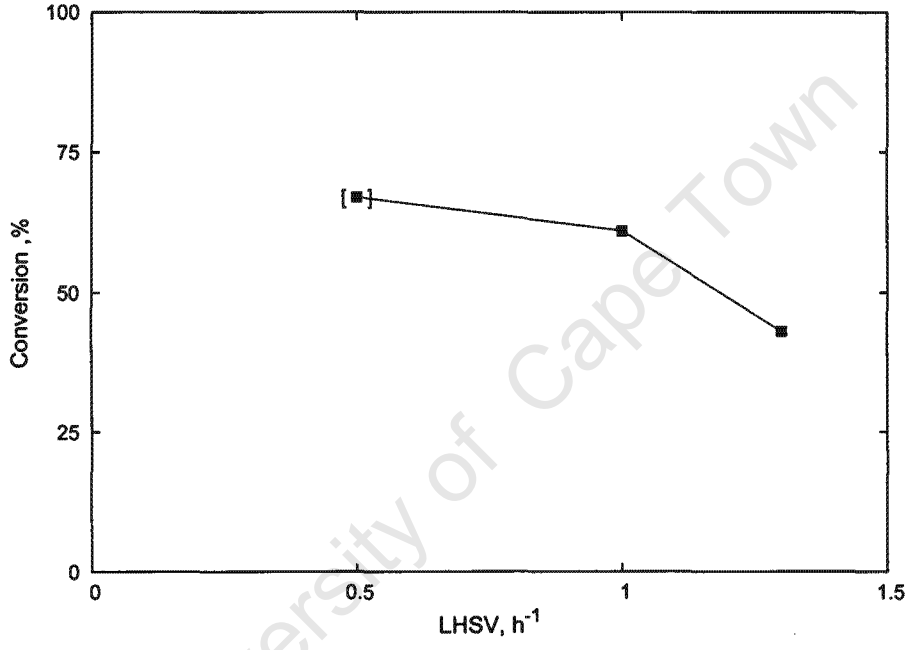

Figure 4.18: The Effect of Space Velocity on Conversion
T=330°C, P=40 bar, H_2/n-C_{14}=10 mol/mol

4.5 Liquid Hourly Space Velocity

Decreasing the space velocity from 1.3 h^{-1} to 1.0 h^{-1} resulted in an 40% increase in the overall conversion (figure 4.18). Note that results from space velocity of 0.5 h^{-1} are somewhat erroneous due to experimental difficulties (see section 3.2.4).

The carbon number distribution curves obtained at 1.3 h^{-1} and 1.0 h^{-1} indicate consistent selectivities over the C_2-C_{11} range and a similar trend of increasing carbon number fraction selectivities beyond C_{11} (figures 4.19 and 4.20). The C_4/C_{10} ratios for these two experiments are identical (table 4.4).

The selectivity of light gases C_1-C_3 increased slightly from a decrease in space velocity

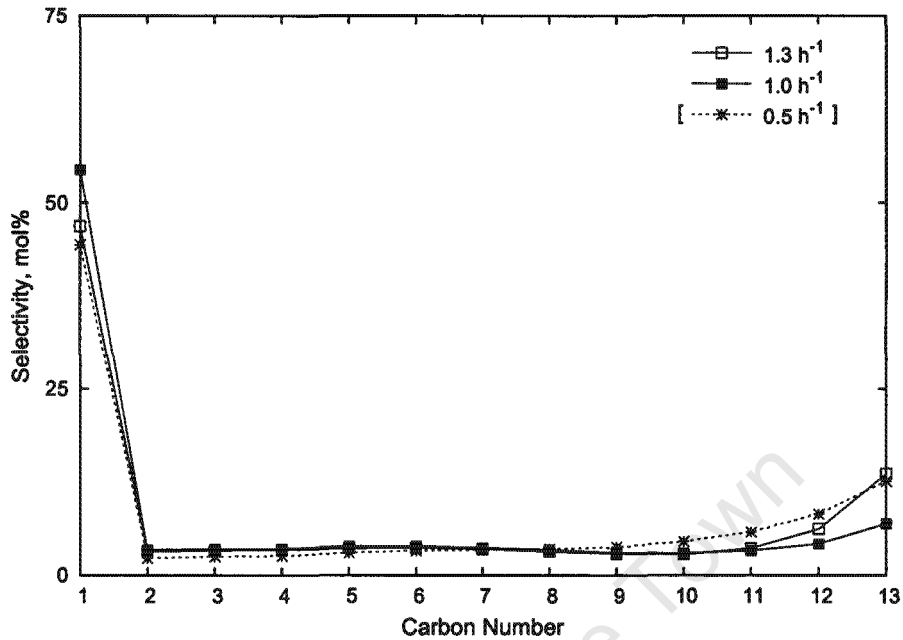

Figure 4.19: Molar Carbon Number Distribution of Products: Effect of Space Velocity
T=330°C, P=40 bar, H_2/n-C_{14}=10 mol/mol

from 1.3 h^{-1} to 1.0 h^{-1} (figure 4.21).

It emerged that results from the run at 0.5 h^{-1} are not only questionable e.g. a C_4/C_{10} ratio less than 1 (table 4.4), highest C_{10}-C_{13} selectivity at lowest C_1 selectivity (figure 4.19) etc. but also do not fit in the trends set by the other runs (tables 4.4 and 4.5, figures 4.18 - 4.25, data, data points or legend in brackets '[ ]').

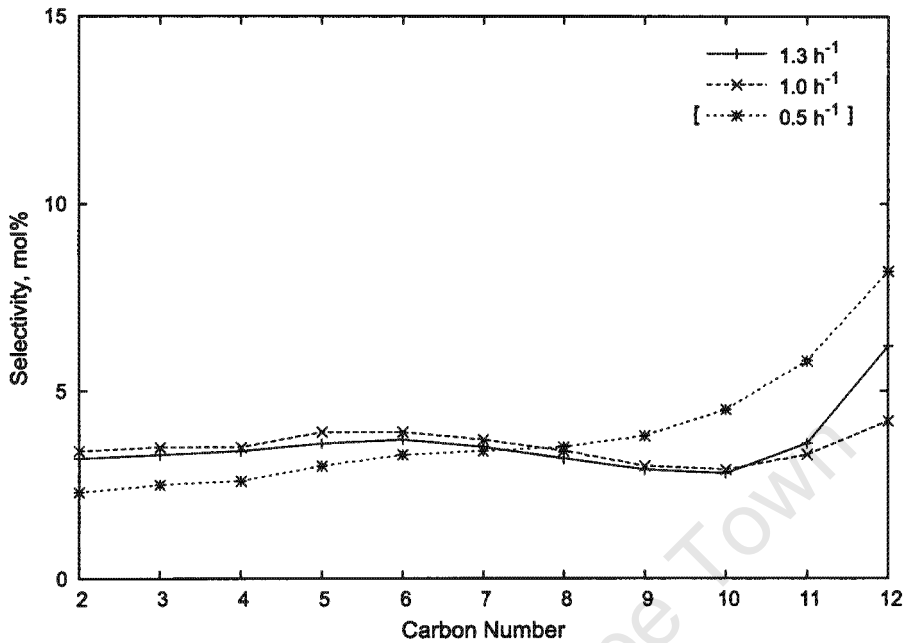

Figure 4.20: Molar Carbon Number Distribution of Products in C_2-C_{12} Range: Effect of Space Velocity
T=330°C, P=40 bar, H_2/n-C_{14}=10 mol/mol

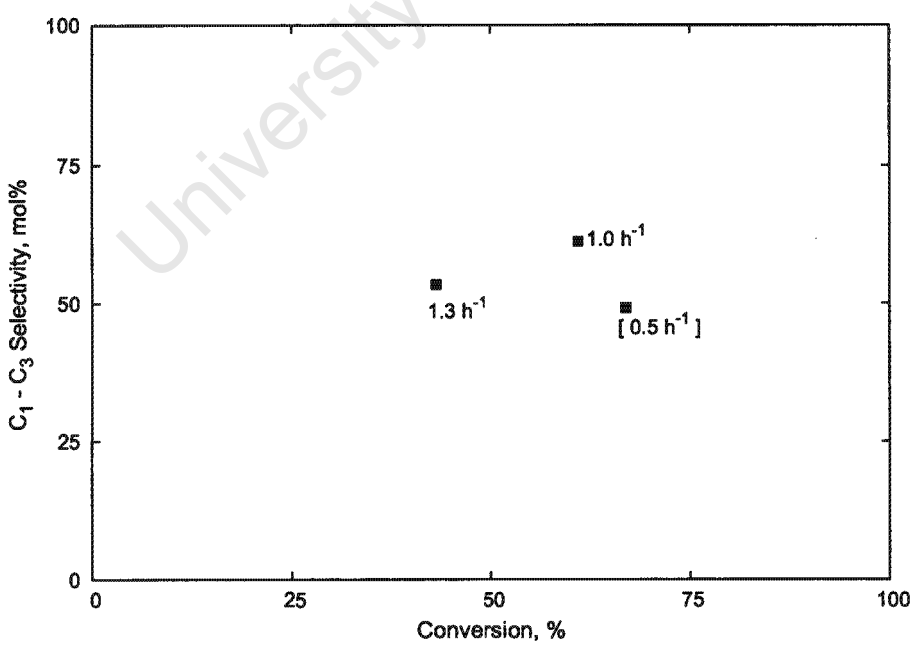

Figure 4.21: Selectivity of Lights: Effect of Space Velocity
T=330°C, P=40 bar, H_2/n-C_{14}=10 mol/mol

Table 4.5: Effect of H_2/n-C_{14} Molar Ratio

T=330°C, P=40 bar LHSV=0.5 h^{-1}

H_2/C_{14}	Conversion	Selectivity, mol%			% Isomers in			Molar Ratio	
Molar Ratio	%	C_1	C_1-C_3	C_{11}-C_{13}	$C_4^{\oslash}$	$C_{10}^{\oslash}$	Total	C_4/C_{10}	C_1/C_{13}
3	46.9	46.6	50.3	28.5	11.6	44.8	20.8	0.5	3.2
[10	67.0	44.4	49.2	26.6	2.3	20.5	10.6	0.6	3.5]
30	99.3	56.4	63.8	4.8	1.6	21.0	4.1	1.3	83.7

$^{\oslash}$Percentage isomers in carbon number fractions

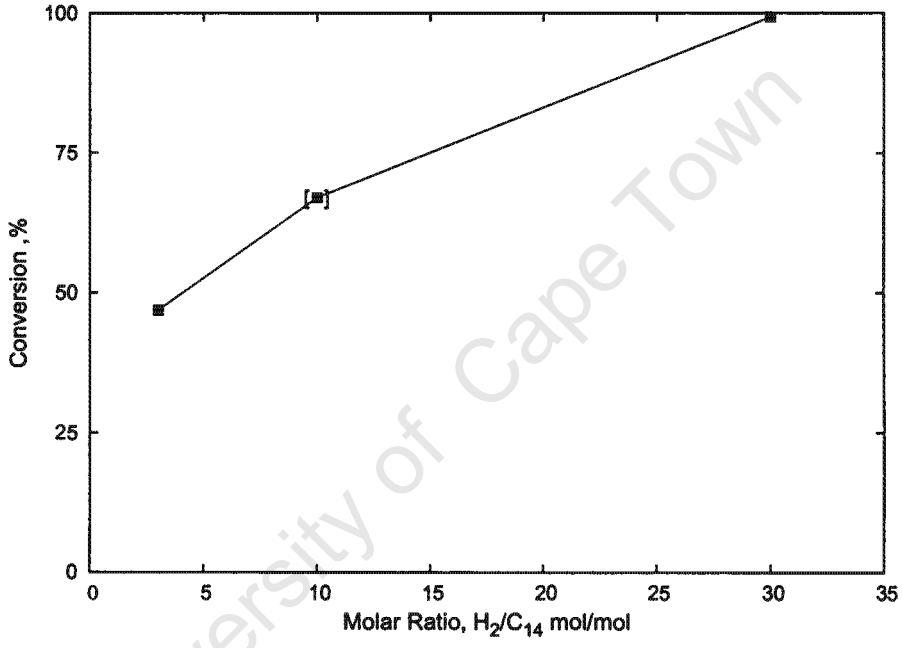

Figure 4.22: The Effect of H_2/n-C_{14} Molar Ratio on Conversion
T=330°C, P=40 bar, LHSV=0.5 h^{-1}

4.6 H_2/n-C_{14} Molar Ratio

As experiments at a space velocity of 0.5 h^{-1} showed that a low C_1-C_3 selectivity is achieved at a high conversion, subsequent experiments to determine the effects of H_2/n-C_{14} molar ratio on cracking reactions were conducted at this space velocity. A slowly increasing overall conversion was observed when the molar ratio was increased (figure 4.22).

Although there was a 20% conversion difference between molar ratios 3 and 10, their distribution curves did not differ significantly over the carbon range, having approximately the same C_4/C_{10} ratio (figures 4.23 and 4.24, table 4.5). The distribution curve at a molar ratio of 30 indicated a C_4/C_{10} ratio close to unity, whereas the C_4/C_{10} ratios were below

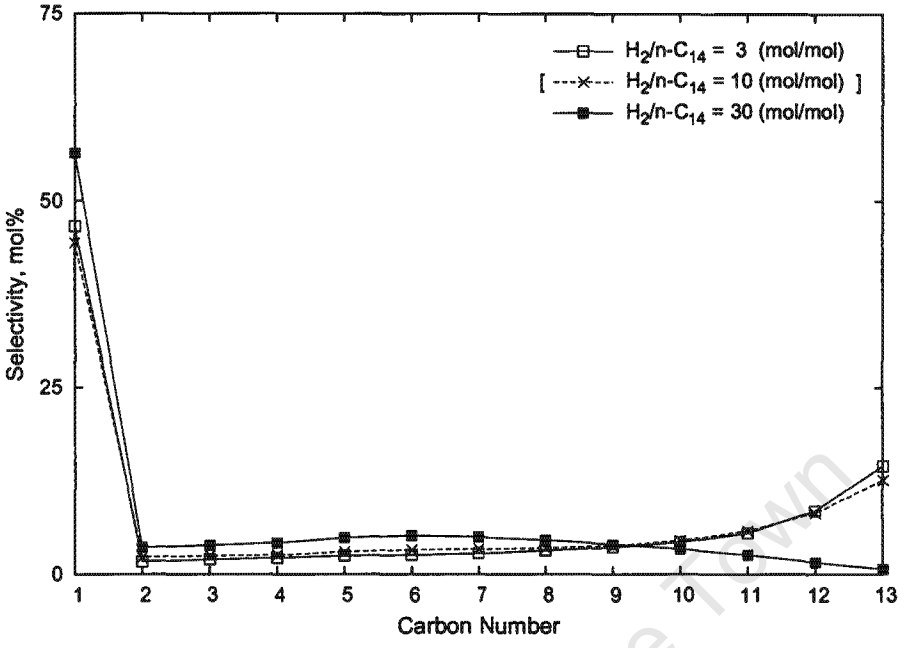

Figure 4.23: Molar Carbon Number Distribution of Products: Effect of H_2/n-C_{14} Molar Ratio
T=330°C, P=40 bar, LHSV=0.5 h^{-1}

unity at lower H_2/n-C_{14} ratios.

There was no distinct mid-carbon range between molar ratios 3 and 10. The distribution curves for these two ratios showed trends of increasing selectivities of carbon numbers above C_8 with a decreasing trend between C_8 and C_2.

A more noticeable C_4-C_{10} mid-carbon range for experiments conducted at 30 mol/mol was observed. The distribution of this curve showed a decreasing C_{11}-C_{13} selectivity as opposed to the increasing trend observed for molar ratios 3 and 10, however, at very high conversion (99.3%).

All molar ratio experiments yielded high selectivities of light gases (consisting predominantly of methane) increasing with increasing molar ratio of H_2/n-C_{14} and conversion (figure 4.25).

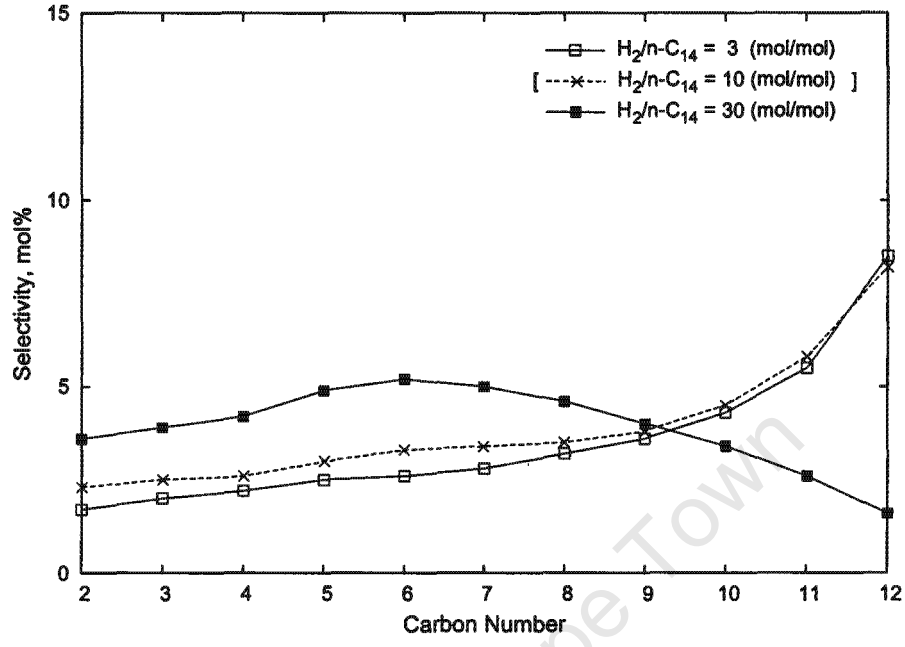

Figure 4.24: Molar Carbon Number Distribution of Products in C_2-C_{12} Range: Effect of $H_2/n\text{-}C_{14}$ Molar Ratio
T=330°C, P=40 bar, LHSV=0.5 h^{-1}

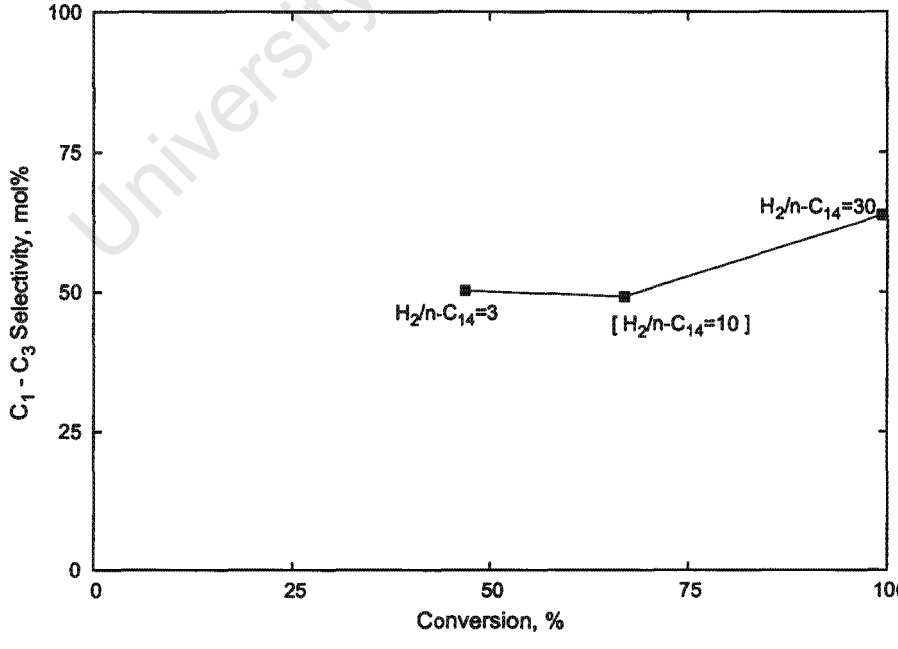

Figure 4.25: Selectivity of Lights: Effect of $H_2/n\text{-}C_{14}$ Molar Ratio
T=330°C, P=40 bar, LHSV=0.5 h^{-1}

5 Discussion

For the purpose of this study all references to isomers are assumed to be structural isomers (including traces of cyclic compounds) with negligible olefin selectivity. This assumption is based on thermodynamic equilibrium calculations (as shown in figure 5.1, for example the 1-butene/n-butane ratio) indicating that olefinic intermediates have a very minor contribution to the isomer selectivity in hydrocracking under the conditions applied. Indeed, no peaks that could be assigned to the typical olefin patterns in hydrocarbon carbon number fractions (e.g. the internal n-olefins that would appear shortly after the n-paraffin peak) were observed in the product chromatograms (see Appendix D).

5.1 Operability - Catalyst Stability

Sections 4.1 and 4.2 deal with catalyst stability and reproducibility of results. Steady state operation was achieved after every change of conditions so that the data could be taken from the steady state results (section 4.1). It was shown, that steady state results were reproducible and no noticeable deactivation occured.

5.2 Hydrocracking vs. Hydrogenolysis

From the results obtained (figures 4.9 - 4.25 and tables 4.2 - 4.5), it is clear that neither 'true' hydrocracking as occurring over a bi-functional catalyst (with a hydrogenation/dehydrogenation and a strong acid function) nor, at a glance, one of the hydrogenolysis mechansisms described (equal reactivity and cleavage of bonds i.e. 'non-selective' hydrogenolysis mechansim, and successive methyl abstraction, respectively) are demonstrated in these figures. However, a combination of the mechanisms for hydrocracking and hydrogenolysis reactions, covered in section 1.4, may explain the observed phenomena.

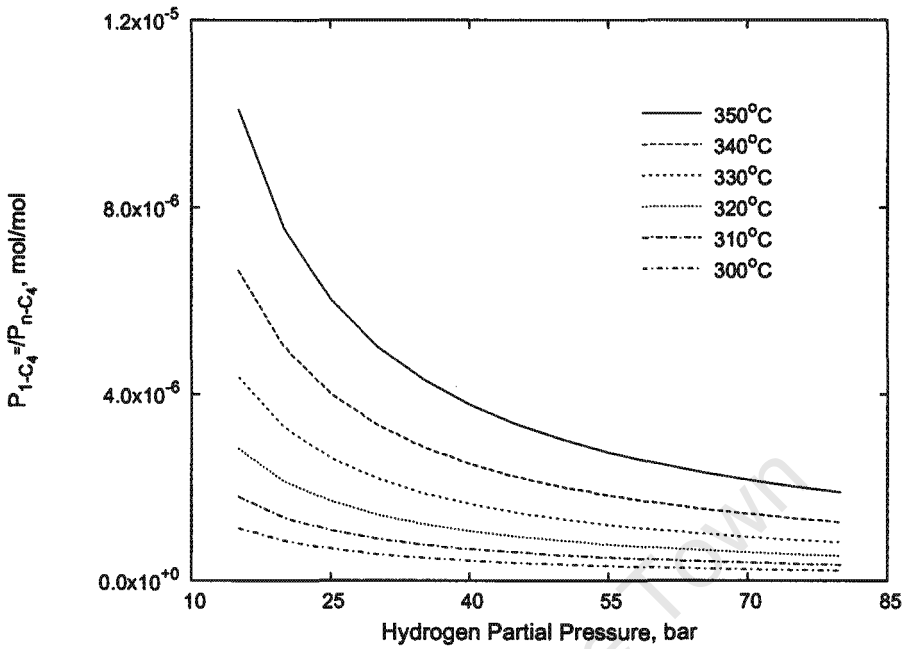

Figure 5.1: Themodynamic Equilibrium of Olefin Intermediates
e.g. 1-Butene to n-Butane
(see Appendix B and table B.7 for calculations)

Table 5.1 compares which product properties are expected from each of the three different possible reaction mechanisms and what was found.

The observed results show that the dominant products were methane with an almost equally distributed mid-carbon number range between C_2 and C_{10} and increasing tail-ends between C_{10}-C_{13} with very little isomerisation over the entire carbon number range. None of the aforementioned features are characteristic of bi-functional, 'true' hydrocracking reactions.

It emerges clearly from table 5.1 that if the 'ideal' shapes of carbon number distributions of the two types of hydrogenolysis reactions, 'non-selective' hydrogenolysis and methyl abstraction, introduced in section 1.4.2 (reproduced in figure 5.2) are combined as shown in figure 5.3, a similar shape is observed to that which was found within this study (see "*Observed*" in table 5.1 and figures 4.1 - 4.8, 4.10, 4.15, 4.19 and 4.23).

Table 5.1: Expected and Observed Results at Low to Medium Conversion for the Various Hydrocracking and Hydrogenolysis Mechanisms

Property	Expected			Observed
	'True' Hydrocracking	Hydrogenolysis		
	Bi-Functional	'Pt - Type'	Methyl Abstraction	
C_1-Selectivity	none	equal to mid-carbon number range	**very high**	very high
C_2-Selectivity	minimal	**equal to mid-carbon number range**	none	equal to mid-carbon number range
C_3-Selectivity	very low	**equal to mid-carbon number range**	none	equal to mid-carbon number range
Mid-Carbon Number Range C_4 - C_{10}	equally distributed	**equally distributed**	none	almost equally distributed
C_4/C_{10} Molar Ratio	**1**	**1**	0	between 0.5 - 1.6
Tail Ends	very low - none mimicking C_1-C_3	equal to mid-carbon number range	**exponentially increasing**	steeply increasing
Degree of Isomerisation	very high	**low**	none	low

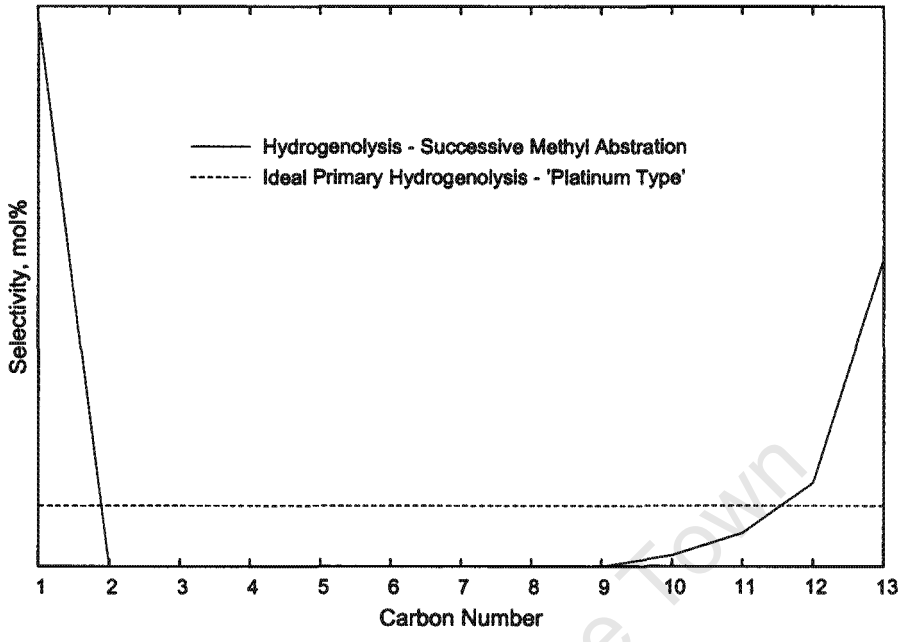

Figure 5.2: Plots of both Successive Methyl Abstration and 'Non-Selective' Hydrogenolysis Carbon Number Distribution (reproduced from figures 1.12 and 1.14)

The above attributes indicate a combination of essentially the following reactions:

- Successive methyl abstraction hydrogenolysis reaction – due to the high selectivity of methane and increasing selectivities of products with carbon numbers above C_{10}
- 'Non-selective' hydrogenolysis reaction – due to the almost equally distributed mid-carbon number range between C_2-C_{10}

It is important to note that, if 'true' bi-functional hydrocracking was taking place, more significant selectivities to isomers would be expected. This is due to the nature of the hydrocracking mechanism (refer to figures 1.4 and 1.6) which suggests that isomerisation occurs readily prior to cracking resulting in high degree of isomerisation before cracking even becomes significant (figure 5.4), which later is reflected in the products. The results showed, however, high preference for producing n-paraffinic cracking products over skeletal isomerised products, corresponding to figure 5.5. This further supports the conclusion that hydrogenolysis reactions are dominant in this study and corresponds to literature (see section 1.7.2) that suggests if a very high metal to acid ratio is present, hydrogenolysis reactions may predominate.

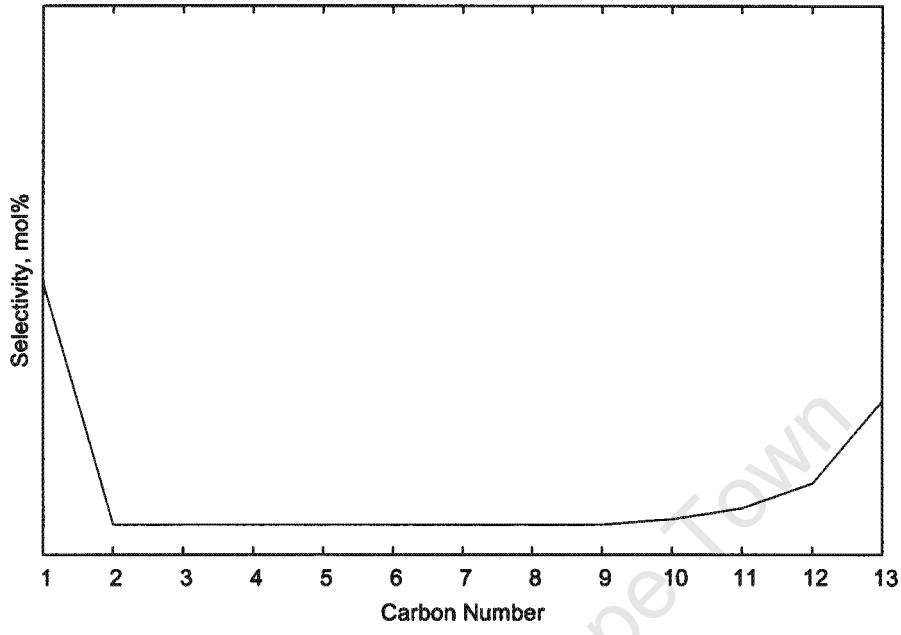

Figure 5.3: Combined Effect of Successive Methyl Abstraction and 'Non-Selective' Hydrogenolysis Carbon Number Distributions

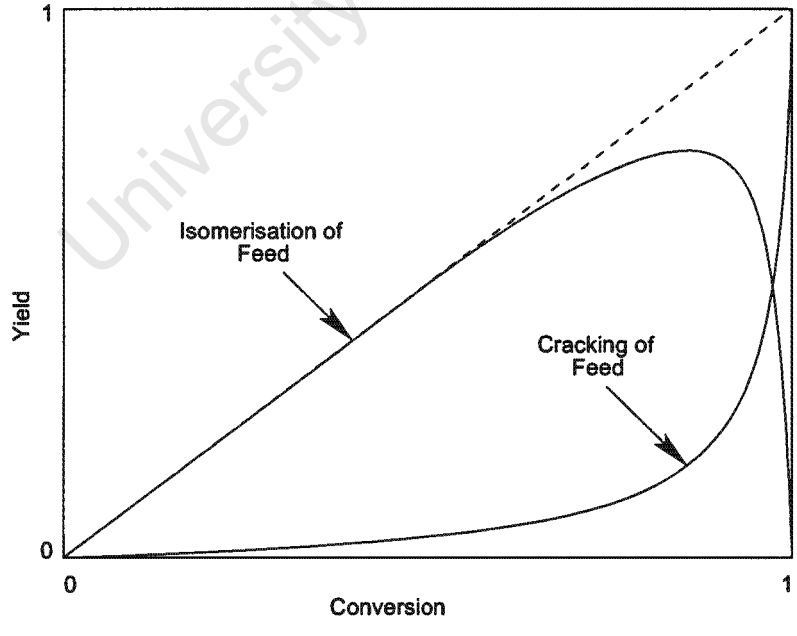

Figure 5.4: Ideal 'True' Hydrocracking: Isomerisation and Cracking Yields over Bi-Functional Catalysts (Martens and Jacobs, 2001)

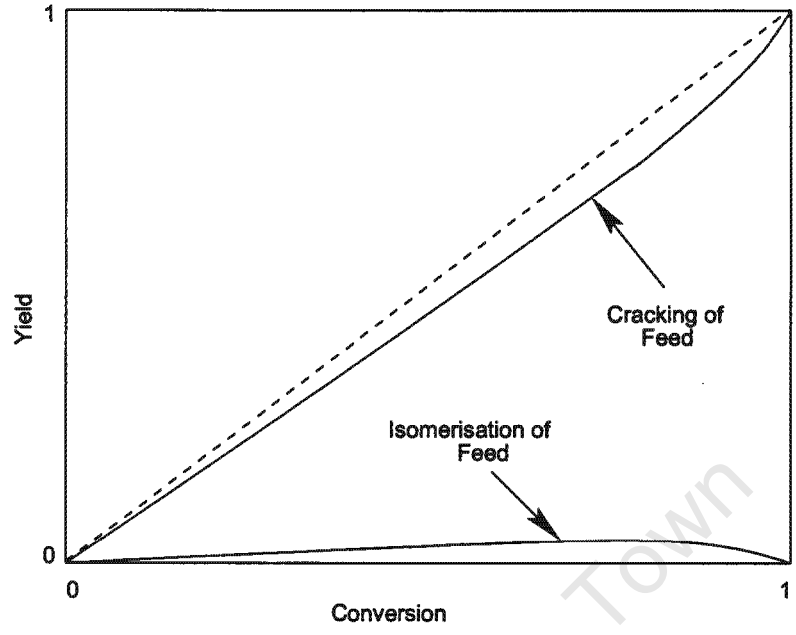

Figure 5.5: Observed Isomerisation and Cracking Yields over 'Non-Selective' Hydrogenolysis Catalysts, such as, Group VIA and VIIIA Mixed Metal Oxide Catalyst

5.2.1 Contribution of Individual Catalyst Constituents

The following section deals with the role of the individual constituents of the catalyst and their contribution to the composition and characteristics of the product.

5.2.1.1 The Carrier – Isomerisation

Even though a catalyst with an acid carrier, $CoMo/SiO_2$-Al_2O_3, was chosen, it appears that the acidity of the carrier did not contribute significantly to the reactions that occured, though the comparably very low activity of the acid catalyst constituent may have contributed to the degree of isomerisation observed (see section 5.6). However, it cannot be said conclusively whether isomerisation was only due to the slight acidity of the catalyst carrier (i.e. formation and isomerisation of carbenium ions) or also a result of the 'non-selective' hydrogenolysis mechanism (with some isomerisation of the adsorbed radicals formed).

5.2.1.2 Metallic Cobalt – Methanolysis

Considering the catalyst composition employed ($CoMo/SiO_2$-Al_2O_3) and recognising that the catalyst is not present in the form of metal sulphides, as is commonly employed in refinery hydrocracking applications, it may be reasonable to ascribe the degree of methanolysis observed to the presence of free cobalt metal, in much the same way as has been reported for free cobalt-sulphide clusters in the case of sulphided CoMo-type hydroprocessing catalysts (Topsøe et al., 1996).

5.2.1.3 The CoMo-Oxide Phase – 'Non-Selective' Hydrogenolysis

A CoMo-oxide phase is known not to differ significantly from a CoMo-sulphide phase in its catalytic properties in hydroprocessing reactions, see sections 1.4.2.3 and 1.4.2.4.

So the product fraction represented by the almost equal carbon number distribution (at low conversion) in the middle range, C_2-C_{10}, and its shift to lower carbon numbers due to secondary cracking at higher conversion can be attributed to 'non-selective' hydrogenolysis reactions over the CoMo-oxide phase.

5.2.2 A Methanolysis Model

To distinguish and explain the trends observed over the entire carbon number range, a simple model was formulated for the methyl abstraction hydrogenolysis mechanism. The model was set-up as follows:

- The C_1/C_{13} molar ratio obtained from the results of the temperature series (see table 4.2) was used as a starting or convergence point for the modelling calculations
- n-C_{14}, used as a basis, undergoes methyl abstraction to form methane and n-C_{13}
- Part of the n-C_{13} desorbs from the catalyst and leaves the system (fraction 1-α) while the rest of the n-C_{13} stays adsorbed on the catalyst (fraction α) to undergo further methyl abstraction to form methane and n-C_{12} etc. (see figure 5.6)
- The number of moles of methane that are produced equals:

$$n_1 = \left\{ \sum_{i=2}^{13} n_i \cdot (14 - i) \right\} + n_2 \tag{5.1}$$

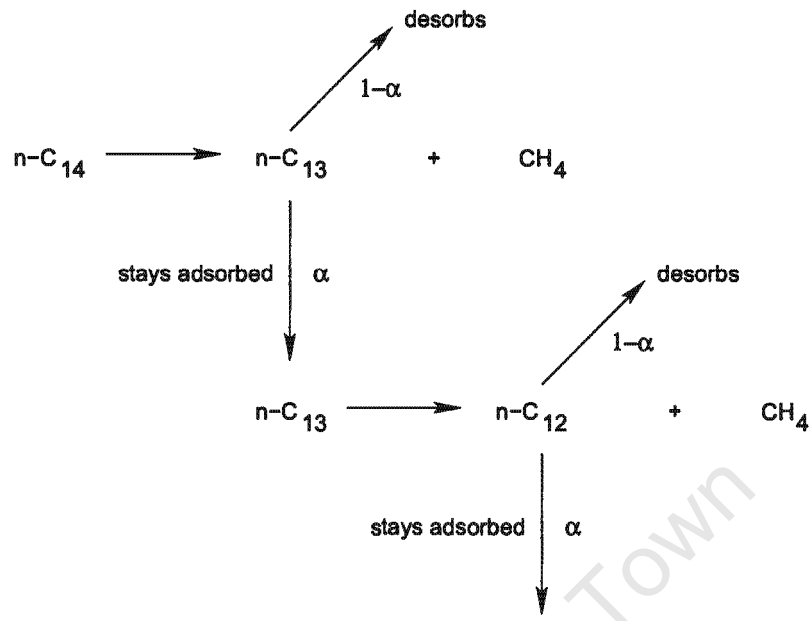

Figure 5.6: Schematic of the Successive Methyl Abstraction Model
'α' represents the probability of the long fragment to stay adsorbed and be demethylated again

i = carbon number of species

n_i = mols of species i

$+ n_2$ considers that the fragment obtained after methyl abstraction from C_2 is another methane molecule

- The fraction of the species that remains adsorbed, α, (see figure 5.6) was determined using Microsoft Excel's SOLVER converging towards the observed C_1/C_{13} molar ratio. The spreadsheet is given in Appendix A.
- Note that the model does not include secondary methanolysis, i.e. further demethylation of the long fragment once desorbed. This is because the reactivities (mainly adsorption kinetics) of C_{13-} compounds, relative to C_{14}, are unknown. In addition, products from the 'non-selective' hydrogenolysis mechanism produced over the CoMo-oxide phase were to be considered. The methanolysis model therefore only holds for low to medium conversion.

The results of the above model, applied to the temperature series, are shown in figures 5.7 and 5.8.

The figure shows a trend that is very similar in shape to what was obtained experimentally (see figure 4.10), namely:

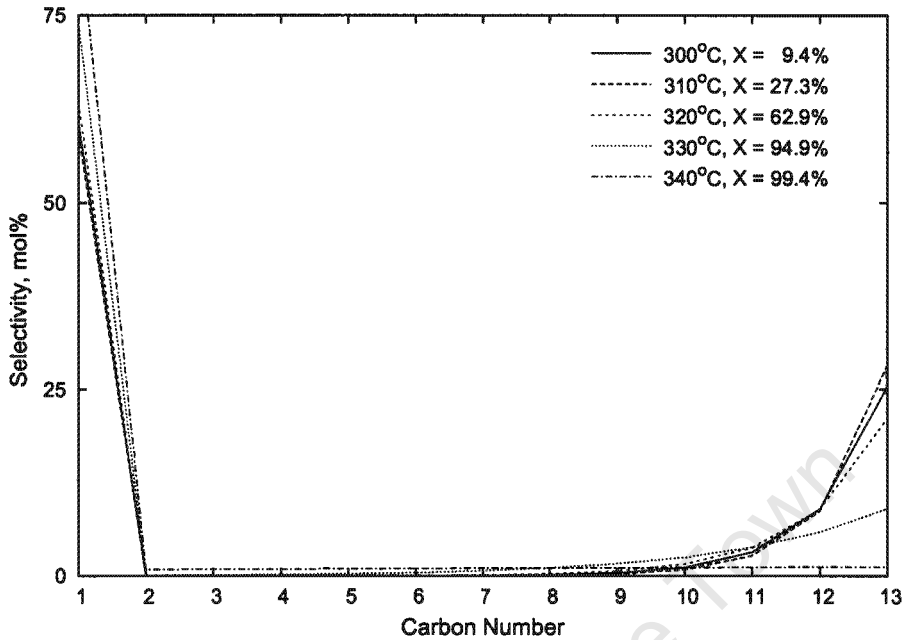

Figure 5.7: Modelled Carbon Number Distribution for the Methyl Abstraction Mechanism
Based on the C_1/C_{13} Molar Ratios Obtained from the Results of the Temperature Series (X=Conversion)

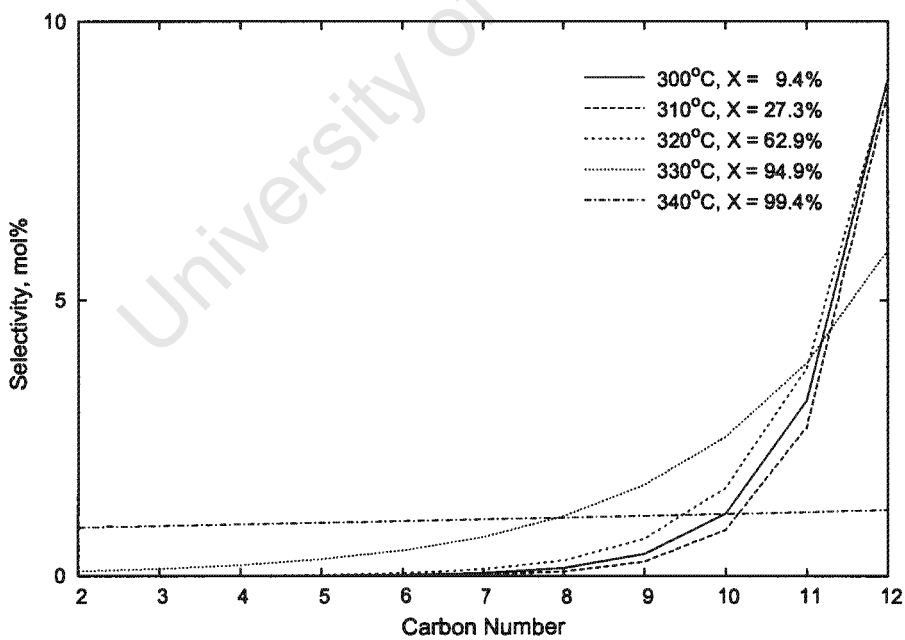

Figure 5.8: Modelled Carbon Number Distribution for the Methyl Abstraction Mechanism, in the C_2-C_{12} range
Based on the C_1/C_{13} Molar Ratios Obtained from the Results of the Temperature Series (X=Conversion)

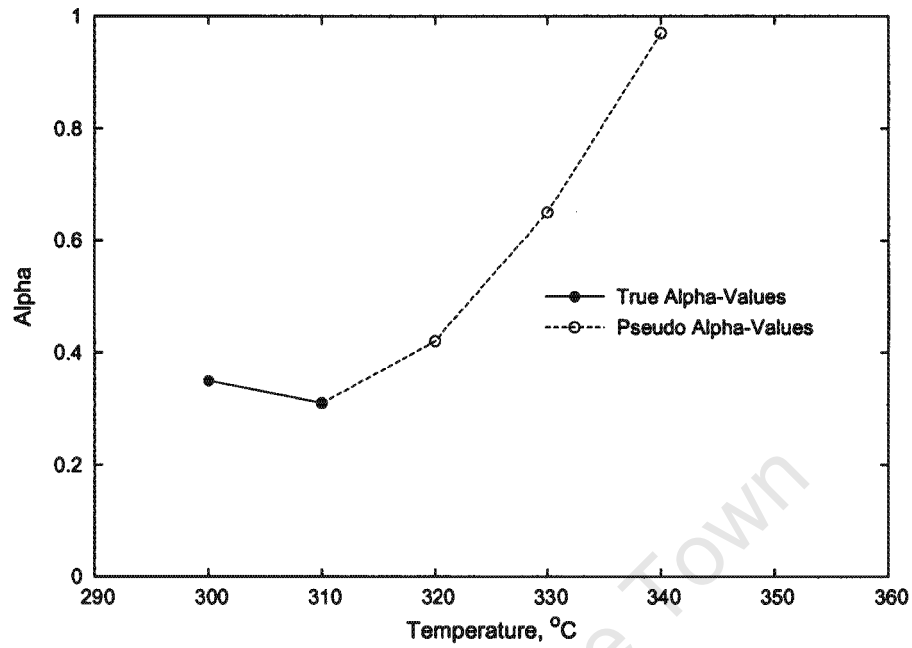

Figure 5.9: α-Values Resulting from the Methanolysis Model Applied on the Product from Hydrocracking of n-C_{14} at Different Temperatures and Conversions, respectively

- very high selectivities of methane
- high tail ends at low to medium conversion

This indicates that carbon number distributions as observed in this study, particularly at low H_2/n-C_{14} ratios (see e.g. figure 4.4) are mainly due to the methyl abstraction mechanism. Differences between the model and the observed trends, i.e. a higher and more equal level in the mid and low carbon number range can then be attributed to the 'non-selective' hydrogenolysis mechanism (see figure 4.10 for the carbon number distributions obtained from the temperature series or the almost 'ideal' curves in figure 4.2 observed from the settling in to steady state in a space velocity experiment).

The model seems to show, additionally, that the methyl abstraction mechanism also contributes to secondary cracking as there seems to be an indication of increased selectivities to lower carbon number fragments at higher temperatures i.e. higher conversions (see the modelled 330°C and 340°C series in figures 5.7 and 5.8) with aforementioned trends seemingly becoming apparent at high conversion in the experimental results (see figure 4.10, obtained from the temperature series and, almost 'ideal', figure 4.15).

However, as mentioned above, the kinetic methyl abstraction model, equation (5.1), does not contain terms that consider secondary reaction steps. So, when applied on very high C_1/C_{13} molar ratios as obtained at high temperature, i.e. high conversion, pseudo α-values result as shown in figure 5.9

α is the fraction of the long fragment from a methanolysis step that stays adsorbed on the catalyst to undergo further methyl abstraction (see figure 5.6). α-values approaching unity cannot be considered as being real. Also, the result of excessive secondary methanolysis would clearly not result in an equal carbon number distribution, C_2-C_{13}, as resulting from the model for high conversion (see figure 5.7) and α-values approaching their upper limit of 1 (figure 5.9).

It can be concluded that α-values obtained at low to medium conversion (300 and 310°C in figure 5.9) eventually represent primary methanolysis. This means that about one third of the long fragment stays adsorbed and undergoes further methyl abstraction.

5.2.3 Mid-Carbon Number Range Distribution

Another feature that was observed, was some preference for medium carbon numbers in the cracked product (i.e. around C_6-C_7) suggesting that the 'non-selective' hydrogenolysis function of the catalyst shows some preference for cleaving centrally situated bonds resulting in a 'hump-like' shape. However, a combination of the carbon number distributions obtained from methanolysis at conversions <99% (see figures 5.7 and 5.8) and secondary hydrogenolysis of the higher carbon number product may produce this 'hump like' shape as well.

5.3 Conversion and Selectivity

It was seen in the results, that a change in the process conditions had a significant effect on the conversion (see tables 4.2 - 4.5 and figures 4.9, 4.14, 4.18 and 4.22).

Indeed, figures 5.11 - 5.15 clearly indicate that the major or only influence on selectivities is by conversion and that there is no or very little direct influence of the process conditions on the selectivity except via conversion. A remarkable influence, to some extent, is only observed when the H_2/n-C_{14} molar ratio is very high (as for the temperature series, see table 4.1).

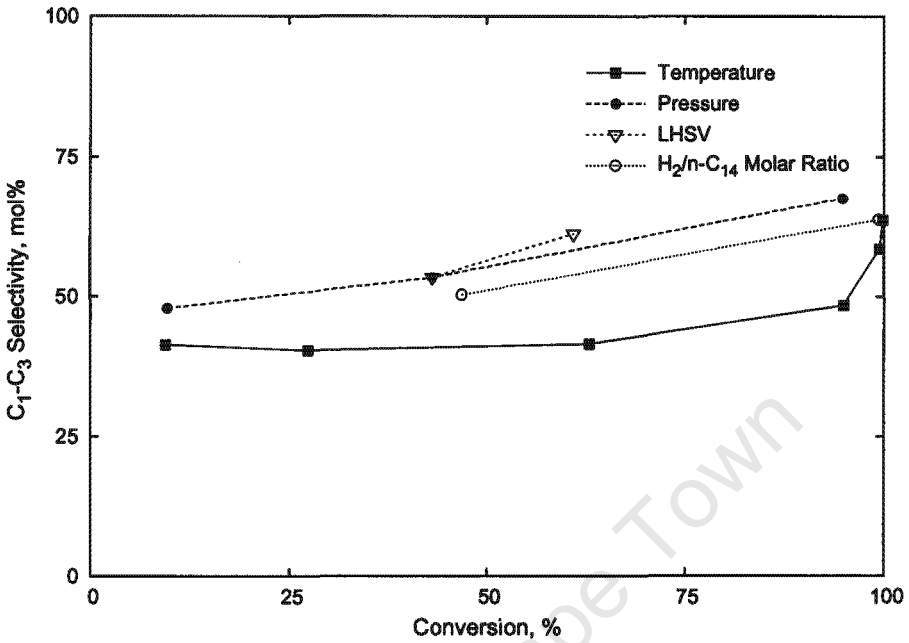

Figure 5.10: C_1-C_3 Selectivity for Different Series of Experiments

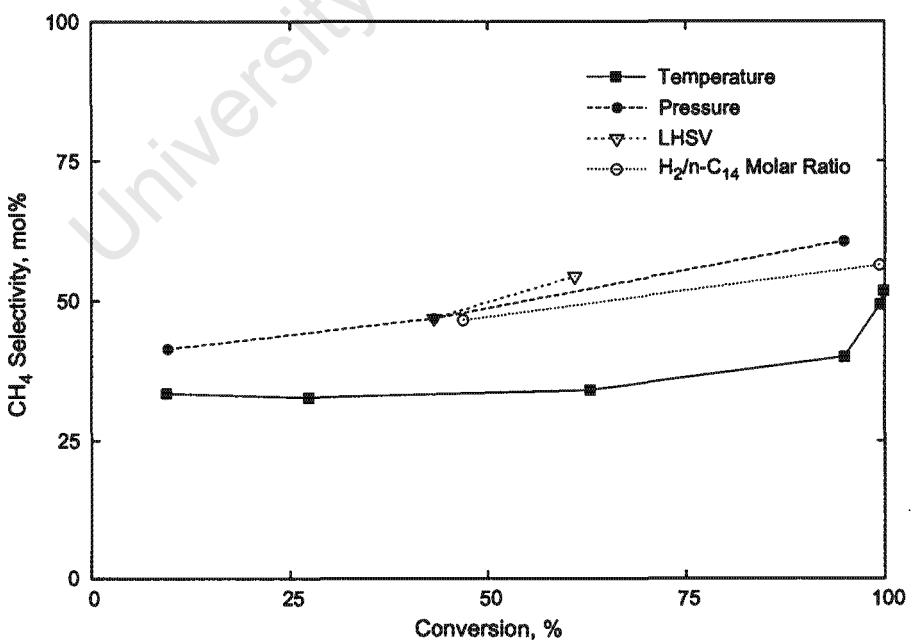

Figure 5.11: CH_4 Selectivity for Different Series of Experiments

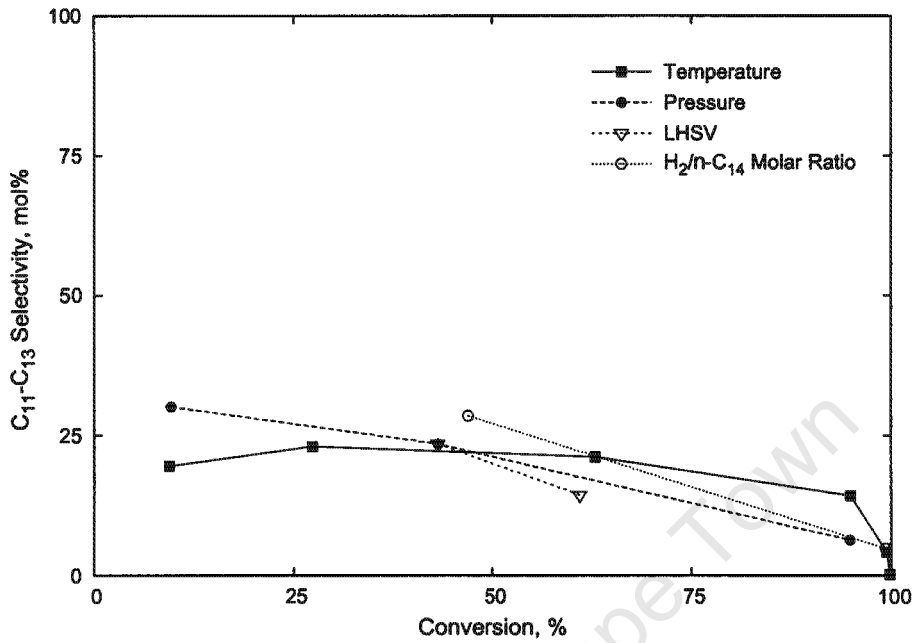

Figure 5.12: C_{11}-C_{13} Selectivity for Different Series of Experiments

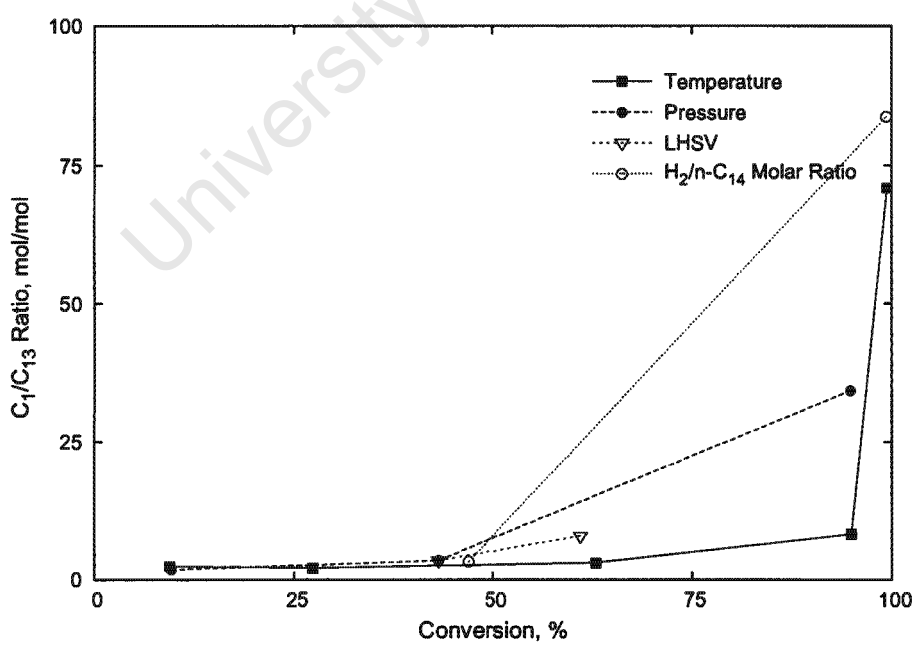

Figure 5.13: C_1/C_{13} Molar Ratio for Different Series of Experiments

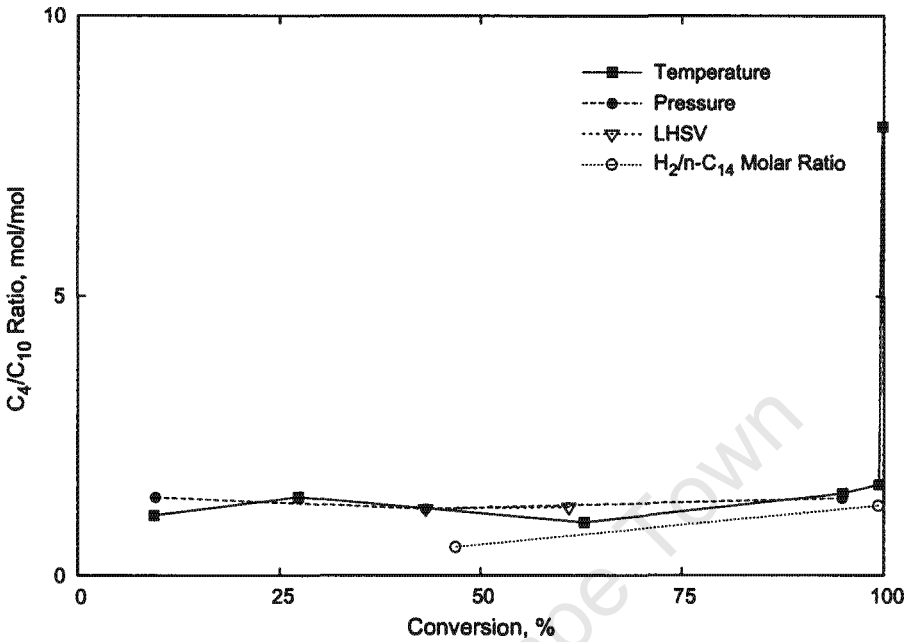

Figure 5.14: C_4/C_{10} Molar Ratio for Different Series of Experiments

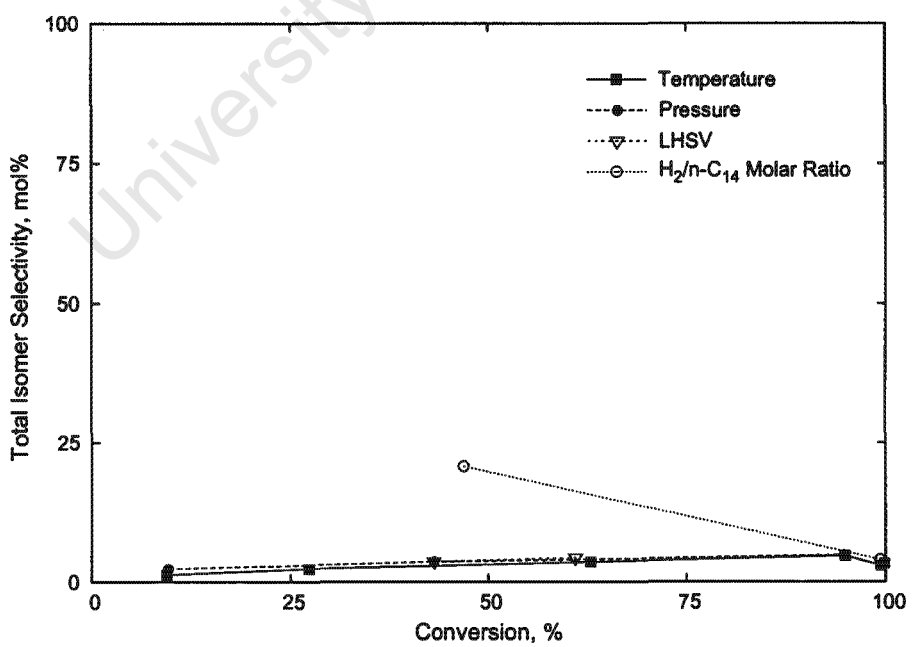

Figure 5.15: Total Isomer Selectivity for Different Series of Experiments

Results show that with increasing conversion there was an increased light gas (C_1-C_3) selectivity especially in methane (see figures 5.10 and 5.11) and decreasing C_{11}-C_{13} selectivity (see figure 5.12). With this observation a shift in the mid-carbon number range to the lower carbon number range was also observed as indicated by increasing C_1/C_{13} and C_4/C_{10} ratios (see figures 5.13 and 5.14). Similar trends appear in figures 4.10 and 4.11 and table 4.2 where conversion is increased by increasing temperature.

The above indicates that with increasing n-C_{14} conversion there is a shift from primary cracking to secondary cracking.

Note the apparent paradox that C_1 selectivity is lower at very high H_2/n-C_{14} molar ratios as was applied for the temperature series (molar H_2/n-C_{14} ratio of 116 instead of 10 for the majority of the other experiments, see figure 5.11).

Figure 5.15 shows that the degree of isomerisation increases significantly with increasing conversion, however still at very low levels <5 mol%. Apparently, a very low H_2/n-C_{14} ratio (3 mol/mol represented by the data point at 46.9%) accelerates isomerisation.

5.4 Effect of Reaction Conditions on Conversion

The temperature series showed increasing conversion with an increase in reaction temperature (see figure 4.9), as expected. Also, as expected, a decrease in space velocity resulted in an increase in conversion (see figure 4.18).

Pressure and H_2/n-C_{14} ratio experiments showed a decreasing conversion with an increase in total pressure (figure 4.14) and an increasing conversion with an increase in H_2/n-C_{14} ratio (see figure 4.22). The former trend was not expected. However, the picture changes when conversion is plotted as a function of partial pressures (figures 5.16 - 5.19). Hydrocracking literature indicates that an increase in hydrogen partial pressure would result in an increase in conversion (see section 1.6.3.2). This was also observed when the H_2 partial pressure increased due to increasing the H_2/n-C_{14} ratio (figure 5.18) but not as a result of increasing the total pressure (figure 5.19). In contrast, conversion changes were consistent when increasing the n-C_{14} partial pressure (i.e. by both decrease of the H_2/n-C_{14} ratio as well as increase of the total pressure, see figure 5.16 and 5.17).

Therefore the pressure effect that is observed in this study is not a result of hydrogen partial pressure, but is rather a result of the n-C_{14} partial pressure. It appears, as if the adsorbed n-C_{14} species are inhibiting the hydrogenolysis reactions.

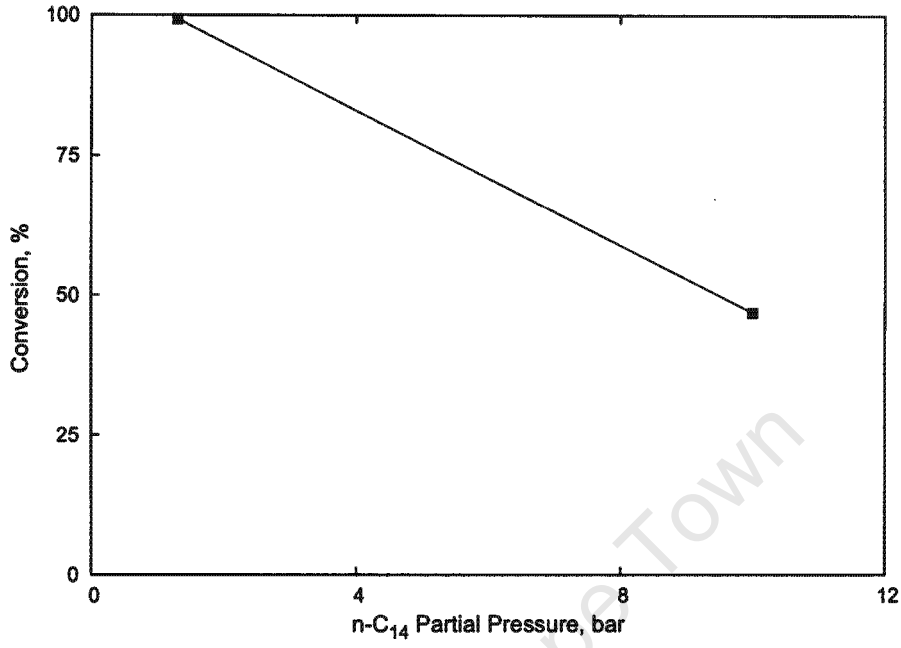

Figure 5.16: Effect of n-C_{14} Partial Pressure on Conversion: Molar Ratio Experiments
T=330°C, P=40 bar, LHSV=0.5 h^{-1}

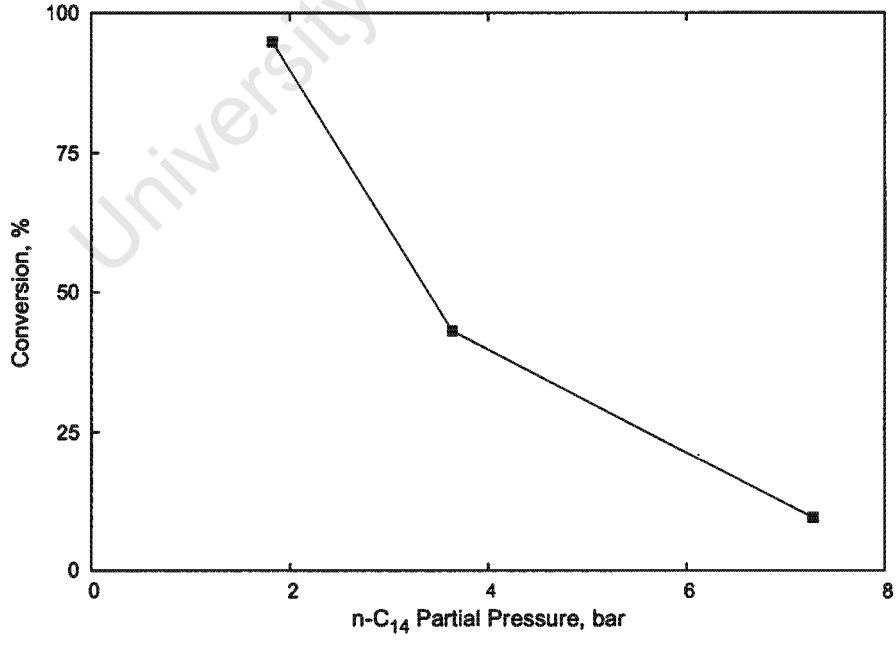

Figure 5.17: Effect of n-C_{14} Partial Pressure on Conversion: Pressure Experiments
T=330°C, LHSV=1.3 h^{-1}, H_2/n-C_{14}=10 mol/mol

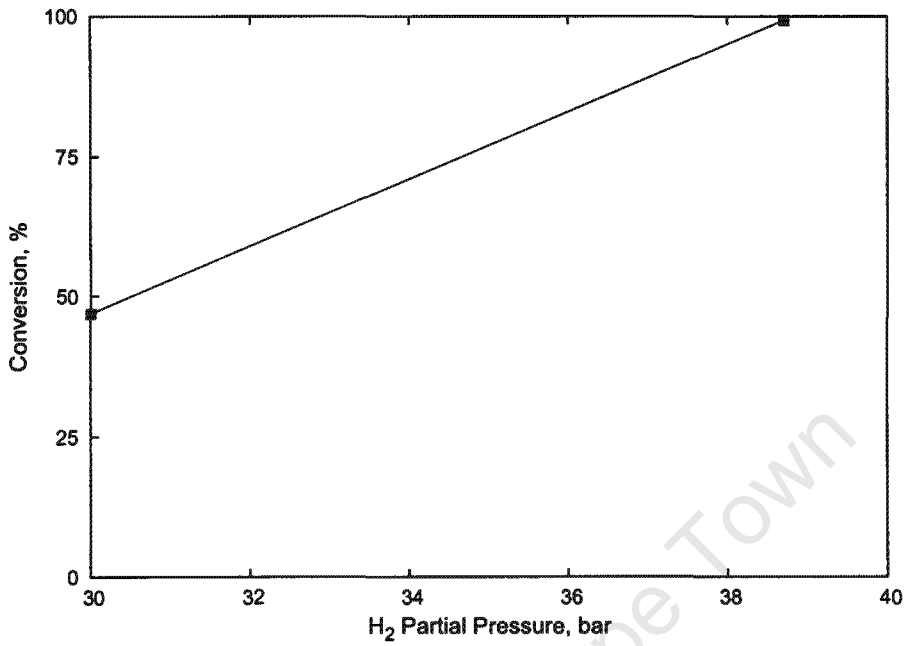

Figure 5.18: Effect of the H_2 Partial Pressure on Conversion: Molar Ratio Experiments
T=330°C, P=40 bar, LHSV=0.5 h^{-1}

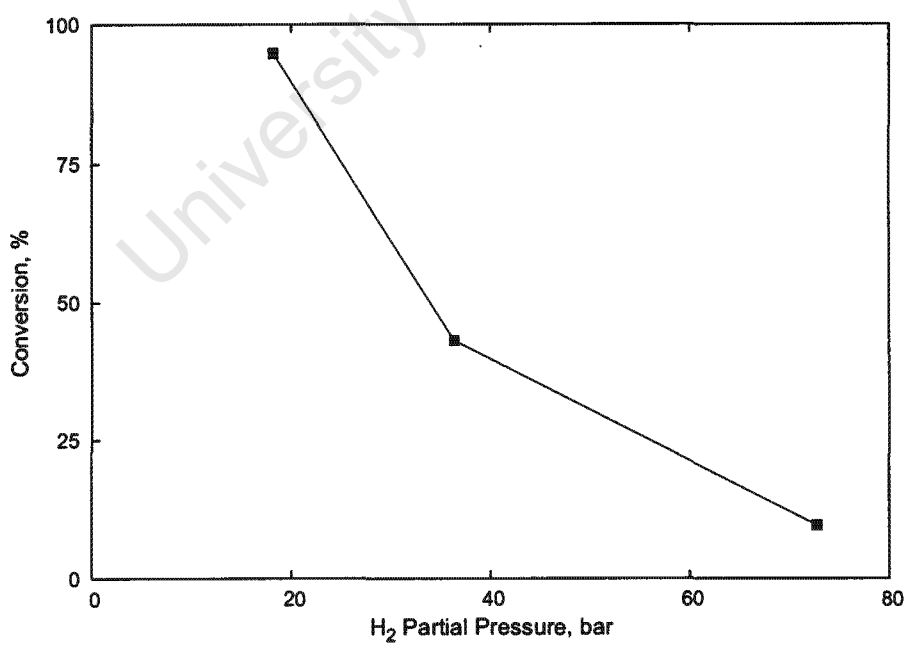

Figure 5.19: Effect of the H_2 Partial Pressure on Conversion: Pressure Experiments
T=330°C, LHSV=1.3 h^{-1}, H_2/n-C_{14}=10 mol/mol

5.5 n-C_{14} Adsorption Effects

Some results appear to be a paradox. Firstly, high n-C_{14} partial pressures reduce conversion, with n-C_{14} apparently having an inhibiting effect. Such inhibiting effects are usually associated with high occupation of the catalyst surface by the respective species. This is not a surprise since many of the experiments were carried out in mixed phase, i.e. with some liquid feed present in the catalyst bed (see table 4.1) or at conditions where the bulk fluid phase is vapour but capillary condensation may still occur in the pores of the catalyst.

Secondly, low C_1 selectivity is observed at high H_2/n-C_{14} ratios i.e. very low n-C_{14} partial pressure. It can be speculated in accordance to Sinfelt (1973), see section 1.4.2.1, that 'non-selective' hydrogenolysis, which results in random bond cleavage over the length of the chain, requires spatially demanding, 'flat' adsorption with a double bond at the central part of the hydrocarbon chain on the catalyst surface, whereas for demethylation the carbon chain might be adsorbed with a double bond at the terminal carbon, i.e. almost perpendicularly to the catalyst surface and in that way requiring less space. Under conditions of high surface occupancy by n-C_{14}, i.e. at high n-C_{14} partial pressure, the 'non-selective' hydrogenolysis mechanism would be suppressed resulting in preference for the methanolysis mechanism, i.e. higher C_1 selectivity.

Finally, methane selectivity does not increase with increasing temperature (as long as conversion is <99%), as one might expect (see table 4.2 and figure 5.11). Accelerated methane formation at higher temperature may be balanced by accelarated 'non-selective' cracking due to the reduced occupation of the catalyst surface.

The three phenomena addressed above are consistent, supporting the conclusion of high surface occupancy by n-C_{14} at high n-C_{14} partial pressure.

5.6 Isomerisation

Increasing selectivity to skeletal isomers was observed with decreasing H_2/n-C_{14} ratio (table 4.2, 330°C data and table 4.5). The lower the H_2/n-C_{14} ratio, i.e. the hydrogen partial pressure, the higher the equilibrium partial pressure of olefins in the reaction system, see figure 5.1. Since olefins are reactive over the acid constituent of the catalyst, namely the SiO_2-Al_2O_3 carrier, acid catalysed isomerisation and possibly acid catalysed isomerisation/cracking (for the mechanism see figures 1.4 and 1.6) are accelerated at low H_2/n-C_{14} ratios (see figure 5.4 and section 5.2) resulting in higher branching of the product.

6 Conclusions

With increasingly stringent legislation in respect of transportation fuel specifications, a growing demand for high quality diesel fuel is likely to be met by synthetic production via proposed GTL plants based on F-T synthesis of heavy hydrocarbon wax followed by hydrocracking of the wax. As this feedstock differs substantially from conventional refinery feedstocks, existing hydrocracking catalysts and processes are not necessarily optimized for use in the GTL environment. Consequently, and recognising the high value of wax feedstock to the GTL hydrocracking stage, selective wax hydrocracking presents a significant opportunity for improving overall GTL performance.

Non-sulphided conventional hydrocracking catalysts, such as $CoMo/SiO_2$-Al_2O_3, proved suitable for F-T wax hydrocracking, although the mechanism appears to be hydrogenolysis and hydrogenolytic methyl abstraction ('methanolysis') rather than 'true', acid catalysed hydrocracking. It must be noted that due to the application of the catalyst in its non-sulphided form, no sulphur is introduced to the product.

The high yields of linear paraffins observed in the mid-carbon number range (C_4 - C_{10}), due to minimal isomerisation through the hydrogenolysis mechanism, would be of interest to high cetane number distillate fuel production from F-T wax. The challenge, therefore, may be to optimise the catalyst in its pretreatment, i.e. avoid/minimise the presence of metallic cobalt, and to optimise reaction conditions (eventually by keeping once through conversion somewhat below 100%) so as to avoid additionally observed high methane and light gas yields which correspond to undesired fuel gas and undesired poor quality gasoline (naphtha) in the case of wax feedstock.

Bibliography

F. Alvarez, F. R. Ribeiro, G. Perot, C. Thomazeau, and M. Guisnet. Hydroisomerization and hydrocracking of alkanes. *Journal of Catalysis*, 162:179–189, 1996.

J. R. Anderson and N. R. Avery. Mechanism of isomerization of aliphatic hydrocarbons at a platinum surface. *Journal of Catalysis*, 7:315–323, 1967.

K. Andrews, F. M. Anderson, A. Baronova, H. Horth, N. Kilde, H. V. Larsen, and T. Zabel. Study on investment and employment related to EU policy on air, water and waste. Technical report, European Commission Directorate General - Environment, WRc Medmenham, Henley Road, Medmenham, Marlow, Bucks, SL7 2HD, 2000. Final report annex 1, Best estimates of costs.

R. C. Archibald, B. S. Greensfelder, G. Holzman, and D. H. Rowe. Catalytic hydrocracking of aliphatic hydrocarbons. *Industrial Engineering Chemistry*, 52:745, 1960.

P. W. Atkins. *Physical Chemistry*. Oxford University Press, Oxford (England), 5^{th} edition, 1994.

A. Cimino, M. Boudart, and H. S. Taylor. Ethane hydrogenation-cracking on iron catalysts with and without alkali. *Journal of Physical Chemistry*, 58:796–800, 1954.

H. L. Coonradt and W. E. Garwood. Mechanism of hydrocracking. Reactions of paraffins and olefins. *Industrial Engineering Chemistry*, 3:38–45, 1964.

M. J. Corke. GTL technologies focus on lowering costs. *Oil & Gas Journal*, (9) 1998.

T. E. Daubert and R. P. Danner. *Physical and thermodynamic properties of pure chemicals: data compilations*. Hemisphere Pub. Corp, New York, 1989.

M. E. Dry. High quality diesel via the Fischer-Tropsch process - A review. *Journal of Chemical Technology and Biotechnology*, 77:43–50, 2001.

M. E. Dry. Practical and theoretical aspects of the catalytic Fischer-Tropsch process. *Applied Catalysis A: General*, 138:319–344, 1996.

M. E. Dry. Chemical concepts used for engineering purposes. *Studies in Surface Science and Catalysis*, 152:196–257, 2004.

P. Dufresne, P.H. Bigeard, and A. Billion. New developments in hydrocracking: low pressure high-conversion hydrocracking. *Catalysis Today*, 1:367–384, 1987.

H.-D. Eichhorn. Die Umsetzung von Chinolin und Wasserstoff an Nickel-Wolfram-Aluminiumoxid-Katalysatoren (The conversion of quinoline and hydrogen over nickel-tungsten-alumina catalysts). *PhD Thesis, University of Karlsruhe, Germany*, 1979.

J. Eilers, S. A. Posthuma, and S. T. Sie. The Shell middle distillate synthesis process (SMDS). *Catalysis Letters*, 7:253–270, 1990.

L. Fernandez and A. A. Keller. Cost-benefit analysis of methyl tert-butyl ether and alternative gasoline formulations. *Environmental Science & Policy*, 3:173–188, 2000.

J. P. Franck and J. F. Le Page. Catalysts for the hydrocracking of heavy gas oils into middle distillates. *Studies in Surface Science and Catalysis*, 7:792–803, 1981.

G. F. Froment. Kinetics of the hydroisomerization and hydrocracking of paraffins on a platinum containing bifunctional Y-zeolite. *Catalysis Today*, 1:455–473, 1987.

B. C. Gates, J. R. Katzer, and G. C. A. Schuit. *Chemistry of catalytic processes.* Chemical Engineering Series. McGraw-Hill, New York, 1979.

C. Kemball and H. S. Taylor. The catalytic decomposition of ethane and ethane hydrogen mixtures. *Journal of American Chemical Society*, 70:348–351, 1948.

C. E. Maier, P. H. Bigeard, J. Lemaire, and J. Taoka. *NPRA Annual Meeting, San Antonio Texas*, 1984.

C. Marcilly and J. P. Franck. Use of zeolite containing catalysts in hydrocracking. *Studies in Surface Science and Catalysis*, 5:93–104, 1980.

J. A. Martens and P. A. Jacobs. Introduction to acid catalysis with zeolites in hydrocarbon reactions. *Studies in Surface Science and Catalysis*, 137:633–671, 2001.

I. E. Maxwell. Zeolite catalysis in hydroprocessing technology. *Catalysis Today*, 1:385–413, 1987.

J. A. Muñoz Arroyo, G. G. Martens, G. F. Froment, G. B. Marin, P. A. Jacobs, and J. A. Martens. Hydrocracking and isomerisation of n-paraffin mixtures and a hydrotreated gasoil on Pt/ZSM-22: confirmation of pore mouth and key-lock catalysis in liquid phase. *Applied Catalysis A: General*, 192:9–22, 2000.

S. I. Sandler. *Chemical and engineering thermodynamics.* Wiley, New York, 1989.

J. Scherzer and A. J. Gruia. *Hydrocracking Science and Technology.* Dekker, New York, 1996.

H. Schulz and H.-D. Eichhorn. Hydrogenative quinoline denitrification on nickel-tungsten-alumina. *Studies in Surface Science and Catalysis*, 7:1474–1475, 1981.

H. Schulz and N. M. Rahman. Elementary steps of hydrogenative sulphur-, nitrogen- and oxygen-removal from organic compounds on sulphided catalysts. *Studies in Surface Science and Catalysis*, 75:585–596, 1993.

H. Schulz, M. Schon, D. Eichhorn, and N. M. Rahman. Comparative study of hydrogenative cleavage of nitrogen from quinoline and isoquinoline. *Chemie Ingenieur Technik*, 59:148–152, 1987.

J. M. Schweitzer, P. Galtier, and D. Schweich. A single events kinetic model for the hydrocracking of paraffins in a three-phase reactor. *Chemical Engineering Science*, 54: 2441–2452, 1999.

SET Laboratories Inc. `http://www.setlaboratories.com/hydrocra.htm`, 2002. Last visited June 2002.

P. P. Shah, G. C. Sturtevant, J. H. Gregor, M. J Humbach, F. G. Padrta, and K. Z. Steigleder. Fischer-Tropsch wax characterisation and upgrading: Final report. Technical report, U.S. Department of Energy, Pittsburgh Energy Technology Center, Pittsburgh, Pennsylvania, 6 June 1988. By UOP Inc., Des Plaines, Illinois, and Allied-Signal Engineering Materials Research Center, Des Plaines, Illinois.

S. T. Sie, M. M. G. Senden, and H. M. H. van Wechem. Conversion of natural gas to transportation fuels via the Shell Middle Distillate Synthesis Process (SMDS). *Catalysis Today*, 8:371–394, 1991.

J. H. Sinfelt. Specificity in catalytic hydrogenolysis by metals. *Advances in Catalysis*, 23: 91–119, 1973.

J. H. Sinfelt. Catalytic hydrogenolysis over supported metals. *Catalysis Reviews*, 3: 175–205, 1969.

J. W. M. Sonnemans, F. J. Plantenga, P. H. Desai, V. J. D'Amico, and P. H. Dixon. Mild hydrocracking of heavy oils in the eighties. Technical report, Akzo Chem. Nederland - Ketjen Catal., Amsterdam, Neth. Natl. Pet. Refiners Assoc., 1984.

D. R. Stull, E. F. Westrum Jr., and C. S. Gerard. *The chemical thermodynamics of organic compounds.* Wiley, New York, 1969.

S. C. Thompson and J. F. Mathews. Characterisation of hydro-cracking catalysts by acidity measurement. *Applied Catalysis*, 47:45–57, 1989.

H. Topsøe, B. S. Clausen, and F. E. Massoth. Hydrotreating catalysis. *Catalysis - Science and Technology*, 11:29–33, 1996.

UOP. Diesel fuel - specifications and demand for the 21^{st} century. `http://www.uop.com/solutions_and_innovations/issues&solutions/UOPDieselfuel.pdf`, 1998. Last visited August 2002.

`http://www.cheresources.com/refining5.shtml`. Students' guide to refining, 2004. Last visited January 2005.

G. E. Weismantel. *Petroleum Processing Handbook.* Dekker, New York, 1992.

J. Weitkamp, P. A. Jacobs, and J. A. Martens. Isomerization and hydrocracking of C_9 through C_{16} n-alkanes on platinum/HZSM-5 zeolite. *Applied Catalysis*, 8:123, 1983.

APPENDICES

Methanolysis Model

A

- Results of Methyl Abstraction Hydrogenolysis Model (section 5.2.2) tables A.1 (300°C, 310°C and 320°C) and A.2 (330°C and 340°C)
- Normalised Selectivity Results of the Methyl Abstraction Model table A.3

Table A.1: Results of Methyl Abstraction Hydrogenolysis Model: 300°C, 310°C and 320°C

Temperature*		300°C			310°C			320°C	
Carbon	Adsorbed mols	Desorbed^{o} mols	C_1#^{o} mols	Adsorbed mols	Desorbed^{o} mols	C_1#^{o} mols	Adsorbed mols	Desorbed^{o} mols	C_1#^{o} mols
1		1.549	1.549		1.449	1.449		1.732	1.732
2	0.00000	0.00001	0.00009	0.00000	0.00000	0.00002	0.00003	0.00004	0.00053
3	0.00001	0.00002	0.00022	0.00000	0.00001	0.00006	0.00008	0.00010	0.00115
4	0.00003	0.00006	0.00057	0.00001	0.00002	0.00018	0.00018	0.00025	0.00248
5	0.00009	0.00016	0.00145	0.00003	0.00006	0.00053	0.00043	0.00059	0.00529
6	0.00025	0.00045	0.00363	0.00009	0.00019	0.00152	0.00102	0.00139	0.01112
7	0.00070	0.00128	0.00897	0.00027	0.00061	0.00428	0.00241	0.00329	0.02303
8	0.00198	0.00361	0.02168	0.00089	0.00197	0.01184	0.00570	0.00779	0.04671
9	0.00560	0.01019	0.05097	0.00286	0.00637	0.03184	0.01348	0.01842	0.09210
10	0.01579	0.02876	0.11503	0.00923	0.02054	0.08218	0.03191	0.04359	0.17434
11	0.04455	0.08112	0.24336	0.02977	0.06629	0.19886	0.07549	0.10313	0.30939
12	0.12567	0.22883	0.45766	0.09606	0.21387	0.42775	0.17862	0.24401	0.48803
13	0.35450	0.64550	0.64550	0.30993	0.69007	0.69007	0.42264	0.57736	0.57736
14	1			1			1		
Calculated C_1/C_{13}**		2.40			2.10			3.00	
Measured C_1/C_{13}**		2.40			2.10			3.00	
Absolute Error		5.08E-08			1.76E-05			6.53E-05	
Alpha (α)		0.35			0.31			0.42	
Sum Mols		2.55			2.45			2.73	

#C_1 = Mols methane formed

*Reaction temperature

**Molar Ratio

^{o} To columns *desorbed mols* and *C_1 formed mols*:

Note that 1 mol of C_{13} desorbed corresponds to 1 mol of C_1 formed. 1 mol of C_{12} desorbed corresponds to 2 mols of C_1 formed, and so on, $C_{14} \rightarrow C_i + (14-i)C_1$ (according to equation 5.1, section 5.2.2)

Table A.2: Results of Methyl Abstraction Hydrogenolysis Model: 330°C and 340°C

Temperature*		330°C			340°C		350°C[x]
Carbon	Adsorbed mols	Desorbed[o] mols	C_1[#o] mols	Adsorbed mols	Desorbed[o] mols	C_1[#o] mols	
1		2.838	2.838		2.168	2.168	
2	0.00612	0.00324	0.03885	0.68886	0.02173	0.26078	
3	0.00935	0.00495	0.05445	0.71059	0.02242	0.24659	
4	0.01430	0.00757	0.07570	0.73301	0.02312	0.23125	
5	0.02187	0.01157	0.10417	0.75613	0.02385	0.21469	
6	0.03345	0.01770	0.14160	0.77998	0.02461	0.19685	
7	0.05115	0.02707	0.18946	0.80459	0.02538	0.17768	
8	0.07822	0.04139	0.24833	0.82997	0.02618	0.15710	
9	0.11960	0.06329	0.31644	0.85616	0.02701	0.13505	
10	0.18289	0.09678	0.38711	0.88317	0.02786	0.11145	
11	0.27967	0.14799	0.44397	0.91103	0.02874	0.08622	
12	0.42766	0.22630	0.45260	0.93977	0.02965	0.05929	
13	0.65396	0.34604	0.34604	0.96942	0.03058	0.03058	
14	1			1			
Calc. C_1/C_{13}**		8.20			70.90		
Actual C_1/C_{13}**		8.20			70.90		
Absolute Error		1.34E-05			2.37E-05		
Alpha		0.65			0.97		
Sum Mols		3.83			2.48		

[#]C_1 = Mols methane formed

*Reaction temperature

[x]No C_{13} compounds found in the product anymore

**Molar Ratio

[o] To columns *desorbed mols* and *C_1 formed mols*:

Note that 1 mol of C_{13} desorbed corresponds to 1 mol of C_1 formed. 1 mol of C_{12} desorbed corresponds to 2 mols of C_1 formed, and so on, $C_{14} \rightarrow C_i + (14-i)C_1$ (according to equation 5.1, section 5.2.2)

Table A.3: Normalised Selectivity Results of the Methyl Abstraction Model

Carbon	300°C	310°C	320°C	330°C	340°C
1	60.77	59.17	63.40	74.06	87.45
2	0.00	0.00	0.00	0.08	0.88
3	0.00	0.00	0.00	0.13	0.90
4	0.00	0.00	0.01	0.20	0.93
5	0.01	0.00	0.02	0.30	0.96
6	0.02	0.01	0.05	0.46	0.99
7	0.05	0.02	0.12	0.71	1.02
8	0.14	0.08	0.28	1.08	1.06
9	0.40	0.26	0.67	1.65	1.09
10	1.13	0.84	1.60	2.53	1.12
11	3.18	2.71	3.77	3.86	1.16
12	8.98	8.73	8.93	5.91	1.20
13	25.32	28.18	21.13	9.03	1.23
Total	100.00	100.00	100.00	100.00	100.00

Calculations

B

- Thermodynamic Equilibrium Data for Paraffins Hydrocracking, table B.1
- Dilution Rates, table B.2
- Reaction Phase Calculations, tables B.3 – B.8
  - Assumes ideal gas
  - Assumes only n-C_{14} present with no lights (crude approach based on the boiling point of n-C_{14})
- Thermodynamic Equilibrium Calculations of Olefins Concentration in the Product, table B.7

Only the overall reaction scheme was considered for thermodynamic evaluation of the hydrocracking of n-paraffins. The following reaction was taken as an example:

$$n\text{-}C_{14} + H_2 \rightleftharpoons 2\, n\text{-}C_7 \tag{B.1}$$

$$K = \frac{P_{C_7}^2}{P_{C_{14}} \cdot P_{H_2}} \tag{B.2}$$

$$\Delta G_R^o = 2\,\Delta G_{f,n-C_7}^o - \Delta G_{f,n-C_{14}}^o \tag{B.3}$$

$$X = \sqrt{\frac{1}{1+\frac{4}{K}}} \tag{B.4}$$

Table B.1: Thermodynamic Equilibrium Data for Paraffins Hydrocracking at 1/1 Molar H_2/n-C_{14} Feed Ratio (thermodynamic data from Daubert and Danner, 1989)

T, °C	T, K	K(T)	$X_{crack,eq}$
150	423	2.67E+06	1.00
160	433	2.00E+06	1.00
170	443	1.52E+06	1.00
180	453	1.16E+06	1.00
190	463	9.04E+05	1.00
200	473	7.10E+05	1.00
210	483	5.63E+05	1.00
220	493	4.51E+05	1.00
230	503	3.64E+05	1.00
240	513	2.97E+05	1.00
250	523	2.44E+05	1.00
260	533	2.02E+05	1.00
270	543	1.68E+05	1.00
280	553	1.41E+05	1.00
290	563	1.19E+05	1.00
300	573	1.01E+05	1.00
310	583	8.60E+04	1.00
320	593	7.38E+04	1.00
330	603	6.36E+04	1.00
340	613	5.52E+04	1.00
350	623	4.80E+04	1.00
360	633	4.20E+04	1.00
370	643	3.69E+04	1.00
380	653	3.25E+04	1.00
390	663	2.88E+04	1.00
400	673	2.55E+04	1.00

Table B.2: Calculated Minimum Dilution Gas Flow Rates for Varying n-C_{14} Space Velocity Based on eq. (3.1), section 3.5.1

(Note that the dilution gas flow rate is made up by both feed hydrogen flow and dilution hydrogen flow. Also note that no additional dilution was required when running at high H_2/n-C_{14} molar ratio of 116:1. Dilution gas flow rate was kept just high enough to maintain pressure control)

LHSV (h^{-1})	**Dilution Gas Flow Rate (sccm)**
0.2	86
0.5	215
1.0	430
1.3	560

Reaction phase calculations:

- Assumes ideal gas
- Assumes only n-C_{14} present with no lights (crude approach based on the boiling point of n-C_{14})

Phase calculations are based on the following formula (Daubert and Danner, 1989):

$$P_{vap}(T) = exp\left\{A + \frac{b}{T} + C \cdot ln(T) + DT^2\right\} \tag{B.5}$$

$A = 140.47$

$B = -1.3231 \times 10^4$

$C = -16.859$

$D = 6.5877 \times 10^{-6}$

The criterion in this crude approach for having pure gas/vapour phase or a mixed phase containing liquid n-C_{14}, was the presence of n-C_{14} at the reaction temperature being higher or lower of what results at the calculated partial pressure of the pure compound.

Table B.3: Phase Calculations for Temperature Reactions (Rep = reproduction)

Temperature	300	310	320	330	340	350	350 Rep	320 Rep
Pressure	80	80	80	80	80	80	80	80
LHSV	0.2	0.2	0.2	0.2	0.2	0.2	0.2	0.2
Molar Ratio	116	116	116	116	116	116	116	116
P_{H_2}	79.3	79.3	79.3	79.3	79.3	79.3	79.3	79.3
$P_{C_{14}}$ in	0.7	0.7	0.7	0.7	0.7	0.7	0.7	0.7
$P_{C_{14}}$ out	0.6	0.4	0.1	0.0	0.0	0.0	0.0	0.1
$P^{vap}_{C_{14}}$ (T)	2.6	3.1	3.7	4.4	5.2	6.0	6.0	3.7
Phase in	vapour	vapour	vapour	vapour	vapour	vapour	vapour	vapour
Phase out	vapour	vapour	vapour	vapour	vapour	vapour	vapour	vapour

Table B.4: Phase Calculations for Pressure Reactions (Rep = reproduction)

Temperature	330	330	330	330 Rep1	330 Rep2
Pressure	80	40	20	40	40
LHSV	1.3	1.3	1.3	1.3	1.3
Molar Ratio	10	10	10	10	10
P_{H_2}	72.0	36.0	18.0	36.0	36.0
$P_{C_{14}}$ in	8.0	4.0	2.0	4.0	4.0
$P_{C_{14}}$ out	6.4	1.3	0.0	0.5	1.4
$P^{vap}_{C_{14}}$ (T)	4.4	4.4	4.4	4.4	4.4
Phase in	mixed	mixed	vapour	mixed	mixed
Phase out	mixed	vapour	vapour	vapour	vapour

Table B.5: Phase Calculations for Space Velocity Reactions

Temperature	330	330	330
Pressure	40	40	40
LHSV	1.3	1.0	0.5
Molar Ratio	10	10	10
P_{H_2}	36.0	36.0	36.0
$P_{C_{14}}$ in	4.0	4.0	4.0
$P_{C_{14}}$ out	1.3	0.6	0.7
$P^{vap}_{C_{14}}$ (T)	4.4	4.4	4.4
Phase in	mixed	mixed	mixed
Phase out	vapour	vapour	vapour

Table B.6: Phase Calculations for H_2/n-C_{14} Molar Ratio Reactions (Rep = reproduction)

Temperature	330	330	330	330 Rep
Pressure	40	40	40	40
LHSV	0.5	0.5	0.5	0.5
Molar Ratio	3	10	30	3
P_{H_2}	26.7	36.0	38.7	26.7
$P_{C_{14}}$ in	13.3	4.0	1.3	13.3
$P_{C_{14}}$ out	4.2	0.7	0.0	8.1
$P^{vap}_{C_{14}}$ (T)	4.4	4.4	4.4	4.4
Phase in	mixed	mixed	vapour	mixed
Phase out	vapour	vapour	vapour	mixed

Table B.7: Calculated Thermodynamic Equilibrium Concentration of Olefins, expressed as 1-Olefin/n-Paraffin Molar Ratio for the Example in the C_4 Fraction

Pressure	$P_{1-Butene}$ / $P_{n-Butane}$ Molar Ratio					
bar	350°C	340°C	330°C	320°C	310°C	300°C
15	1.01E-05	6.67E-06	4.37E-06	2.83E-06	1.80E-06	1.13E-06
20	7.55E-06	5.01E-06	3.28E-06	2.12E-06	1.35E-06	8.50E-07
25	6.04E-06	4.00E-06	2.62E-06	1.70E-06	1.08E-06	6.80E-07
30	5.03E-06	3.34E-06	2.18E-06	1.41E-06	9.02E-07	5.67E-07
35	4.31E-06	2.86E-06	1.87E-06	1.21E-06	7.73E-07	4.86E-07
40	3.77E-06	2.50E-06	1.64E-06	1.06E-06	6.77E-07	4.25E-07
45	3.35E-06	2.22E-06	1.46E-06	9.42E-07	6.01E-07	3.78E-07
50	3.02E-06	2.00E-06	1.31E-06	8.48E-07	5.41E-07	3.40E-07
55	2.74E-06	1.82E-06	1.19E-06	7.71E-07	4.92E-07	3.09E-07
60	2.52E-06	1.67E-06	1.09E-06	7.07E-07	4.51E-07	2.83E-07
65	2.32E-06	1.54E-06	1.01E-06	6.52E-07	4.16E-07	2.62E-07
70	2.16E-06	1.43E-06	9.36E-07	6.06E-07	3.87E-07	2.43E-07
75	2.01E-06	1.33E-06	8.74E-07	5.65E-07	3.61E-07	2.27E-07
80	1.89E-06	1.25E-06	8.19E-07	5.30E-07	3.38E-07	2.13E-07

Thermodynamic Equilibrium Concentration of Olefins.

As an example the 1-butene/n-butane ratio is calculated (thermodynamic data, $\Delta G_f^o(T)$, obtained from Stull et al., 1969 and calculations based on Sandler, 1989)

$$n\text{-}C_{14} \rightleftharpoons H_2 + 1\text{-}C_4^= \tag{B.6}$$

$$\Delta G_R^o = \Delta G_{f,1-C_4^=}^o - \Delta G_{f,n-C_4}^o \tag{B.7}$$

$$K = exp\left\{\frac{-\Delta G_R^o}{RT}\right\} = \frac{P_{1-C_4^=} \cdot P_{H_2}}{P_{n-C_4}} \tag{B.8}$$

$$\frac{P_{1-C_4^=}}{P_{n-C_4}} = \frac{1}{P_{H_2}} \cdot exp\left\{\frac{-\Delta G_R^o}{RT}\right\} \tag{B.9}$$

Table B.8: Phase Calculations for Conditions Screening Reactions (Rep = reproduction)

Temperature	320	330	350	330 Rep	350
Pressure	80	80	80	80	40
LHSV	1.3	1.3	1.3	1.3	1.3
Molar Ratio	10	10	10	10	10
P_{H_2}	72.0	72.0	72.0	72.0	36.0
$P_{C_{14}}$ in	8.0	8.0	8.0	8.0	4.0
$P_{C_{14}}$ out	7.2	6.4	1.7	7.0	0.0
$P_{C_{14}}^{vap}$ (T)	3.7	4.4	6.0	4.4	6.0
Phase in	mixed	mixed	mixed	mixed	vapour
Phase out	mixed	mixed	vapour	mixed	vapour

Reactor Temperature Profiles

C

- Temperature Profiles over Reactor at:
  - 350°C
  - 330°C

Table C.1: Data of Temperature Profiles Over Reactor Length at Certain Set Temperatures

(bold numbers indicate the position of the catalyst bed)

Length	350°C	350°C REP*	330°C	330°C REP*
0	351	353	332	329
1	352	353	332	329
2	353	353	332	329
3	353	353	333	329
4	354	353	333	329
5	354	352	332	329
6	354	352	331	329
7	353	351	330	329
8	353	351	329	329
9	353	351	328	329
10	352	350	328	329
11	352	350	328	329
12	352	349	328	329
13	352	349	328	329
14	352	349	328	329
15	**352**	**350**	**328**	**329**
16	**352**	**350**	**328**	**330**
17	**352**	**350**	**328**	**330**
18	**352**	**350**	**328**	**330**
19	**352**	**350**	**328**	**330**
20	**352**	**350**	**328**	**330**
21	352	350	329	330
22	352	350	329	331
23	352	350	329	331
24	352	350	330	332
25	352	350	330	332
26	352	350	330	332
27	352	350	330	332
28	352	350	329	331
29	352	350	327	329
30	352	349	324	327
31	352	347	323	326
32	352	346	318	322
33	352	344	312	316
34	352	340	306	310
35	352	338	300	304

*Reproduced Profiles

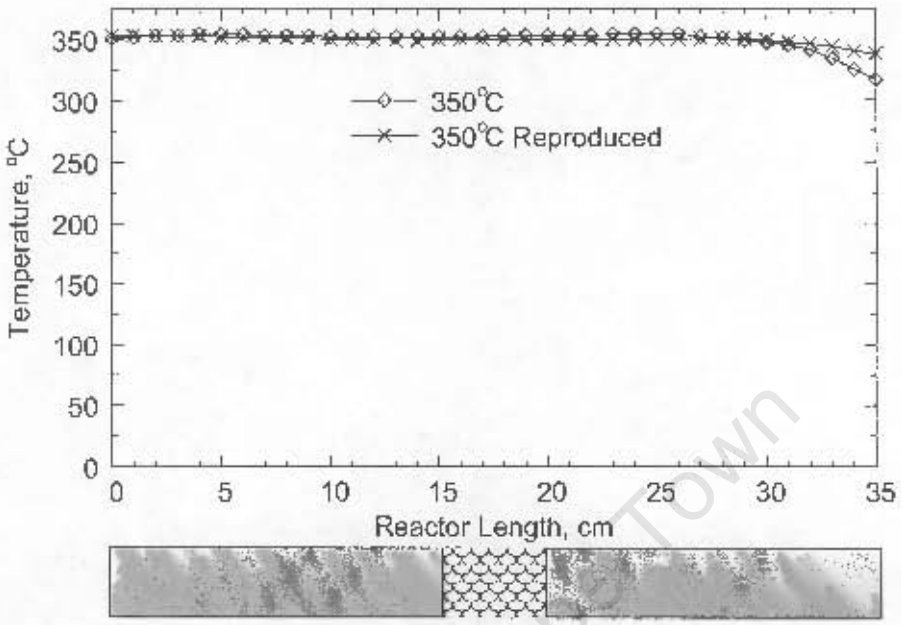

Figure C.1: Temperature Profile Over Reactor at 350°C Set Temperature

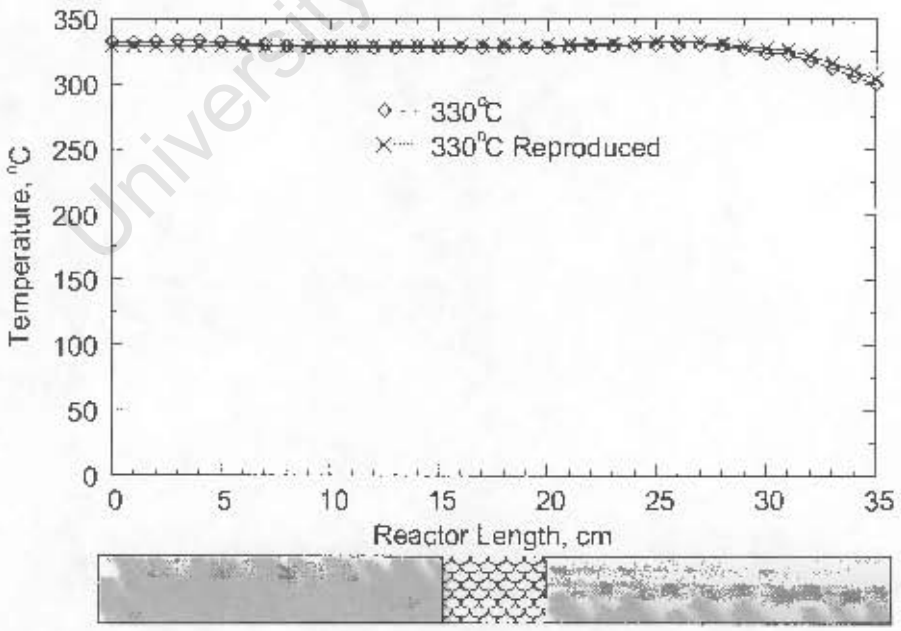

Figure C.2: Temperature Profile Over Reactor at 330°C Set Temperature

Data

D

- Gas Chromatogram of Hydrocracking Product, figure D.1

- Achieving Steady State Conditions for:
  - Temperature Experiments, table D.1
  - Pressure Experiments, table D.2
  - Space Velocity Experiments, table D.3
  - H_2/n-C_{14} Molar Ratio Experiments, table D.4

- Effect of Temperature
  - Iso + Normal Paraffins, table D.5
  - Normal Paraffins, table D.6
  - Iso Paraffins, table D.7
- Effect of Pressure
  - Iso + Normal Paraffins, table D.8
  - Normal Paraffins, table D.9
  - Iso Paraffins, table D.10
- Effect of Space Velocity
  - Iso + Normal Paraffins, table D.11
  - Normal Paraffins, table D.12
  - Iso Paraffins, table D.13
- Effect of H_2/n-C_{14} Molar Ratio

  - Iso + Normal Paraffins, table D.14
  - Normal Paraffins, table D.15
  - Iso Paraffins, table D.16

- Conditions Screening Experiments
  - Iso + Normal Paraffins, table D.17
  - Normal Paraffins, table D.18
  - Iso Paraffins, table D.19

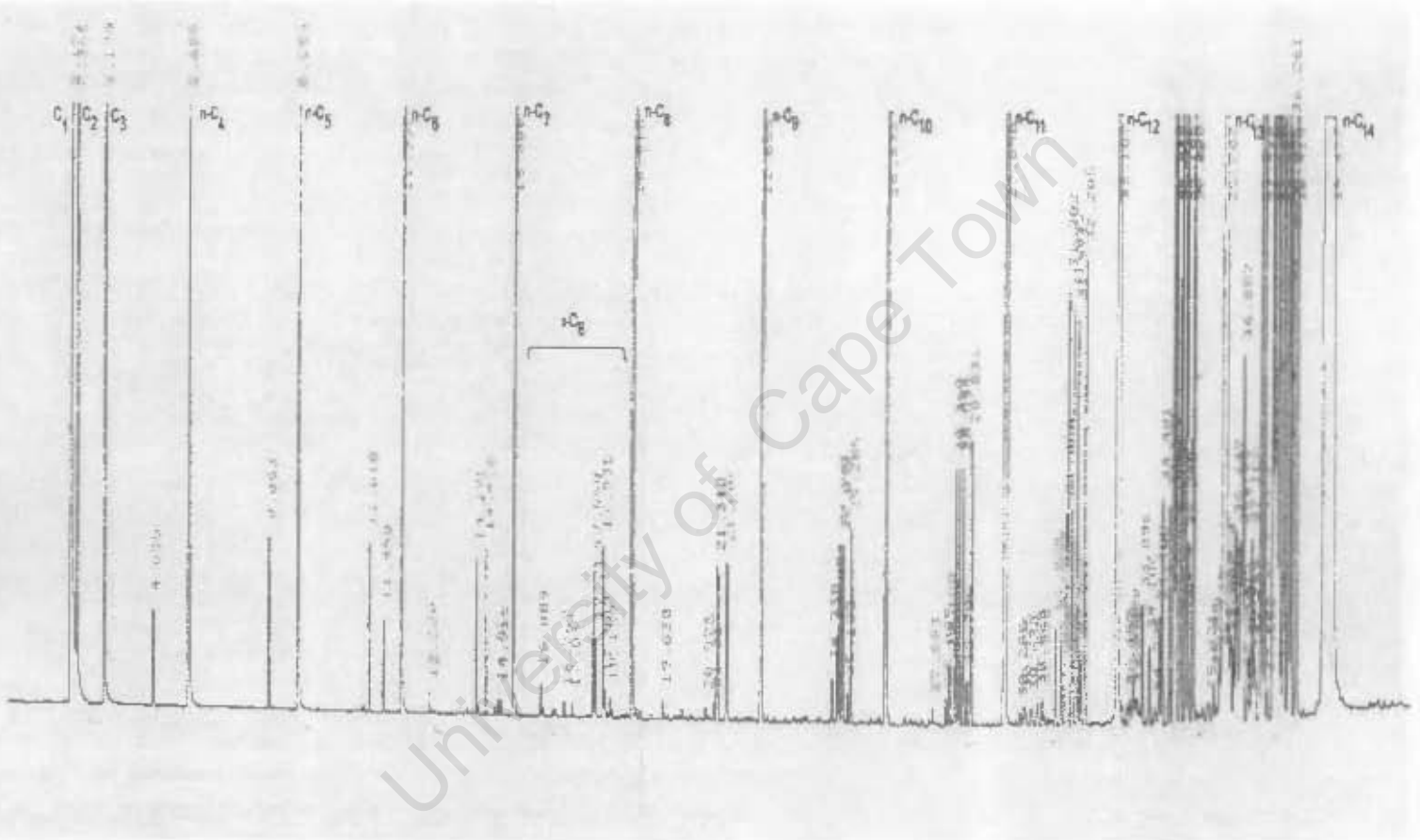

Figure D.1: Gas Chromatogram of Hydrocracking Product
(The series of high peaks marks the n-paraffins. All peaks between two n-paraffins are considered as isomers of the higher one, see for example i-C_8. No products higher than the feed compound, n-C_{14}, are obtained)

Table D.1: Achieving Steady State Conditions for Temperature Experiments

C_{14} Conversion and Selectivity to Iso + Normal Paraffins (mol%)
T=350°C, P=80 bar, LHSV=0.2 h^{-1}, H_2/n-C_{14}=116 mol/mol,
Phase in: Vapour, Phase out: Vapour

	TOS				
Carbon No.	+48h	72h	96h	120h	123h
1	64.5	47.9	50.8	52.7	51.8
2	3.2	5.1	5.4	5.6	5.6
3	3.7	5.6	6.1	6.1	6.3
4	4.0	5.9	6.6	6.8	6.9
5	4.7	6.9	7.6	7.8	7.6
6	4.5	6.7	7.3	7.3	7.7
7	4.0	6.1	6.3	6.3	6.4
8	3.5	5.2	4.7	4.1	4.2
9	2.8	4.0	3.1	2.2	2.4
10	1.9	3.1	1.4	0.8	0.9
11	1.3	2.1	0.5	0.2	0.2
12	1.1	1.1	0.1	0.0	0.0
13	0.8	0.3	0.0	0.0	0.0
14	0.0	0.0	0.0	0.0	0.0
Total	100.0	100.0	100.0	100.0	100.0
Conversion (%)	93.2	98.0	98.2	97.8	99.8

Table D.2: Achieving Steady State Conditions for Pressure Experiments

C_{14} Conversion and Selectivity to Iso + Normal Paraffins (mol%)
P=40 bar, T=330°C, LHSV=1.3 h^{-1}, H_2/n-C_{14}=10 mol/mol,
Phase in: Mixed, Phase out: Vapour

	TOS					
Carbon No.	+48h	50h	74h	170h	194h	196h
1	48.6	48.1	49.6	44.2	49.7	46.9
2	3.2	3.1	3.8	2.9	3.1	3.2
3	3.3	3.2	3.2	3.1	3.3	3.3
4	3.2	3.3	3.3	3.1	3.4	3.4
5	3.8	3.6	3.6	3.6	3.8	3.6
6	3.8	3.5	3.7	3.7	3.8	3.7
7	3.6	3.4	3.6	3.6	3.7	3.5
8	3.3	3.1	3.4	3.2	3.4	3.2
9	3.0	2.9	3.1	3.0	3.0	2.9
10	2.9	2.7	3.2	3.3	2.7	2.8
11	3.5	3.2	4.0	5.5	3.1	3.6
12	5.7	5.9	5.2	8.4	5.2	6.2
13	12.2	14.0	10.3	12.4	11.8	13.6
Total	100.0	100.0	100.0	100.0	100.0	100.0
Conversion (%)	43.1	39.0	46.3	43.0	41.8	43.1

Table D.3: Achieving Steady State Conditions for Space Velocity Experiments

C_{14} Conversion and Selectivity to Iso + Normal Paraffins (mol%)
LHSV=0.5 h^{-1}, T=330°C, P=40 bar, H_2/n-C_{14}=10 mol/mol, Phase in: Mixed, Phase out: Vapour

	TOS									
Carbon No.	148h	72h	96h	99h	101h	125h	127h	151h	152h	155h
1	45.5	40.0	36.8	41.8	44.1	43.9	45.7	46.5	44.9	44.4
2	2.4	2.0	1.8	2.1	2.2	2.3	2.3	2.4	2.3	2.3
3	2.6	2.2	2.0	2.3	2.5	2.5	2.6	2.7	2.5	2.5
4	2.8	2.3	2.1	2.4	2.6	2.6	2.7	2.8	2.7	2.6
5	3.2	2.7	2.5	2.8	3.0	3.0	3.1	3.2	3.1	3.0
6	3.4	2.9	2.7	3.1	3.3	3.3	3.4	3.5	3.3	3.3
7	3.5	3.1	2.9	3.3	3.5	3.5	3.5	3.6	3.4	3.4
8	3.4	3.3	3.2	3.6	3.7	3.7	3.7	3.7	3.6	3.5
9	3.4	3.8	3.6	4.0	3.9	4.1	4.0	3.9	3.9	3.8
10	4.0	4.9	4.9	4.4	4.2	4.5	4.6	4.5	4.5	4.5
11	5.6	6.7	7.1	5.9	5.1	5.5	5.4	5.3	5.6	5.8
12	8.8	9.9	11.1	8.9	7.8	8.0	7.4	7.1	8.0	8.2
13	11.4	16.2	19.4	15.2	14.3	13.3	11.6	10.9	12.1	12.6
Total	100.0	100.0	100.0	100.0	100.0	100.0	100.0	100.0	100.0	100.0
Conversion (%)	79.6	62.0	55.0	58.8	58.2	65.6	67.2	69.8	65.9	67.0

Table D.4: Achieving Steady State Conditions for H_2/n-C_{14} Molar Ratio Experiments

C_{14} Conversion and Selectivity to Iso + Normal Paraffins (mol%)
H_2/n-C_{14}=3 mol/mol, P=40 bar, T=330°C, LHSV=0.5 h^{-1}
Phase in: Liquid, Phase out: Vapour

	TOS			
Carbon No.	+51h	147h	149h	151h
1	35.7	48.3	49.5	46.6
2	1.6	1.7	2.1	1.7
3	1.9	2.0	2.0	2.0
4	2.1	2.2	2.2	2.2
5	2.4	2.5	2.4	2.5
6	2.7	2.6	2.6	2.6
7	2.9	2.8	2.8	2.8
8	3.3	3.1	3.1	3.2
9	3.7	3.5	3.5	3.6
10	4.3	4.1	4.0	4.3
11	6.0	5.2	5.0	5.5
12	10.6	8.2	7.7	8.5
13	22.8	13.8	12.9	14.5
Total	100.0	100.0	100.0	100.0
Conversion (%)	35.4	47.5	46.8	46.9

Table D.5: Effect of Temperature

Selectivity to Iso + Normal Paraffins (mol%)

P=80 bar LHSV=0.2 h^{-1}, H_2/n-C_{14}=116 mol/mol

Carbon	300°C	310°C	320°C	330°C	340°C	350°C	350°C Rep	320°C Rep
1	33.5	32.8	34.1	40.0	49.4	51.8	57.9	49.3
2	3.6	3.5	3.5	3.9	4.4	5.6	6.0	4.0
3	4.3	4.1	3.9	4.4	4.7	6.3	6.6	4.5
4	4.7	4.6	4.4	4.9	5.2	6.9	7.3	5.2
5	5.8	5.4	5.1	5.8	6.4	7.6	8.4	6.6
6	6.3	5.9	5.4	6.3	6.6	7.7	6.9	7.3
7	6.2	6.2	5.7	6.6	6.1	6.4	4.4	5.2
8	5.8	6.0	6.0	6.3	5.4	4.2	1.9	2.6
9	6.1	5.3	6.2	4.1	4.3	2.4	0.5	1.9
10	4.3	3.2	4.5	3.3	3.2	0.9	0.1	1.6
11	2.8	3.1	4.2	4.1	2.2	0.2	0.0	1.7
12	2.9	4.2	5.7	5.3	1.4	0.0	0.0	3.0
13	13.9	15.7	11.3	4.9	0.7	0.0	0.0	7.0
Total	100.0	100.0	100.0	100.0	100.0	100.0	100.0	100.0

For conversions see table 4.2

Table D.6: Effect of Temperature

Selectivity to Normal Paraffins (mol%)

P=80 bar LHSV=0.2 h^{-1}, H_2/n-C_{14}=116 mol/mol

Carbon	300°C	310°C	320°C	330°C	340°C	350°C	350°C Rep	320°C Rep
1	33.5	32.8	34.1	40.0	49.4	51.8	57.9	49.3
2	3.6	3.5	3.5	3.9	4.4	5.6	6.0	4.0
3	4.3	4.1	3.9	4.4	4.7	6.3	6.6	4.5
4	4.7	4.5	4.3	4.9	5.1	6.7	7.2	5.2
5	5.6	5.3	5.0	5.7	6.3	7.3	8.1	6.5
6	6.3	5.8	5.3	6.1	6.4	7.3	6.5	7.2
7	6.2	6.0	5.6	6.3	5.8	5.7	3.9	5.1
8	5.8	5.9	5.8	5.9	5.0	3.5	1.6	2.5
9	5.5	4.9	5.9	3.7	3.8	1.6	0.4	1.9
10	4.2	3.1	4.2	3.0	2.7	0.6	0.1	1.6
11	2.8	2.9	3.9	3.5	1.7	0.1	0.0	1.7
12	2.9	4.1	5.1	4.2	1.0	0.0	0.0	2.8
13	13.5	14.7	9.8	3.6	0.5	0.0	0.0	6.4
Total	98.7	97.7	96.4	95.3	97.1	96.6	98.3	98.7

Table D.7: Effect of Temperature

Selectivity to Iso Paraffins (mol%)

P=80 bar LHSV=0.2 h^{-1}, H_2/n-C_{14}=116 mol/mol

Carbon	300°C	310°C	320°C	330°C	340°C	350°C	350°C Rep	320°C Rep
1	0.0	0.0	0.0	0.0	0.0	0.0	0.0	0.0
2	0.0	0.0	0.0	0.0	0.0	0.0	0.0	0.0
3	0.0	0.0	0.0	0.0	0.0	0.0	0.0	0.0
4	0.0	0.1	0.1	0.1	0.1	0.1	0.1	0.0
5	0.1	0.1	0.1	0.1	0.1	0.3	0.2	0.1
6	0.0	0.1	0.1	0.2	0.2	0.5	0.4	0.1
7	0.0	0.1	0.2	0.3	0.3	0.6	0.5	0.1
8	0.0	0.1	0.2	0.4	0.4	0.7	0.3	0.1
9	0.6	0.4	0.2	0.4	0.4	0.8	0.1	0.0
10	0.1	0.1	0.3	0.4	0.5	0.3	0.0	0.1
11	0.0	0.1	0.3	0.6	0.5	0.1	0.0	0.1
12	0.0	0.2	0.6	1.1	0.3	0.0	0.0	0.2
13	0.4	1.0	1.6	1.3	0.2	0.0	0.0	0.5
Total	1.3	2.3	3.6	4.7	2.9	3.4	1.7	1.3

Table D.8: Effect of Pressure

Selectivity to Iso + Normal Paraffins (mol%)

T=330°C, LHSV=1.3 h^{-1}, H_2/n-C_{14}=10 mol/mol

Carbon	80 bar	40 bar	20 bar	40 bar REP	40 bar REP2
1	41.5	46.9	60.6	51.3	51.7
2	3.1	3.2	3.2	3.5	2.9
3	3.3	3.3	3.7	3.5	2.9
4	3.3	3.4	3.7	3.7	3.0
5	3.7	3.6	4.1	4.2	3.4
6	3.7	3.7	4.3	4.3	3.4
7	3.3	3.5	4.2	4.2	3.4
8	3.0	3.2	3.8	3.8	3.5
9	2.7	2.9	3.2	3.4	3.0
10	2.4	2.8	2.7	3.1	2.6
11	2.5	3.6	2.4	3.4	3.3
12	4.2	6.2	2.2	4.5	5.1
13	23.4	13.6	1.8	7.1	11.9
Total	100.0	100.0	100.0	100.0	100.0

For conversions see table 4.3

Table D.9: Effect of Pressure

Selectivity to Normal Paraffins (mol%)

T= 330°C, LHSV=1.3 h^{-1}, H_2/n-C_{14}=10 mol/mol

Carbon	80 bar	40 bar	20 bar	40 bar REP	40 bar REP2
1	41.5	46.9	60.6	51.3	51.7
2	3.1	3.2	3.2	3.5	2.9
3	3.3	3.3	3.7	3.5	2.9
4	3.3	3.4	3.6	3.6	2.9
5	3.6	3.6	3.9	4.1	3.3
6	3.7	3.6	4.0	4.2	3.4
7	3.3	3.4	3.8	3.9	3.2
8	3.0	3.1	3.2	3.6	3.3
9	2.7	2.7	2.6	3.1	2.7
10	2.4	2.6	2.1	2.8	2.4
11	2.5	3.3	1.7	2.9	3.0
12	4.2	5.6	1.4	3.7	4.4
13	21.2	11.8	1.1	5.8	10.0
Total	97.6	96.3	95.1	95.9	96.1

Table D.10: Effect of Pressure

Selectivity to Iso Paraffins (mol%)

T=330°C, LHSV=1.3 h^{-1}, H_2/n-C_{14}=10 mol/mol

Carbon	80 bar	40 bar	20 bar	40 bar REP	40 bar REP2
1	0.0	0.0	0.0	0.0	0.0
2	0.0	0.0	0.0	0.0	0.0
3	0.0	0.0	0.0	0.0	0.0
4	0.0	0.0	0.1	0.1	0.1
5	0.0	0.1	0.2	0.1	0.1
6	0.0	0.1	0.3	0.1	0.1
7	0.0	0.1	0.4	0.2	0.1
8	0.0	0.2	0.6	0.3	0.2
9	0.0	0.2	0.6	0.3	0.2
10	0.0	0.2	0.6	0.4	0.2
11	0.0	0.3	0.7	0.5	0.3
12	0.1	0.7	0.7	0.8	0.7
13	2.2	1.8	0.7	1.3	1.9
Total	2.4	3.7	4.9	4.1	3.9

Table D.11: Effect of Space Velocity

Selectivity to Iso + Normal Paraffins (mol%)

T=330°C, P=40 bar, H_2/n-C_{14}=10 mol/mol

Carbon	1.3	1.0	0.5
1	46.9	54.4	44.4
2	3.2	3.4	2.3
3	3.3	3.5	2.5
4	3.4	3.5	2.6
5	3.6	3.9	3.0
6	3.7	3.9	3.3
7	3.5	3.7	3.4
8	3.2	3.4	3.5
9	2.9	3.0	3.8
10	2.8	2.9	4.5
11	3.6	3.3	5.8
12	6.2	4.2	8.2
13	13.6	6.9	12.6
Total	100.0	100.0	100.0

For conversions see table 4.4

Table D.12: Effect of Space Velocity

Selectivity to Normal Paraffins (mol%)

T=330°C, P=40 bar, H_2/n-C_{14}=10 mol/mol

Carbon	1.3	1.0	0.5
1	46.9	54.4	44.4
2	3.2	3.4	2.3
3	3.3	3.5	2.5
4	3.4	3.5	2.6
5	3.6	3.8	2.9
6	3.6	3.8	3.1
7	3.4	3.5	3.1
8	3.1	3.1	3.1
9	2.7	2.7	3.2
10	2.6	2.5	3.6
11	3.3	2.7	4.3
12	5.6	3.3	5.7
13	11.8	5.5	8.6
Total	96.3	95.6	89.4

Table D.13: Effect of Space Velocity

Selectivity to Iso Paraffins (mol%)

T=330°C, P=40 bar, H_2/n-C_{14}=10 mol/mol

Carbon	1.3	1.0	0.5
1	0.0	0.0	0.0
2	0.0	0.0	0.0
3	0.0	0.0	0.0
4	0.0	0.1	0.1
5	0.1	0.1	0.1
6	0.1	0.2	0.2
7	0.1	0.2	0.3
8	0.2	0.3	0.4
9	0.2	0.3	0.6
10	0.2	0.4	0.9
11	0.3	0.6	1.5
12	0.7	0.9	2.5
13	1.8	1.4	4.0
Total	3.7	4.4	10.6

Table D.14: Effect of H_2/n-C_{14} Molar Ratio

Selectivity to Iso + Normal Paraffins (mol%)

T=330°C, P=40 bar, LHSV=0.5 h^{-1}

Carbon	3 mol/mol	10 mol/mol	30 mol/mol	3 mol/mol REP
1	46.6	44.4	56.4	24.4
2	1.7	2.3	3.6	1.0
3	2.0	2.5	3.9	1.2
4	2.2	2.6	4.2	1.6
5	2.5	3.0	4.9	2.3
6	2.6	3.3	5.2	3.5
7	2.8	3.4	5.0	4.5
8	3.2	3.5	4.6	4.4
9	3.6	3.8	4.0	4.8
10	4.3	4.5	3.4	4.1
11	5.5	5.8	2.6	4.8
12	8.5	8.2	1.6	10.6
13	14.5	12.6	0.7	32.7
Total	100.0	100.0	100.0	100.0

For conversions see table 4.5

Table D.15: Effect of H_2/n-C_{14} Molar Ratio

Selectivity to Normal Paraffins (mol%)

T=330°C, P=40 bar, LHSV=0.5 h^{-1}

Carbon	3 mol/mol	10 mol/mol	30 mol/mol	3 mol/mol REP
1	46.6	44.4	56.4	24.4
2	1.7	2.3	3.6	1.0
3	2.0	2.5	3.9	1.2
4	1.9	2.6	4.1	1.5
5	2.1	2.9	4.8	2.1
6	2.1	3.1	5.0	3.1
7	2.1	3.1	4.7	3.7
8	2.1	3.1	4.1	3.4
9	2.2	3.2	3.4	3.6
10	2.4	3.6	2.7	2.8
11	2.7	4.3	1.9	3.1
12	4.0	5.7	1.1	6.7
13	7.3	8.6	0.4	18.6
Total	79.2	89.4	95.9	75.1

Table D.16: Effect of H_2/n-C_{14} Molar Ratio

Selectivity to Iso Paraffins (mol%)

T=330°C, P=40 bar, LHSV=0.5 h^{-1}

Carbon	3 mol/mol	10 mol/mol	30 mol/mol	3 mol/mol REP
1	0.0	0.0	0.0	0.0
2	0.0	0.0	0.0	0.0
3	0.0	0.0	0.0	0.0
4	0.3	0.1	0.1	0.2
5	0.4	0.1	0.1	0.3
6	0.5	0.2	0.2	0.5
7	0.7	0.3	0.4	0.8
8	1.0	0.4	0.5	1.0
9	1.4	0.6	0.6	1.2
10	1.9	0.9	0.7	1.4
11	2.8	1.5	0.7	1.7
12	4.5	2.5	0.5	3.9
13	7.2	4.0	0.2	14.1
Total	20.8	10.6	4.1	24.9

Table D.17: Conditions Screening Experiments

Selectivity to Iso + Normal Paraffins (mol%)

P=80 bar, LHSV=1.3 h^{-1}, H_2/n-C_{14}=10 mol/mol

Carbon	320C	330C	350C	330C REP	350C 40 bar
1	43.5	41.5	51.8	12.3	65.6
2	3.2	3.1	3.8	0.9	5.2
3	3.3	3.3	4.0	0.9	5.7
4	3.4	3.3	4.0	0.8	5.5
5	3.6	3.7	4.3	0.9	5.0
6	3.6	3.7	4.2	1.2	3.7
7	3.1	3.3	3.7	2.8	2.8
8	2.7	3.0	3.4	4.0	1.9
9	2.5	2.7	3.0	4.7	1.4
10	2.2	2.4	2.8	6.5	1.0
11	2.3	2.5	3.1	8.4	0.8
12	3.9	4.2	4.5	11.3	0.7
13	22.5	23.4	7.4	45.3	0.6
Total	100.0	100.0	100.0	100.0	100.0
Conversion (%)	4.3	9.6	53.9	9.4	97.1

Table D.18: Conditions Screening Experiments

Selectivity to Normal Paraffins (mol%)

P=80 bar, LHSV=1.3 h^{-1}, H_2/n-C_{14}=10 mol/mol

Carbon	320°C	330°C	350°C	330°C REP	350°C 40 bar
1	43.5	41.5	51.8	12.3	65.6
2	3.2	3.1	3.8	0.9	5.2
3	3.3	3.3	4.0	0.9	5.7
4	3.4	3.3	4.0	0.8	5.3
5	3.6	3.6	4.2	0.9	4.7
6	3.6	3.7	4.0	1.2	3.4
7	3.1	3.3	3.4	2.8	2.5
8	2.7	3.0	3.1	4.0	1.6
9	2.5	2.7	2.7	4.7	1.1
10	2.2	2.4	2.4	6.5	0.8
11	2.3	2.5	2.7	8.2	0.6
12	3.9	4.2	3.8	11.1	0.4
13	22.2	21.2	6.3	44.2	0.3
Total	99.7	97.6	96.3	98.4	97.2

Table D.19: Conditions Screening Experiments

Selectivity to Iso Paraffins (mol%)

P=80 bar, LHSV=1.3 h^{-1}, H_2/n-C_{14}=10 mol/mol

Carbon	320°C	330°C	350°C	330°C REP	350°C 40 bar
1	0.0	0.0	0.0	0.0	0.0
2	0.0	0.0	0.0	0.0	0.0
3	0.0	0.0	0.0	0.0	0.0
4	0.0	0.0	0.1	0.0	0.2
5	0.0	0.0	0.1	0.0	0.3
6	0.0	0.0	0.1	0.0	0.3
7	0.0	0.0	0.2	0.0	0.3
8	0.0	0.0	0.3	0.0	0.3
9	0.0	0.0	0.3	0.0	0.3
10	0.0	0.0	0.3	0.0	0.3
11	0.0	0.0	0.5	0.1	0.3
12	0.0	0.1	0.7	0.3	0.3
13	0.3	2.2	1.1	1.1	0.2
Total	0.3	2.4	3.7	1.6	2.8